REVIEW

Materials Science

Energy & Environmental Materials WILEY

Membrane Engineering for Battery Systems: Bridging Design Principles and Frontier Applications

*Xiaoqun Zhou**, *Justice Delali Akoto*, *Rui Tan**, *and Jun Ma**

Electrochemical energy storage systems (EESSs) stand as linchpins in the global transition toward carbon neutrality, yet their performance and safety remain fundamentally constrained by the underappreciated component: membrane separators. This review delivers a paradigm-shifting synthesis of separator science across redox flow batteries (RFBs), lithium-ion batteries (LIBs), and solid-state batteries (SSBs), unraveling the universal principles that govern ion selectivity, interfacial stability, and long-term cyclability. By critically analyzing the interplay among material architecture, ion transport mechanisms, and electrochemical degradation pathways, we establish a unified framework for designing next-generation separators that overcome the persistent trade-off between ionic conductivity and molecular-level discrimination. Recent advances in porous crystalline materials, polymer electrolytes, and hybrid composites are dissected through the lens of size-exclusion, Donnan-exclusion, and dynamic adaptive interactions, revealing how tailored pore geometries and functional group engineering enable the precise modulation of cation/anion flux. Emphasis is placed on the emerging role of computational modeling in decoding separator–electrolyte couplings, guiding the rational design of membranes with atomic-scale precision. The review further addresses critical challenges, including dendritic growth in alkali metal batteries, crossover losses in aqueous RFBs, and interfacial instability in solid-state systems. This integrative analysis establishes a cross-cutting roadmap for separator innovation, where the synergistic design of material architectures, ion transport physics, and computational-guided interfaces converge to unlock the full potential of electrochemical energy storage systems.

1. Overview

1.1. Electrochemical Energy Storage

The net-zero emissions (NZE) outline a decarbonization pathway to achieve global CO_2 neutrality by 2050, fueled by clean energy investments and electrification, visualized in **Figure 1**. By 2030, clean energy jobs will rise by 14 million, offsetting 5 million fossil fuel job losses, though regional disparities and skill mismatches risk exacerbating inequities. Global GDP grows despite stark revenue declines for fossil fuel producers (80% lower by 2050) and import-dependent economies (90% drop in fossil fuel tax revenues). Energy systems pivot sharply: fossil fuel production contracts, while firms repurpose expertise for low-emissions technologies, and electricity demand surges 2.5-fold by 2050, centered on renewables, grid upgrades, and industrial decarbonization (e.g., green hydrogen), with energy storage systems critical for grid stability and integrating variable renewables. Universal energy access for 1 billion people by 2030 requires 40 billion USD per year, adding less than 0.2% to CO_2, with 75% of the required behavioral shifts dependent on policy mandates. Equity remains critical, as household energy costs stabilize in developing economies despite rising demand. Success hinges on cross-sectoral governance, addressing energy security risks (critical minerals and grid reliability), accelerating innovation (50% of 2050 emissions cuts depend on nascent technologies), and global cooperation to align standards and infrastructure. Delays in multilateral collaboration could defer net-zero progress by decades, underscoring the urgency of coordinated action.

Energy storage technologies are mechanistically categorized into four principal paradigms: Mechanical systems (e.g., pumped hydro, compressed air, flywheels) that store energy through kinetic/potential energy conversion; Thermal storage systems capturing heat via phase-change materials or sensible heat carriers; Hydrogen/power-to-X (P2X) chemical energy vectors enabling electrical-to-chemical energy interconversion,[2–4] and Electrochemical devices – with this final category dominating modern applications from microelectronics to renewable energy grids due to its unparalleled scalability and roundtrip efficiency.

As shown in **Figure 2**, batteries outperform other technologies in efficiency (80–90% roundtrip), response speed, and scalability, making them ideal for grid-scale applications (1 kW–10 MW). Beyond their common benefits, different types of batteries each possess unique constructions and properties and face distinct challenges. Redox Flow Batteries (RFBs), Lithium-Ion Batteries (LIBs), and Solid-State Lithium-Ion Batteries (SSBs) are the topics of interest in this review. Lithium-ion

X. Zhou, Prof. J. Ma
State Key Laboratory of Urban-Rural Water Resource & Environment, School of Environment, Harbin Institute of Technology, Harbin 150090, China
E-mail: 21b329008@stu.hit.edu.cn
E-mail: majun@hit.edu.cn
J. D. Akoto, Dr. R. Tan
Department of Chemical Engineering, Swansea University, Swansea SA1 8EN, UK
E-mail: rui.tan@swansea.ac.uk
The ORCID identification number(s) for the author(s) of this article can be found under https://doi.org/10.1002/eem2.70192.

DOI: 10.1002/eem2.70192

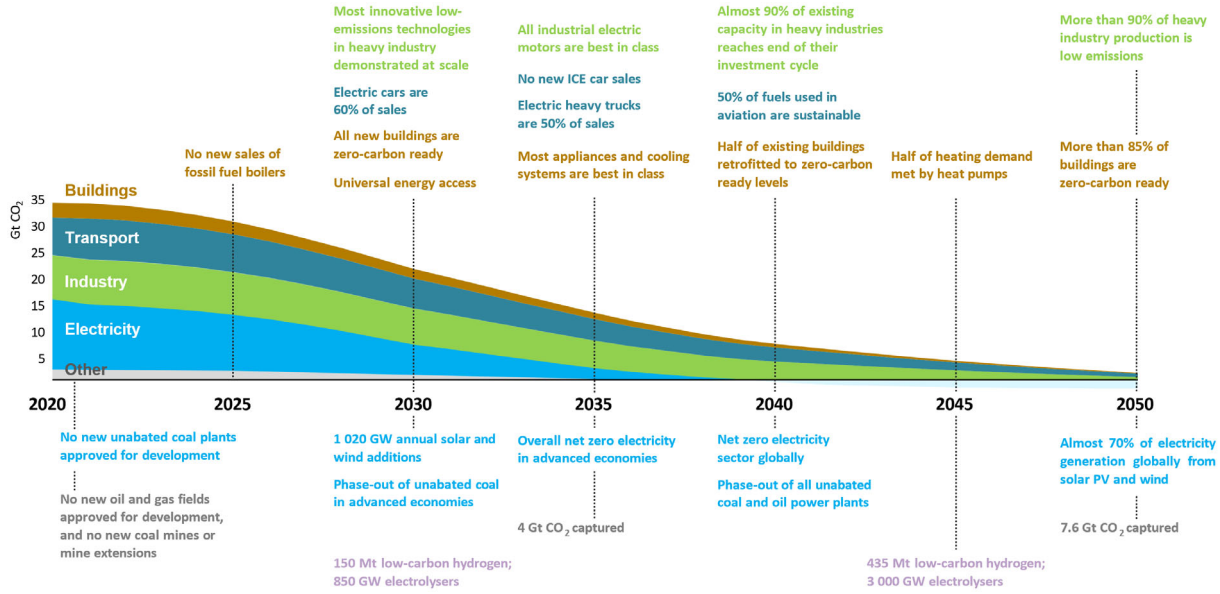

Figure 1. Key milestones for policies, infrastructure, and technology deployment in the pathway to net zero.[1] Copyright 2022, IEA, World Energy Outlook.

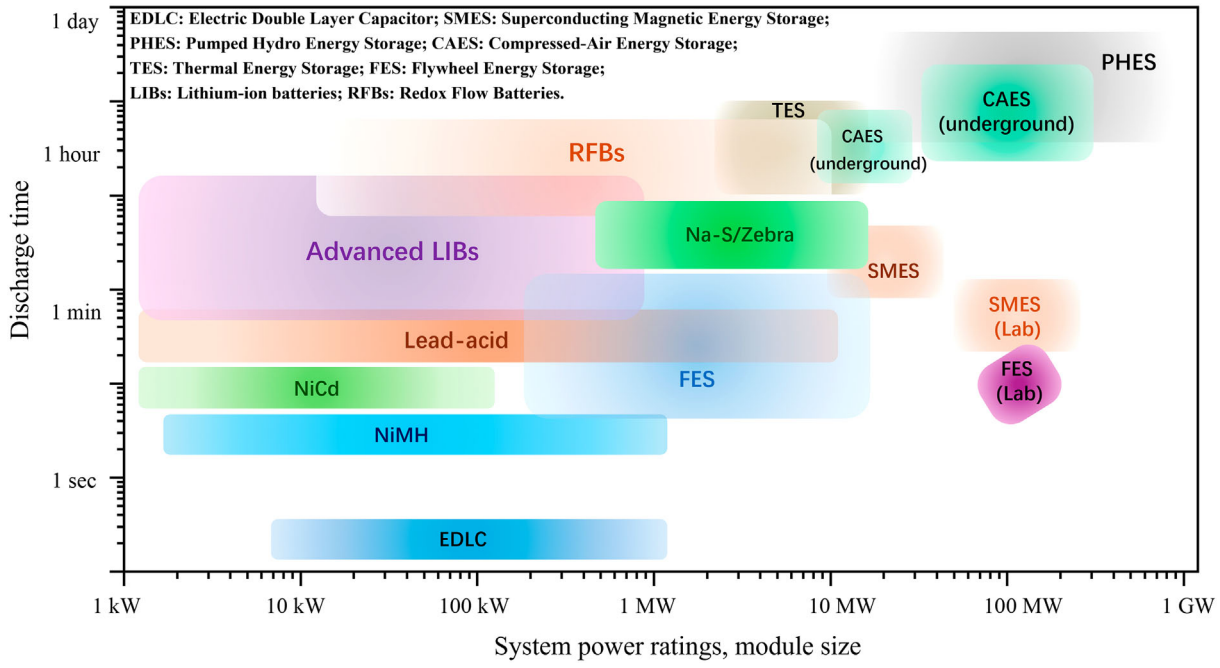

Figure 2. Comparison of discharge duration and power for various energy storage technologies. Data adopted from the references.[5,6]

batteries (LIBs), redox flow batteries (RFBs), and solid-state alternatives (SSBs) are focal points here due to their distinct advantages and challenges (**Table 1**).

LIBs dominate portable electronics and electric vehicles (EVs) due to their high energy density (300 Wh kg^{-1} in NMC811 vs 110 Wh kg^{-1} in 2010) and scalability (8.8 GWh installed in 2019 vs 0.25 GWh for RFBs).[7] However, safety concerns (thermal runaway) and high maintenance costs hinder their grid-scale deployment. RFBs, with decoupled power/energy scaling and long lifespans (20 000 cycles), are promising for stationary storage but face challenges in active material cost and membrane selectivity.[8]

Membrane separators are critical to both systems, influencing efficiency, safety, and cost. In RFBs, membranes account for 40% of stack cost and dictate 75% of energy efficiency via redox-species crossover suppression.[9] In LIBs, polyolefin separators (polyethylene/polypropylene) enable high energy density (150–250 Wh kg^{-1}) but suffer from poor thermal stability, leading to dendrite formation and fire risks.[10,11] Therefore, the

Table 1. Comparison of the performance, advantages, and limitations of commercial LIBs and RFBs.

Storage chemistry	Roundtrip efficiency (%)	Duration (h)	Capital cost ($ kWh^{-1})	Life span (years)	Advantages	Limitations
Commercial RFBs (Vanadium Redox)	70–80	4–12	500–1100	>20	• Two tank system with low maintenance cost • Aqueous system without fire risk • Long cycle life and fast response • Stable at all charges	• Low energy densities of actives • **High cost of actives and membranes** • Crossover of actives through membrane, leading to a low cycling efficiency
Commercial LIBs	80–90	1–4	300–1000	5–20	• Light weight and a high energy density • High roundtrip efficiency • Moderate cycle life. • High output voltage (>3.4 V)	• Fire risk due to the use of flammable organic electrolytes • **Sensitive to high temperature due to the thermally instable separators** • Maintenance cost

Bolded text in the table indicates key weaknesses of the system.

development of advanced membrane separators is required, and it is the primary focus of this work.

1.2. Membrane Separators in RFBs, LIBs, and SSBs

Membrane separators play a critical role in electrochemical devices by electrically isolating electrodes while enabling selective ion transport to maintain charge balance.[12] This dual functionality is essential for optimizing energy efficiency and safety across diverse systems, including redox flow batteries (RFBs), lithium-ion batteries (LIBs), and solid-state batteries (SSBs). However, the design requirements for these membranes vary significantly depending on the operational principles and materials chemistry of each system.[12]

1.2.1. RFBs

In RFBs, typical components include two external tanks containing catholytes and anolytes, current collectors, electrodes, and membrane separators (**Figure 3a**). During operation, redox-active electrolytes are pumped into the cells, and electrochemical reactions occur on the surface of the electrodes. The ion-conductive membrane prevents cross-mixing of redox species while allowing charge carriers to be transported (as illustrated in Figure 3c).[14,15] The ability to transport charge carriers and block redox species is referred to as "selectivity" or "permselectivity", a vital metric for RFB membranes. An ideal membrane should exhibit high ionic conductivity, high selectivity, good mechanical strength, high electrochemical and thermal stability, low area-specific resistance, ease of processing, and cost-effectiveness. Figure 3b presents the commercial Nafion perfluorinated membrane, which is now widely used in commercial RFB stacks. However, its high cost and poor selectivity toward redox materials (e.g., vanadium-based actives) pose significant challenges for the scale-up of RFB stacks.[16–18] Commercial Nafion perfluorinated membranes, despite their dominance in current RFB stacks,[16] face two critical limitations: prohibitively high costs (>$500 m^{-2}) and suboptimal selectivity for transition-metal-based redox couples.[18] This has driven a decade-long pursuit of non-perfluorinated alternatives, including cation/anion-exchange membranes (CEMs/AEMs), nonionic architectures, and porous polymeric systems.[10] While advanced fabrication methods, such as phase inversion for polybenzimidazole membranes[19] and thin-film composite (TFC) architectures,[20] have improved performance, persistent challenges remain: thickness-selectivity trade-off, interfacial instability (delamination between selective and support layers under prolonged cycling[21]), and chemical degradation (oxidative attack by high-potential catholytes (e.g., >1.5 V vs SHE)[14]).

Despite significant progress in materials engineering and process optimization,[22] the development of a "universal membrane" that simultaneously satisfies all seven performance metrics remains elusive.[17] This underscores the need for breakthroughs in molecular-level pore design and interfacial reinforcement strategies to enable scalable RFB systems.

1.2.2. LIBs and SSBs

The architecture of conventional lithium-ion batteries (LIBs) features a porous polyolefin separator (primarily polyethylene/polypropylene) sandwiched between a graphite anode and a metal oxide cathode (Figure 3c), with organic liquid electrolyte permeating its pores to enable Li^+ transport.[23] A typical LIB pack using polyolefin separators can deliver a gravimetric energy density of 150 Wh kg^{-1} and a volumetric energy density of 250 Wh L^{-1}, these values fall short of the US Department of Energy's 2025 targets for electric vehicles (250 Wh kg^{-1} and 500 Wh L^{-1}).[13,24] This gap drives research toward two transformative strategies: functional porous separators for lithium-metal anodes[25] and solid-state electrolytes.[24]

Functional porous separators (**Figure 4**): Functional porous separators require precise engineering: thickness control (20–25 μm), mechanical strength >98 MPa, thermal stability (<5% shrinkage at 90 °C), and pore architecture matching Li^+ transport kinetics.[26] Conventional polyolefin membranes (e.g., Celgard separators, Figure 4a) undergo plasma treatment, inorganic coatings, or polymer grafting to enhance wettability and ionic conductivity.[26] Emerging alternatives (Polyvinylidene fluoride (PVDF),[22,30] poly(vinylidene fluoride-co-hexafluoropropylene) (PVDF-HFP),[31,32] polyacrylonitrile (PAN),[25,27,28] poly(methyl methacrylate) (PMMA),[33] etc., Figure 4b,c) have also been manufactured into porous separators or composite membranes loaded with other organic or inorganic materials. Polymers of intrinsic microporosity (PIMs) emerge as selective microporous separators (Figure 4d), demonstrating improved performance in Li-S batteries and LIBs,[29,34–36] which form composite separators with tailored porosity through dry/wet phase-inversion processes,[33]

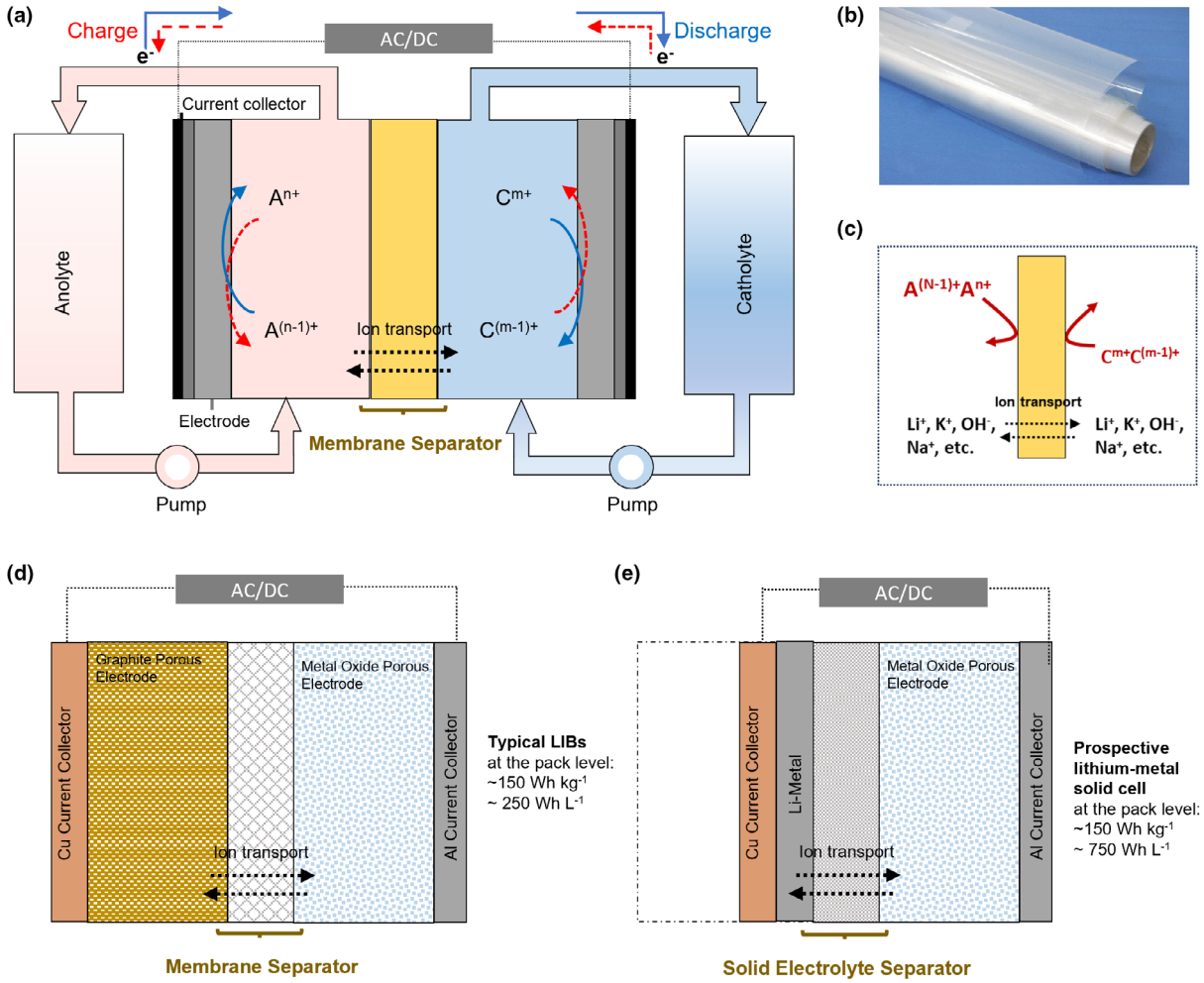

Figure 3. a) Working principle of a typical RFB. b) Photo showing a commercial perfluorosulfonic membrane. c) Diagram of the function of ion-conductive and molecular-selective membrane. Anolyte: $A^{(n-1)+/n+}$ and Catholyte: $C^{(m-1)+/m+}$. d) Configuration of a typical LIB. e) Configuration of an advanced LIB using lithium metal anode and solid electrolyte separator. Reproduced with permission.[13] Copyright 2017, Nature Energy.

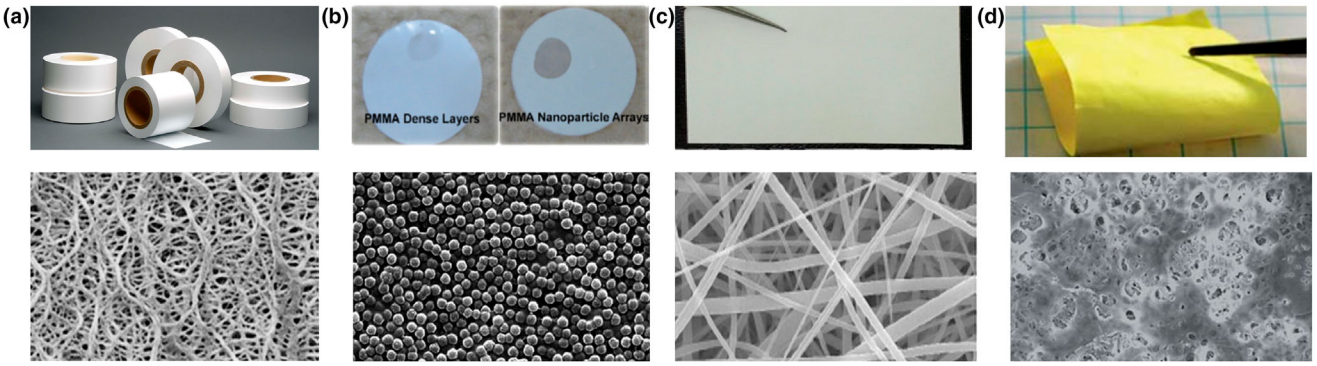

Figure 4. Photos and SEM images of a) Celgard separator, reproduced with permission,[26] Copyright 2014, Royal Society of Chemistry; b) PMMA coated separators, reproduced with permission,[27] Copyright 2010, Springer-Verlag; c) nonwoven PAN separator. Reproduced with permission.[28] Copyright 2018, Elsevier B.V.; d) PIM-1/S separator, reproduced with permission.[29] Copyright 2019, The Royal Society of Chemistry.

shown in Figure 4d. Despite advancements in electrospun[37] and self-assembled architectures, flammable liquid electrolytes remain a critical safety concern.[33]

Solid electrolytes: Solid-state electrolytes offer a paradigm shift by eliminating volatile components and enabling dendrite-suppressing architectures. The inorganic electrolyte, $Li_{10}GeP_2S_{12}$, is the major advance over

the last decade, but the ionic conductivity remains low.[38] Conventional polymeric electrolyte membranes are mainly formed from polyethylene oxides (PEO) and PEO derivatives, which have relatively low ionic conductivity at room temperature. Solid composite electrolyte is a promising concept which integrates the mechanically robust inorganic with ion-conductive organic liquid or ionic liquid. For example, $Li_{1.5}A_{0.4}Ge_{1.5}(PO_4)_3$ and ionic liquid were dispersed in PEO/PVDF-HFP organic matrix to form a hybrid electrolyte, which offers good flexibility, outstanding ionic conductivity, and improved thermal stability.[39] However, large-scale production of the inorganic electrolyte or composite electrolyte is challenging due to the poor handleability of the inorganic component.

This work provides a cross-cutting analysis of electrochemical energy storage systems that reveals shared scientific challenges in developing functional membrane separators: achieving rapid and selective ion transport while maintaining mechanical integrity and electrochemical stability. Overcoming these limitations is critical for advancing energy efficiency, cycle life, and safety across lithium-metal batteries, redox flow batteries, and solid-state systems. Building on this foundation, this review proposes innovative design paradigms for next-generation separators by leveraging subnanometer-scale microporous materials. These architectures—tailored to the unique demands of targeted energy storage systems—offer precise control over pore-channel dimensions, enabling unprecedented selectivity for charge carriers. Through systematic analysis of recent breakthroughs in materials science and interfacial engineering, the review establishes key structure–property–function relationships that govern separator performance. By bridging fundamental insights with scalable manufacturing strategies, this work aims to accelerate the translation of laboratory innovations into industrial applications, ultimately guiding the development of advanced membrane technologies for sustainable electrochemical energy storage.

1.2.3. Cutting-Edge Mircroporous Materials for Battery Separators

Microporous materials, including covalent organic frameworks (COFs), porous organic cages, metal–organic frameworks (MOFs), and polymers of intrinsic microporosity (PIMs), have emerged as functional electrolyte separators in electrochemical devices due to their tailored porosity and ion transport properties. COFs, such as PBI/COF composites,[40] leverage crystalline porous structures to enhance V^+/H^+ selectivity in redox flow batteries (RFBs), though standalone fabrication challenges persist. Pelletized COFs (e.g., cucurbit[6]uril COF.[41]) demonstrate ionic conductivities up to 7.2 mS cm^{-1} with low activation energy (0.1 eV) when functionalized with imidazole or borate groups,[41–43] but their insolubility hinders flexible separator development. Porous organic cages, like TdA cages, host liquid electrolytes (1 M LiTFSI/DME) to achieve 1.0 mS cm^{-1} conductivity and stable oxidative windows (4.7 V vs Li/Li^+),[37] though processability limitations remain. MOFs, such as ZIF-7,[44], ZIF-8,[45,46] and UiO-66,[47,48] utilize tunable pore chemistry to suppress polysulfide crossover and immobilize anions in lithium batteries, with polymer blending or in situ growth enabling flexible membranes despite potential pore blockage by binders.[49] PIMs, pioneered by McKeown et al.,[50] employ rigid, contorted backbones to achieve high microporosity (e.g., PIM-EA-TB with >1000 m^2 g^{-1} surface area[51]) and solution-processability, enabling thin-film separators for energy storage.[52]

2. Design Principles and Performance Metrics of Membrane Separation

2.1. Fundamental Knowledge about Electrochemical Process in Battery Systems

2.1.1. Overpotentials in Redox Flow Batteries

The fundamental operation of electrochemical energy storage relies on exothermic redox reactions, $C_{oxi} + A_{red} \leftrightarrow C_{red} + A_{oxi}$ $(\Delta H \ll 0)$, where electrons transfer from the anode (reductant) to the cathode (oxidant) via an external circuit, while ions migrate through an electrolyte-separator medium to maintain charge neutrality. The theoretical cell voltage $V_{cell} = V_C - V_A$, derived from the Nernst equation:

$$V = U_0 + \frac{RT}{nF}\ln\left(\frac{a_{oxi}}{a_{red}}\right) \quad (1)$$

where U_0 is the standard potential of electrodes, n is the number of electrons, a is the chemical activity that relates to the physical concentrations c, by $a = \gamma c$. γ refers to the activity coefficient. Thus, the Nernst equation can be equivalently described as:[53]

$$V = U_0 + \frac{RT}{nF}\ln\left(\frac{c_{oxi}}{c_{red}}\right) + \frac{RT}{nF}\ln\left(\frac{\gamma_{oxi}}{\gamma_{red}}\right) \quad (2)$$

when charging, cathode/catholyte undertakes reactions to provide electrons that move from the cathode/catholyte to the anode/anolyte through the external circuit, so $c_{oxi,cathode}$ and $c_{red,anode}$ increase while $c_{red,cathode}$ and $c_{oxi,anode}$ decrease. As a result, the cathode potential, V_c, increases and the potential of anode, V_a, decreases, leading to the decrease of the overall potential, V_{cell}.

However, practical battery performance deviates significantly from the ideal Nernstian predictions, highlighting the critical role of separators in mediating ion transport and interfacial processes. The theoretical discharging curve predicted from the ideal Nernst equation (γ_{oxi}, γ_{red} are unity) is presented in **Figure 5**a. Clearly, the ideal discharge curve is totally different from the process of practical batteries. Gaining insight into ideal and practical battery curves would support us to understand the process and the influence of the separator. This may pave a way to designing a useful separator and an improved battery system.

Real-world voltage losses arise from three primary overpotentials:

Ohmic overpotential (V_{ohmic}): The solid-phase resistance (e.g., resistances of the component contacts), electrolyte resistance, and the resistance of current collectors could be treated as constant impedance and described as:

$$R_{ohmic} = R_e + R_{con} + R_{cc} + R_{ele} \quad (3)$$

where R_e refers to the resistance of electrolytes and separators, R_{con} is the contact resistance, R_{cc} and R_{ele} are the ohmic resistance of current collectors and electrodes. Thus, the voltage drops due to the ohmic resistance is $V_{ohmic} = i \times R_{ohmic}$. In lithium-ion batteries (LIBs), solid-state LIBs, and redox flow batteries (RFBs), R_e dominates the overall value of R_{ohmic} as the ion transport through the electrolyte membrane becomes a limiting process. Reducing the R_e could lower the ohmic overpotential and significantly increase the output power density at a specific current.

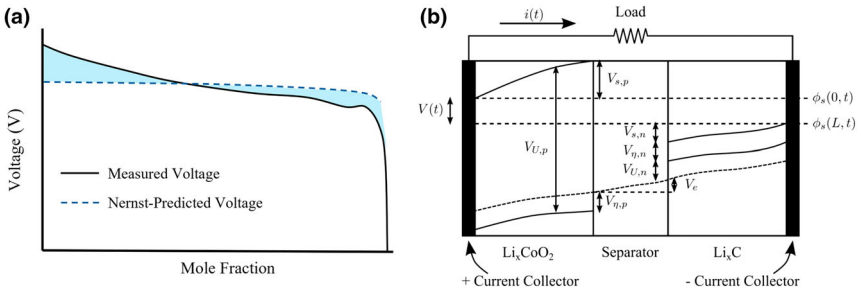

Figure 5. a) Comparison of an ideal discharging curve derived from the classical Nernst equation with the curve of a practical battery. Reproduced with permission.[54] Copyright 2013, The Prognostic and Health Management Society. b) Battery voltages of a practical Li-ion battery. Reproduced with permission.[54] Copyright 2013, The Prognostic and Health Management Society.

Surface overpotential (V_η): The surface overpotential is governed by charge-transfer kinetics at the electrode-electrolyte interface, described by the Butler–Volmer equation:[55]

$$j_i = j_0\left(\exp\left(\frac{(1-\alpha)F}{RT}(V_c - V_{c,0})\right) - \exp\left(-\frac{\alpha F}{RT}(V_c - V_{c,0})\right)\right) \quad (4)$$

where α is the symmetry factor, $V_c - V_{c,0}$ stands for the surface overpotential, V_η, and j_0 refers to the exchange current density. The symmetry factor in the case of LIBs is 0.5.

j_0 is the intrinsic kinetic parameter representing the rate of electron transfer at equilibrium, and it is a combined parameter proportional to the density of accessible reaction sites, redox-species concentration, and the rate constant of electron transfer. The density of accessible reaction sites refers to the number of active sites per unit area where redox reactions occur (e.g., defects, dopants, or surface functional groups), and the rate constant of electron transfer refers to the intrinsic speed of electron transfer between the electrode and adsorbed species. In practical batteries, the exchange current is closely associated with the surface structure properties of electrodes, for example, the surface roughness, formed passivating SEI layer, and absorbed species.

Surface roughness enhances the effective surface area of electrodes, creating micro/nano-features (e.g., pores) that increase active sites for redox reactions, thereby elevating the exchange current density (j_0). However, excessive roughness introduces dead zones or interfacial voids, increasing ohmic resistance and charge-transfer resistance (R_{ct}), which raises overpotential (V_η). The SEI layer acts as a selective ion barrier but suppresses j_0 by coating electrodes, reducing accessible active sites and electron transfer. Its low ionic conductivity, orders of magnitude below bulk electrolytes, amplifies R_{ct} ($\propto d/\sigma$, where d = thickness, σ = conductivity). Higher R_{ct} increases V_η to sustain current density, as seen in aged batteries where SEI thickening elevates charge–discharge voltages and accelerates capacity fade. Adsorbed species influence kinetics through competitive site blocking or interfacial energetic modulation. Strongly adsorbed anions occupy Li^+ intercalation sites, lowering j_0. Conversely, weakly bound solvated ions stabilize transition states, reducing activation energy (E_a) and enhancing j_0. Strongly bound adsorbates distort surface potentials, increasing E_a and V_η. In summary, surface roughness optimizes j_0 via expanded active areas but risks V_η increases from heterogeneous resistance. SEI layers reduce j_0 and elevate V_η due to resistive barriers, with thickness/composition dictating trade-offs. Adsorbed species dynamically regulate j_0 and V_η based on binding strength, balancing site blocking against energetic stabilization.

Membrane separators also play a critical role in affecting the surface overpotential; functional microporous separators mitigate side reactions and ensure uniform ion flux, minimizing localized overpotentials.[56,57]

Concentration overpotential: When the battery is operating, electrochemical reactions occur on the surface of electrodes, leading to the concentration gradient within the bulk of electrodes or in the catholyte/anolyte. The concentration gradient could be minimized in a flow mode in RFBs. In LIBs, fabricating highly porous and electron-conductive electrodes could diminish the influence of concentration gradients in the electrode bulk. Generally, the overpotential caused by the concentration gradients in the electrodes of batteries is small.

2.1.2. Battery Voltage and Roles of Separator

The battery voltage could be expressed as the following equation by considering the different types of overpotentials, $V_{cell} = V_c - V_a - V_{ohmic} - V_{\eta,c} - V_{\eta,a}$.

To maximize the output voltage, V_{cell}, substantial efforts are being devoted to developing high-voltage cathode materials and enlarging the equilibrium potential difference of electrodes, that is, $V_c - V_a$. Surface engineering has also been employed to enhance the reactions of the electrode surface. Developing functional separator emerges as a new strategy to further improve the device powers. Although the separator is a redox-inactive material, it plays a very important role in diminishing the ohmic resistance and surface overpotentials, V_{ohmic} and V_η, respectively. As shown in **Figure 6**, improving the ionic conductivity of the electrolyte separator or reducing the effective thickness could enhance the ion conduction and mitigate the ohmic overpotential. The membrane can possess some functions to selectively transport supporting ions and separate redox species. This function could improve the lithium-ion transference number and ensure the homogenous Li^+ transport in LIBs. It can also prevent the shuttle of redox species in RFBs, which not only maintains the cycling capacity but also avoids the side reaction caused by the crossover mixing of redox species.

2.2. Understanding the Basis of Ion Conduction in Separator for Battery Systems

Ions in the electrolyte (e.g., aqueous electrolytes, organic liquid electrolytes) perform a random Brownian motion with the collision time, τ. When applied with the electric field E, the current density of the electrolyte can be described as Equation 5.

$$J_{electrolyte} = n_i \frac{q^2}{m_i}\tau E \quad (5)$$

where n_i is the number of ions per unit volume, q is the charge, and m_i is the mass of an ion. Here, $\frac{q}{m_i}\tau$ refers to the mobility of ions, μ_i. Based on the ohmic law, the conductivity of this electrolyte can be expressed as:

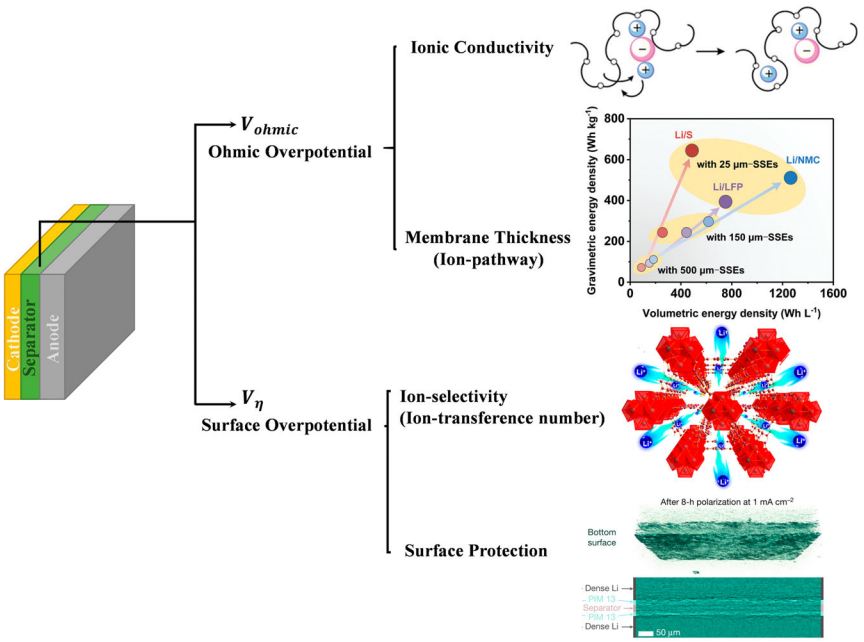

Figure 6. Essential influence of electrolyte separators on the resistance of batteries. Figures adapted from references. (Reproduced with permission.[58] Copyright 2021, RSC publishing; Reproduced with permission.[59] Copyright 2021, Springer Nature; Reproduced with permission.[60] Copyright 2015, Royal Society of Chemistry).

$$\sigma = \frac{J_{electrolyte}}{E} = n_i \frac{q^2}{m_i} \tau = n_i q \mu_i \quad (6)$$

Applying this classical equation, highlighting three universal strategies to enhance conductivity: increasing ion concentration, optimizing mobility, and selecting low-mass charge carriers. These principles serve as the foundation for analyzing ion transport in solid polymer, inorganic, and composite electrolytes, as well as their applications in redox flow batteries (RFBs), lithium-ion batteries (LIBs), and solid-state electrolytes (SSEs).

Ion exchange, vehicle, and Grotthuss mechanisms are fundamental to understanding proton and ion transport in various media, summarized in **Table 2**. The Grotthuss mechanism involves the transfer of protons through a network of hydrogen bonds, where protons hop between water molecules or other hydrogen-bonded structures, facilitating efficient proton transport without the physical movement of the molecules themselves.[61] This mechanism is particularly efficient in systems like aqueous phosphoric acid, where proton hopping is essential for long-range diffusion, although it can be limited by ionic correlations that reduce conductivity. In contrast, the vehicular mechanism involves the physical movement of protonic defects, such as hydronium ions, through the medium, often aided by solvation environments that facilitate their transport. This mechanism is characterized by the movement of entire molecular entities, which can be influenced by factors such as hydration levels and temperature, as seen in hydroxide ion transport in anion-exchange membranes. The ion-exchange mechanism, often discussed in the context of anion-exchange membranes, involves the swapping of ions between the membrane and the surrounding solution, which can be influenced by the membrane's hydration and structural properties.

2.2.1. *Ionic Conduction in Solid Polymer Electrolyte (SPE)*

Polyethylene oxide (PEO) is the most developed and representative solid polymer electrolyte, of which the ion-conducting mechanism was proposed in **Figure 7**a. The hopping of Li-ions highly depends on the flexible ether chains of PEO. Li-ions can coordinate with ether oxygen atoms in ether groups and move by inter/intrachain hopping through ether chains. The continuous dis-/solvation of Li-ions via exchanging the coordination centers realizes a long-range migration of Li ions. This migration type is named as "vehicular" movement that is induced by the phase change.[62] However, the ionic conductivity is low at the temperature close to the glass transition temperature of PEO due to the slow segmental motions of polymer chains.

The ionic conductivity against temperature could be fitted to the Vogel–Fulcher–Tammann function as described below:

$$\sigma = \frac{\sigma_0}{\sqrt{T}} \exp\left(-\frac{E_a}{k_B(T - T_0)}\right) \quad (7)$$

where σ_0 is the pre-exponential factor, E_a is the activation energy and T_0 stands for the temperature at which the ability of free volume within SPEs to conduct ions is zero. T_0 is identical to the glass transition temperature of polymers. Besides SPEs, the temperature

Table 2. Comparison of ion transport mechanisms: ion exchange, vehicle mechanism, and grotthuss mechanism focusing on primary carrier species, spatial requirements, and key dependencies.

	Ion exchange	Vehicle mechanism	Grotthuss mechanism
Primary carrier	Fixed functional groups with mobile counterions	Polymer segment-coordinated mobile protonic/ionic species	Protons hopping via H-bond networks
Spatial requirement	Ion-exchange sites (static functional groups fixed in polymer matrix)	Polymer segment-coordinated solvation environments (dynamic, polymer-dependent)	Continuous H-bond pathways (flexible, H-bond donor/acceptor density-dependent)
Key dependency	Hydration-induced swelling (to activate fixed functional groups)	Polymer segmental mobility/free volume (to enable solvation shell rearrangement)	H-bond availability and stability (to maintain hopping pathways)

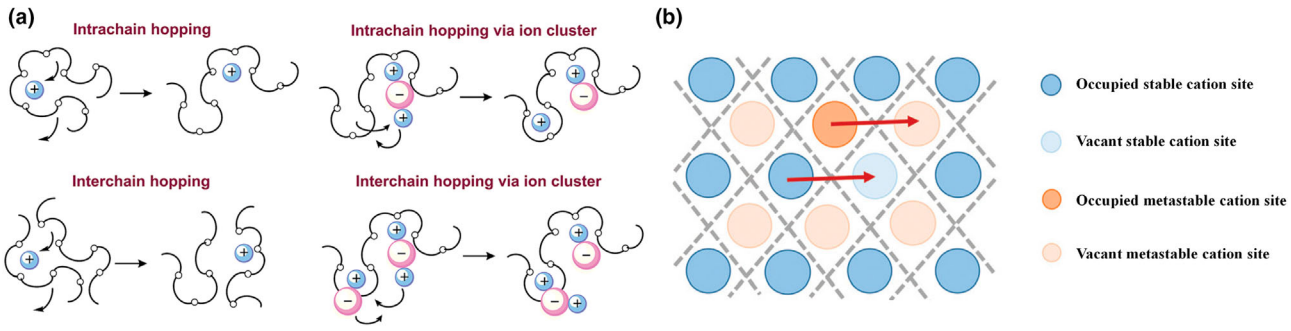

Figure 7. a), Mechanism of the ion transport in solid polymer electrolytes. Reproduced with permission.[60] Copyright 2015, Royal Society of Chemistry. b) Mechanism of the ion transport in solid inorganics. Reproduced with permission.[58] Copyright 2021, RSC publishing.

dependence of ionic conductivity of glasses and some crystalline ion conductors, for example, $Li_{0.5}La_{0.5}TiO_3$, fit the above empirical equations.[63]

Polymer chain dynamics, including segmental motion and free volume distribution, play a crucial role in the efficiency of the vehicle mechanism for ion migration in polymer electrolytes. Segmental motion refers to the local movement of polymer chain segments, which is essential for facilitating ion transport as ions often migrate by coordinating with these moving segments. In poly(ethylene oxide) (PEO)-based electrolytes, the segmental dynamics are significantly influenced by the presence of additives such as SiO2 nanoparticles or ionic liquids, which can enhance the polymer's flexibility and thus improve ionic conductivity.[64,65] The free volume within the polymer matrix, which refers to the unoccupied space that allows for molecular movement, is another critical factor. An increase in free volume generally correlates with enhanced ionic conductivity, as it provides more pathways for ion migration.[66] Studies using positron annihilation spectroscopy have shown that modifications in free volume characteristics, induced by nanoparticle loading, can alter the semi-crystalline morphology of PEO, thereby affecting ion transport.[33] Furthermore, the decoupling of ion transport from segmental motion, particularly in rigid polymer backbones, can lead to high ionic conductivity even when segmental dynamics are restricted.[67,68] This decoupling is crucial for designing high-performance solid polymer electrolytes, as it allows for efficient ion transport without relying solely on segmental motion.[68] Thus, the interplay between segmental dynamics and free volume is considered fundamental to understanding and optimizing the vehicle mechanism in polymer electrolytes, as it directly influences the pathways and efficiency of ion migration.[69]

2.2.2. *Ionic Conduction in Solid Inorganic Electrolytes (SIE)*

In the ideal crystalline material, mobile ions must overcome a high energy barrier E_a, usually delivering a very low ion diffusivity and conductivity. In usable SIEs, the mobile ions could hop through the lattice defect (e.g., vacancies and interstitials) or so-called "charged defects" where co- or counter-ions are missing from their local sites.[58,70]

With the absence of an electrical field E, the probability (per unit time) for a mobile ion to hop from one site to an adjacent site can be expressed as:

$$P = v_0 \exp\left(-\frac{E_a}{k_B T}\right) \tag{8}$$

where v_0 is the attempt frequency and E_a is the energy barrier or activation energy. The energy barrier is changed by the applied electrical field. If the possibility of the ion to hop in the same direction with the electrical field, the activation energy, E_a', increases to $E_a + \frac{1}{2}qE\alpha$ where α is the lattice constant. Similarly, the activation energy, E_a'', is $E_a - \frac{1}{2}qE\alpha$ when the ion migrates in the opposite direction of the electrical field. Accordingly, the overall probability of the ion migration in terms of hyperbolic function, $\sinh(x) = \frac{e^x - e^{-x}}{2}$, could be denoted as:

$$P' = v_0 \exp\left(-\frac{E_a}{k_B T}\right) \times 2\sinh\left(\frac{qE\alpha}{2k_B T}\right) \tag{9}$$

Typically, the potential of applied electrical field is generally low, resulting in $qE\alpha \ll 2k_B T$, so the probability can be transformed to the following equation:

$$P' = \frac{qE\alpha v_0}{k_B T} \exp\left(-\frac{E_a}{k_B T}\right) \tag{10}$$

Combining the relationship between the velocity (v_i) and probability, $v_i = P \times \alpha$ with the relationship of the ionic conductivity, mobility, and velocity, the ionic conductivity can be expressed as:

$$\sigma = n_i q \mu_i = n_i q \frac{v_i}{E} = n_i \frac{q^2 \alpha^2 v_0}{k_B T} \exp\left(-\frac{E_a}{k_B T}\right) \tag{11}$$

where n_i is the numbers of ions, q is the charge of an ion, and μ_i is the mobility of ions. The term $n_i \frac{q^2 \alpha^2 v_0}{k_B T}$ is normally considered as the pre-exponential factor, σ_0, and the above equation could be simplified in the form:

$$\sigma = \sigma_0 \exp\left(-\frac{E_a}{k_B T}\right) \text{ or } \ln\sigma = \ln\sigma_0 - \frac{E_a}{k_B T} \tag{12}$$

The Nernst–Einstein relation can be further employed to correlate ionic conductivity with the diffusivity (D_i) of ions as $\sigma = \frac{n_i q^2 D_i}{k_B T}$.

According to the above equation, the ionic conductivity of a solid could be enhanced by increasing the concentration of charge carriers (Li-ions in solid-state LIBs), increasing defect/interstitial concentrations, and lowering the energy barrier for ion-hopping and migration.[70] The Arrhenius equation can fit the pure ionic conductor and most liquid electrolytes very well and even works for the composite electrolytes and quasi-solid electrolytes.

2.2.3. *Ionic Conduction in Composite Electrolyte Separator*

The composite electrolyte separators generally contain ion-conductive liquid (e.g., organic electrolyte, RTIL) and functional or non-functional matrices. For the composite electrolyte separator with a non-functional matrix (**Figure 8**a), the effective ionic conductivity depends on the conductivity of the confined liquid, that is, $\sigma_e = \frac{\varepsilon}{\tau}\sigma_d$ where ε and τ are physical attributes of the matrix, porosity, and tortuosity, respectively. The maximum conductivity of this composite is accordingly the value of the bulk of liquid electrolyte, σ_d. Introducing straight pore channels and increasing porosity could maximize the apparent conductivity, which has been adopted as an efficient strategy to develop solid-like electrolyte for LIBs.

The ion transport mechanism is rather complicated in the solid-like composite electrolytes that consist of a polar matrix or a matrix with functional groups. Currently, the Arrhenius model and empirical Vogel–Fulcher–Tammann models are two acceptable theories to interpret the mechanism.[71] However, ion separators follow different pathways in this electrolyte, for example, ion conduction in the matrix, within the confined liquid, or along the interface. The well-known effective medium theory and percolation theory were employed to estimate the overall conductivity of solid–solid composites by considering the volumetric fractions and geometric features.[72] The interaction at the interfaces was not fully understood.

The space charge model, where "space charge" refers to the localized accumulation of charge carriers within a material or at its interface, forming a nonuniform charge density distribution that significantly influences electrochemical, electronic, or optical properties, was adopted to describe the interface interaction.[62,70,73] The fundamental concept is the charge carriers could be attracted or repulsed by the interfacial cores (Figure 8b). For a solid–solid composite electrolyte, the interface between oriented grains of two phases can produce the narrow-charged zone due to the surface defects. This could be expressed as $M \leftrightarrow S_M^{\cdot} + M_V^{\prime}$ when A attracts M and $M \leftrightarrow M_M + M_i^{\cdot}$ when A repulses M. Here, $S_M^{\cdot}$ and $M_i^{\cdot}$ refer to the charged defects and M_M and $M_V^{\prime}$ are metal ion vacancies. This model could properly fit the LiI-Al_2O_3 solid composite electrolyte.[74] The enhanced ionic conductivity, $\Delta\sigma$, is affected by the geometric size (r, radius) of inert particles Al_2O_3, and the volume fracture (f), that is, $\Delta\sigma = \frac{1}{r}\frac{f}{1-f}$. This model can quantitatively explain (not predict) the roles of interface in promoting ionic conductivity of organic–inorganic composite electrolytes. The modified space charge model is necessary to describe the function of interfaces within a solid–liquid system and a particle-concentrated system.

2.2.4. *Ionic Conductivity in RBFs*

Ionic conductivity is a fundamental property related to the ion transport and dynamics within the membrane, which is driven by coupled forces derived from diffusion driven by concentration gradient, migration under a certain electric field, and the convection of fluids. For aqueous electrolytes, strategies of creating ion channels in membranes can effectively promote the migration of charge carriers and increase the overall ionic conductivity of membranes. Functionalizing the membranes with hydrophilic ionic groups could favorably facilitate the ion transport, such as negative groups sulfonate ($-SO_3^-$), carboxylate($-COO^-$), phosphate ($-PO_3^{2-}$), hydrogen phosphate ($-PO_3H^-$), phenolate ($-C_6H_4O^-$) and positive groups ammonium ($-NH_3^+$, $-NR_2H^+$, $-NR_3^+$) and sulfonium ($-SR_2^+$).[19] However, conventional ion-exchange membranes with significantly improved ionic conductivity might result in swollen membranes along with an increased crossover of active species (**Figure 9**b). Crossover of redox species in membranes must be considered during the optimization of ionic conductivity.

Controllable microstructure plays critical roles in promoting the ionic conductivity and mitigating redox-active permeability. The commercial perfluorinated sulfonic acid (PSFA) has hydrophilic sulfonate acid domains interconnected by narrow water channels with a diameter of around 1.0 nm. When the membrane is exposed to water, phase separation occurs due to the assembly of hydrophilic side chains and hydrophobic backbones, leading to the formation of hydrophilic domains with water clustering. The hydrophilic domains spontaneously formed in PSMs could provide more nanoscale space for ion transport while selectively transferring ions or redox species through interconnected bottlenecks (Figure 9b). This narrow ion channel could prevent

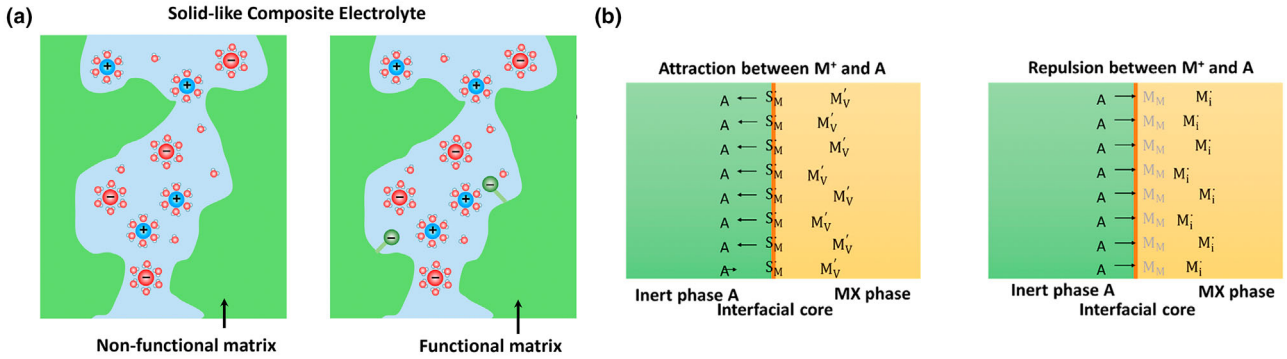

Figure 8. a) Schematic illustration of the composite electrolytes with a non-/functional matrix. b) Space charge theory. Reproduced with permission.[62] Copyright 2020, American Chemical Society.

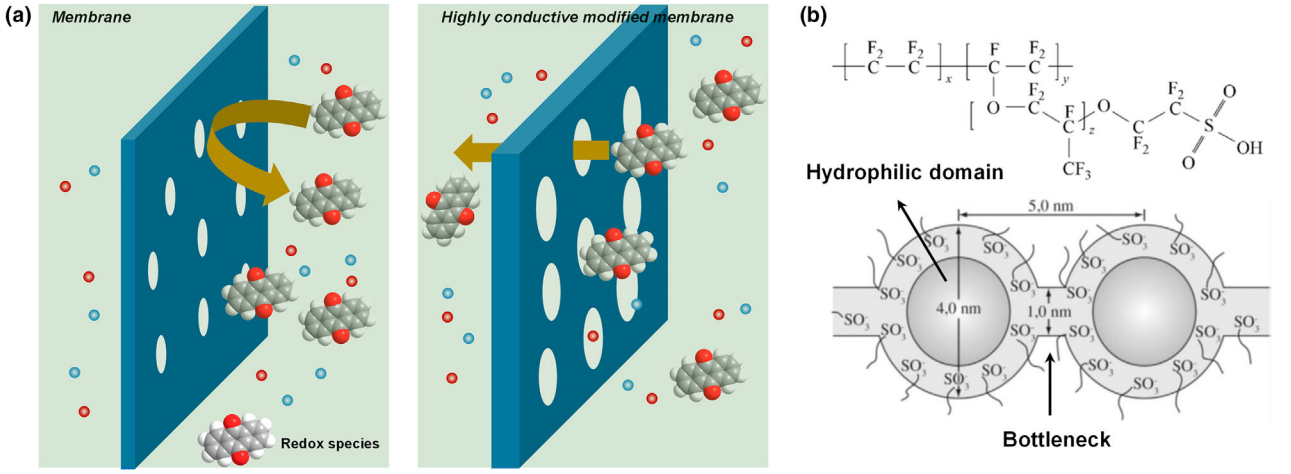

Figure 9. Diagram of redox-species crossover and typical structure of Nafion membranes. a) Schematics showing the permeation of redox species through nonswollen and swollen RFB separators. The pores just stand for the hydrophilic channels within the membranes. b) Diagram of proposed structure for a phase-separated membrane. Reproduced with permission.[15] Copyright 2018, Elsevier B.V.

the crossover of large redox species. Nafion is the most developed and commercially available PSFA membrane.[15] Recent experimental and computational results suggested the diameter of water channels in Nafion membranes is around 2.4 nm.[75]

Over the past 30 years, extensive efforts have been made to synthesize hydrocarbon ion-exchange membranes by controllably tuning the phase-separated microstructure in polymeric materials. One way to induce membrane phase separation is by partially functionalizing materials with hydrophilic groups or side chains, such as sulfonated poly(p-phenylene),[76] sulfonated poly-ether-ether-ketone (S-PEEK),[77] 2-methoxyethoxy (sidechain) grafted polybenzimidazole,[78] quaternized poly (arylene ether),[79] and so on. However, the strategy of solely introducing hydrophilic functional groups demonstrates the difficult control of membrane hydrophilicity. Hydrophobic groups are therefore integrated with hydrophilic groups to induce membrane phase separation and control membrane swelling. For example, polysulfone modified with hydrophilic trimethylammonium and hydrophobic hexylamine groups can result in a phase-separated morphology and provide high ionic conductivity with a limited water uptake.[80]

Apart from the phase-separated microstructure, the pore architecture and pore size distribution are very important factors that impact ionic conductivity. Pores can be created through several ways, such as the phase-inversed membrane preparation,[81] incorporating templating agents (e.g., cyclodextrin), and exploiting nonsolvent polymers (e.g., poly(ethylene glycol)).[82] However, these methods generally create pores with a relatively large size, which might lead to significant crossover of redox species.

2.2.5. *Ionic Conductivity in LIBs*

The lithium-ion transference number, t_{Li}, is a key parameter to differentiate the non-ion-selective and ion-selective separators. It associates with the electrolyte overpotentials and battery power densities. t_{Li} refers to the fraction of the overall ionic conductivity originating from Li-ions, $t_{Li} \propto \sigma_{Li}/\sigma_d$. In the commercial lithium-ion electrolytes, t_{Li} is in the range of 0.2–0.4. This means anions with a transference number of 0.6–0.8 dominate the ion transport process,[83] which can result into a distinct concentration gradient of ions and increase the internal resistance in batteries.

The ionic conductivity of electrolyte-filled separator is related to the wettability and porosity of the separator, and the conductivity of absorbed electrolyte, σ_d. The low separator porosity will lead to a high internal resistance due to the insufficient absorbed electrolyte. In contrast, the high separator porosity could contribute to a low internal resistance, but along with the sacrifice of the mechanical strength. The porosity ε (or fractural free volume) of a separator could be measured by the weight of absorbed liquid and calculated according to Equation 13.[84]

$$\varepsilon = \left(\frac{W_{dry} - W_{wet}}{\rho_L \times V}\right) \times 100\% \quad (13)$$

where the W_{after} and W_{before} refer to the weights of the separator after and before absorbing liquid, ρ_L is the density of liquid, V is the geometric volume of the wet membrane separator. The maximum ionic conductivity of a nonionic conductive separator (e.g., PP, PE, PVDF, PAN, cellulose separators) is the conductivity of the salt-based electrolyte. Accordingly, the effective conductivity, σ_e, can be defined by the following Equation 14.

$$\sigma_e = \frac{\varepsilon}{\tau}\sigma_d \quad (14)$$

where ε and τ are the porosity and tortuosity, respectively. For a given organic electrolyte, the ionic conductivity is infinite, and related to the concentration, c, of the salts and the diffusion coefficients of lithium ions and anions: $\sigma_d \propto c \times (D_{Li} + D_{anion})$.[85] To improve the ion transport, one practical strategy is to increase the concentration of lithium salts. For example, the conductivity of $LiPF_6$-containing electrolytes will quasi-linearly increase with the increase of concentration from 0 to 1.0 M. However, after leveling off, the ionic conductivity decreases strongly in the concentrated electrolyte (>1.0 M). In addition, increasing the porosity or reducing the tortuosity of membrane separators could contribute to an improved effective ionic conductivity.

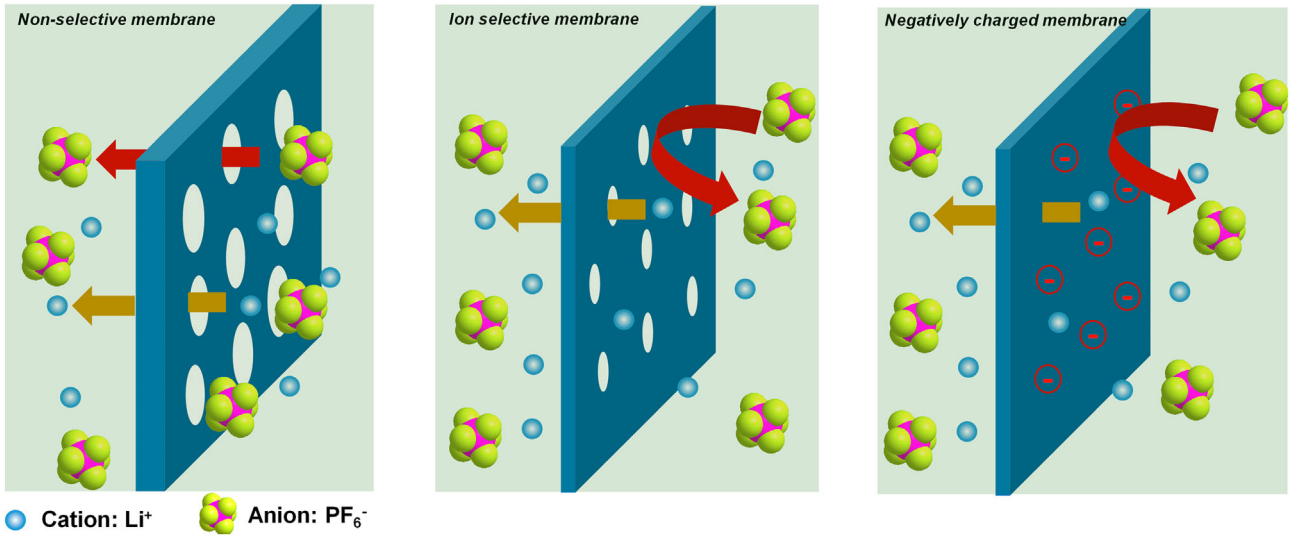

Figure 10. Schematic illustration of ion transport through a non-selective porous membrane, an ion-selective membrane, and a negatively charged membrane.

Wettability is another important property, which can be defined by the ratio of the resistance of the electrolyte-filled membrane to the resistance of the electrolyte, that is, MacMullin number (Equation 15).

$$\text{Wettability} = \frac{R_{overall}}{R_{el}} \tag{15}$$

The wettability, effective ionic conductivity, and membrane tortuosity could be defined in specific directions, providing an approach to distinguish the ion transport through-plane or in-plane. For example, Celgard separators possess very different properties in the machine direction (MD) and transverse direction (TD).[86]

To improve the lithium-ion systems, membrane separators play a very important role. As shown in **Figure 10**, both cations and anions can pass through the non-selective porous membranes (e.g., Celgard PP/PE separator). Such membranes cannot regulate ion transport and immobilize the large anions. Membranes with narrow ion channels or negatively charged functional groups can effectively block anions by the size-exclusion and Donnan-exclusion mechanisms so as to improve the Li ion transference number. The incorporation of the selective property in LIB separators is receiving more interest (**Figure 11**).

2.2.6. *Ionic Conductivity in SSEs*

Ionic conductivity is one of the important metrics to evaluate the operational capability of solid electrolytes. In contrast to liquid electrolytes, SSE (solid-state electrolyte) intrinsically possesses a higher energy barrier and low ionic conductivity (**Figure 12**). In solid inorganics or solid polymers, there is little space for ions to transport. The ion diffusion will strongly depend on the defects in the solid inorganics and the mobility of polymer chains in solid polymers. In solid inorganics, point defects, such as Frenkel and Schottky defects (Figure 12a), have significant influences on ion conduction. Integrating substitutional/interstitial atoms within the crystalline structure is a practical way to increase ionic conductivity.[87] In solid polymers, the ions can coordinate with the polar structure and transport along with the motion of polymer chains (Figure 12b).[88] Compared with crystalline polymers, amorphous polymers deliver relatively higher ionic conductivity.

The ionic conductivity in SSEs can be generally expressed by

$$\sigma_i = n_i e \mu_i \tag{16}$$

where e is the ion charge, n_i and μ_i are the concentration and mobility of ions. In solid crystals, n_i is closely associated with the defect concentration. The ion conduction under an electric field is the motion of vacancies. In solid polymers, the interaction between polymer chains and ions, such as interaction of ether units and Li-ions, determines the effective number of transport ions, n_i. For a practical and usable SSE, electronic conductivity is undesirable. The transference number of electrons can be defined as the following equation:

$$t_e = \frac{\sigma_e}{\sigma_e + \sigma_i} \approx 0 \tag{17}$$

In solid electrolytes, the grain boundaries can undesirably increase the resistance and decrease the overall ionic conductivity. As presented in **Figure 13**, there remain two depressed semicircles that can be attributed to the bulk of the electrolyte and the grain boundaries among the particles. The value of grain-boundary resistance R_{gb} is $R_t - R_b$. The intergrain impedance along with a high activation energy E_{gb} is generally 2–3 times higher than the impedance of grains in the well-sintered solid particles. This phenomenon is not only observed in solid inorganic electrolytes but also exists in the solid composite electrolyte and semi-solid electrolyte. Fabricating a grain-boundary free electrolyte is generally an approach to maximizing the ionic conductivity.

EIS is frequently used to measure the ionic conductivity of SSEs. Typically, SSEs are tested at varied temperatures with a small bias amplitude of 10 mV in 10^6–10 Hz. The resistance of bulk electrolyte can be obtained from the EIS profile (Figure 13a). However, grain boundaries

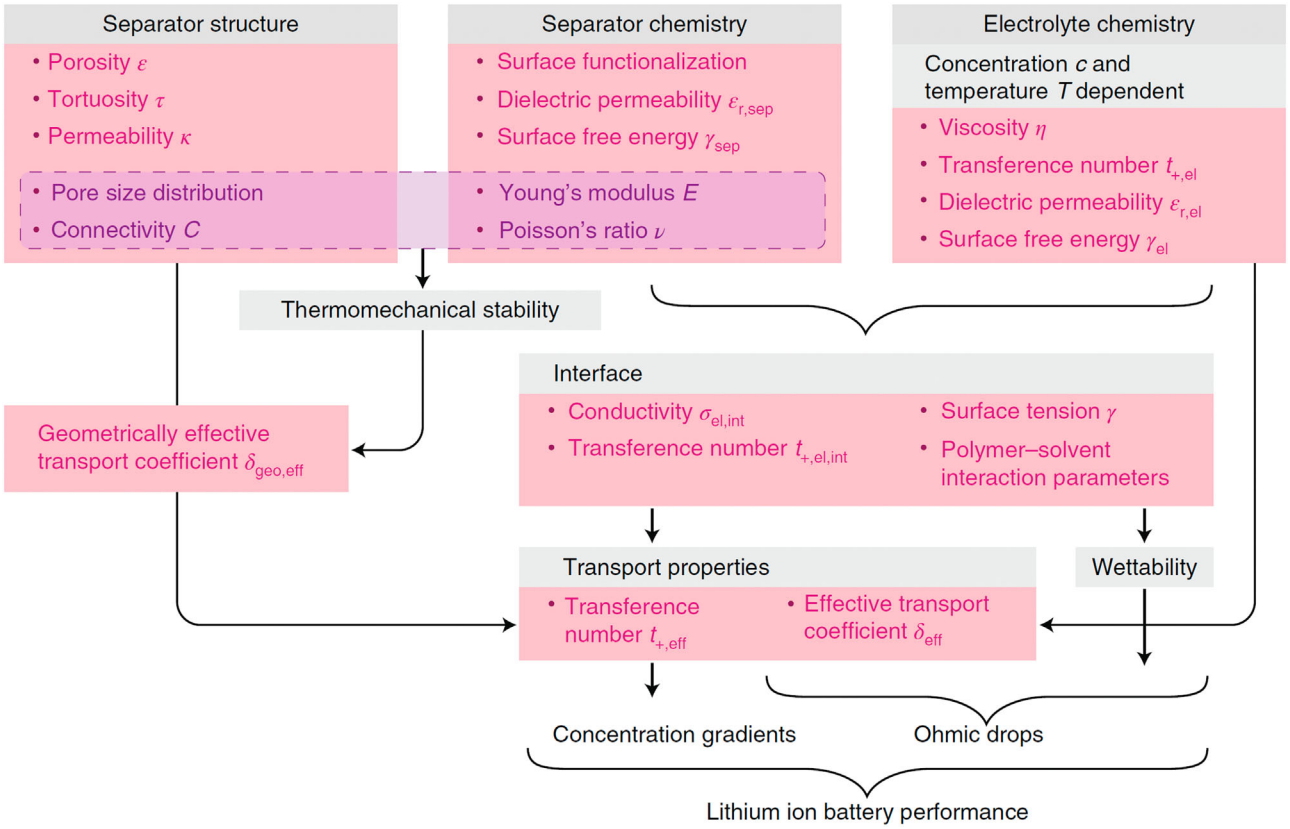

Figure 11. Relationship between properties and battery performance. Reproduced with permission.[85] Copyright 2018, Springer Nature Limited.

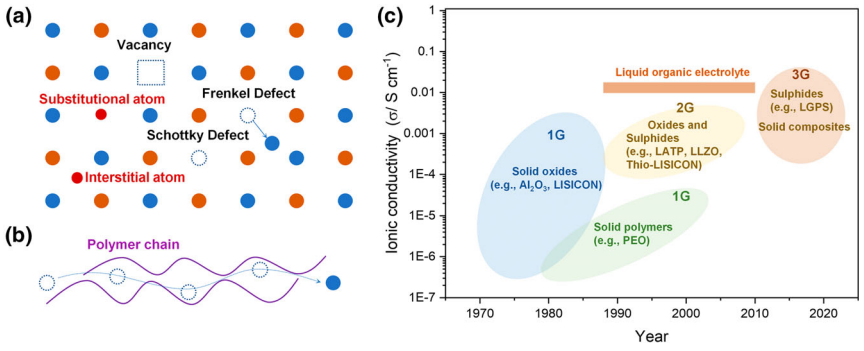

Figure 12. Schematics illustrating the types of defects, ion transport in polymers, and three generations of SSEs. a) Schematic illustration of types of defects in solid inorganics. b) Schematic diagram showing the ion transport in a solid polymer. c) A general summary of the development of SSEs and their ionic conductivity.

cannot be easily alleviated in a pelletized SSE, which undesirably increases the overall resistance and lowers the apparent ionic conductivity.[91] This issue needs to be solved when SSEs are used in practical devices.

Currently, the ionic conductivity of liquid organic electrolyte is above 10 mS cm^{-1}, surpassing that of most SSEs (Figure 13c). The first-generation (1st G) solid oxides and solid polymers only possess low ionic conductivity in the range of 10^{-5}–10^{-2} mS cm^{-1}. The ionic conductivity of second-generation solid oxides is about two orders of magnitude higher than that of first-generation solid oxides, mainly due to the effective strategy of creating defects within solid inorganic electrolytes.

2.3. Pathways to Achieve Selectivity

2.3.1. Fundamental Selectivity Mechanisms

Selective ion transport in battery separators is governed by two core mechanisms: the Donnan-exclusion effect and size-sieving. These principles dictate how membranes regulate ion migration to suppress redox-species crossover and dendritic growth:

Donnan Exclusion: Fixed charges controlling ion migration (e.g., sulfonic acid groups repelling multivalent ions);

Size-Sieving: Pore dimensions matching target ion/molecule sizes block larger species via steric hindrance (**Figure 14**).

Selectivity denotes the ratio of the permeation of species i, to the permeation of specie *s*. In a battery system, the permeation of species i (including redox actives) driven by electric force, concentration gradients and pressure gradients, could be characterized by the Equation 18.[92]

The first phase $\frac{t_i}{Z_i F} i$ is due to the migration under a certain electric field where F is the Faraday constant, *I* is the applied current density, t_i and Z_i are the transference number and charge number. The second

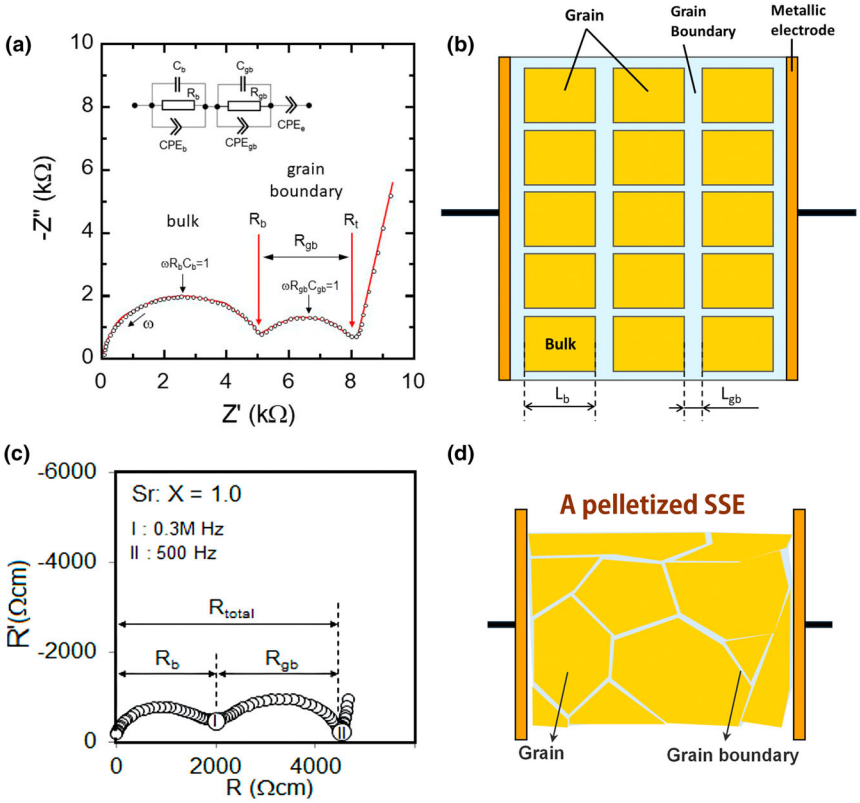

Figure 13. a and b) Nyquist plots of a grain-boundary involved solid state electrolyte. Reproduced with permission.[89] Copyright 2020, MDPI. c) Electrochemical impedance spectroscopy of a typical pelletized solid electrolyte and d) the relevant diagram of a pelletized SSE. Reproduced with permission.[90] Copyright 2016, Ohta, Kihira, and Asaoka.

$$N_i = \frac{t_i}{z_i F} I + L_i^{\tau} \frac{\partial \tau}{\partial x} - L_i^{p} \frac{\partial p}{\partial x} - D_{ii} \frac{\partial c_{s/i}}{\partial x} - \sum_{s/j \neq 0, s/i} D_{ij} \frac{\partial c_{s/j}}{\partial x} \quad (17)$$

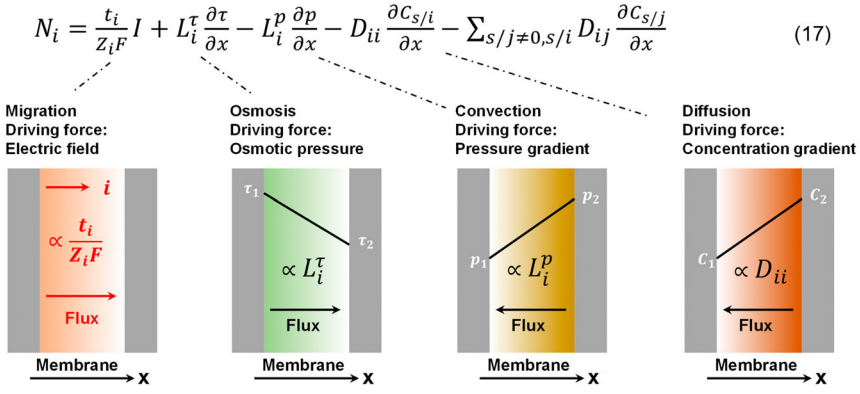

Figure 14. Different driving forces related to the permeation of redox species.

phase is the flux caused by the osmotic pressure, which is proportional to the osmotic transport coefficient, L_i^{τ} and the concentration of species i. In diluted battery systems, the influence of osmotic pressure is negligible. The third term is the flux from the hydraulic pressure, often occurring when the volume of electrolytes changes a lot during the operation. The fourth phase is due to the diffusion of species i, driven by the concentration gradients of different supporting salts s/i. D_{ii} is the diffusion coefficient of species i. The fifth phase means the flux of specie could be negatively influenced by the diffusion of other constituent salts s/j or redox species. According to this equation, the engineering approaches to reducing the crossover of species i is i) balancing the osmotic pressure using supporting ions, ii) applying external hydraulic pressure, and iii) introducing other species to diffuse against redox actives. However, these methods may introduce other complexities in the battery system.

2.3.2. *Separator Selectivity Design Strategies*

Regarding the design of a required selective separator, fundamentals need to be introduced. Similar to the derivation of the Arrhenius equation for the ionic conductivity, the solute permeability can also be described by the Arrhenius-type equation:[93]

$$P = A' \exp\left(-\frac{E_a}{RT}\right) \quad (18)$$

where A' is the pre-exponential factor and E_a is the energy barrier for the solute transport. Transition-state theory can illustrate the behavior of the species diffusion through subnanometer pores.[94,95] The energy barrier, E_a, refers to the actual energy for the activation and diffusion of a specific solute through a membrane (**Figure 15**). As we discussed, the operating conditions (e.g., hydraulic pressure, solution compositions) and the interaction between the solutes can affect the diffusion and change the activation energy. The energy barrier of the solute diffusion can also be influenced by the membrane chemistries and properties, including the size of pores and pore aperture, electrostatic state, dielectric state, the influence of van der Waals (vdW) forces, viscous effects, and frictional effects.

The steric hindrance and electrostatic repulsion/attraction are based on the theories of size-exclusion and Donnan effects (i–ii, in Figure 15), which dominate the working principles of selective membranes. Besides, dielectric effects (iii, in Figure 15) may lead to partial desolvation (the process by which a solute is liberated from its solvation shell in a solution or composite material) of a solute and lower the transport energy barrier. Ions with smaller size typically hold the solvation shells tightly with a high solvation energy. Narrowing the pore size and introducing the oppositely charged sites are efficient approaches to reducing the desolvation-based energy barriers. Additionally, the polarizable membrane materials can interact with non-charged solutes via the weak vdW forces (iv, in Figure 15) and reduce the diffusion barrier. When the permeated

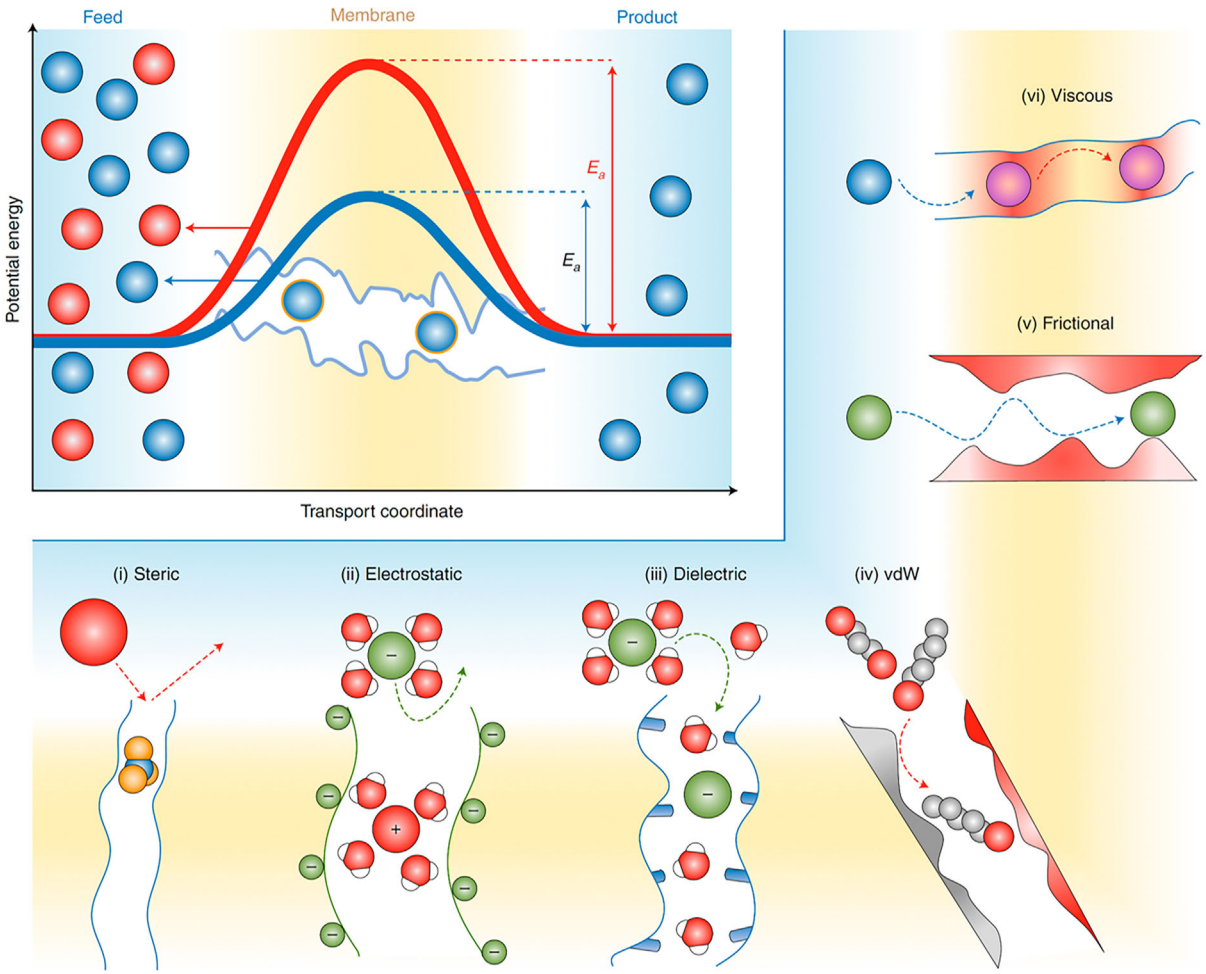

Figure 15. Mechanisms of different effects on the increase of the energy barrier for the species permeation. Reproduced with permission.[93] Copyright 2020, Springer Nature Limited.

solutes are confined in the membranes, the transport is hindered due to frictional effects (v, in Figure 15) originating from the roughness of pore walls and adhesive effects due to the chemical affinity (vi, in Figure 15).

Apart from the optimization of operating conditions to improve the selectivity (or lower the permeation of a target species), the effective methods for the design of selective separators include i) narrowing down the pore size of the membranes; ii) introducing the binding sites or oppositely charged functional groups to facilitate ion transport; iii) reducing the distance between adjacent binding sites, which could increase the repulsive forces between these two binding sites and reduce the attractive force toward the target species.

Selectivity in Battery Systems

LIB separator: The selectivity of a LIB separator can be indicated by the value of the Li ion transference number. Theoretically, the Li ion transference number was defined as the ratio of Li-ionic conductivity to the overall ionic conductivity, which can also be considered as the ratio of the permeation of Li-ions to the permeation of anions. Improving the transference number of Li-ions is very meaningful for the homogenous transport of Li-ions and limiting the growth of Li-ion dendrites. PEO was selected as a typical example to demonstrate the relationship between dendrite growth and the Li-ion transference number (**Figure 16**). In this phase-map, the single-ion conductor with a Li ion transference number of about 1 exhibited the stable deposition of Li ions.

Additionally, size-exclusion and Donnan-exclusion are introduced to improve Li ion transference number, such as producing narrow pores in membranes, introducing the negatively charged functional groups, and grafting the anions in the structure of membranes.

Selectivity in RFB separator: Stability and size of redox species play an important role in the cycling stability and lifetime of RFBs. Active materials should be chemically and electrochemically stable over the whole electrochemical process, particularly in the deep charged/discharged states (0 and 100% SOC). The size of redox species relates to their crossover through a membrane separator.[99] As presented in **Figure 17**, active materials with a smaller size could easily permeate through the membrane separator, leading to capacity decay in an operating battery. Employing redox actives with a relatively large size could limit the crossover and extend the lifetime of RFBs.

Selectivity is a very important property that directly determines the current efficiency and longevity of RFBs. As discussed, the optimization of ionic conductivity is accompanied by the increased permeability of

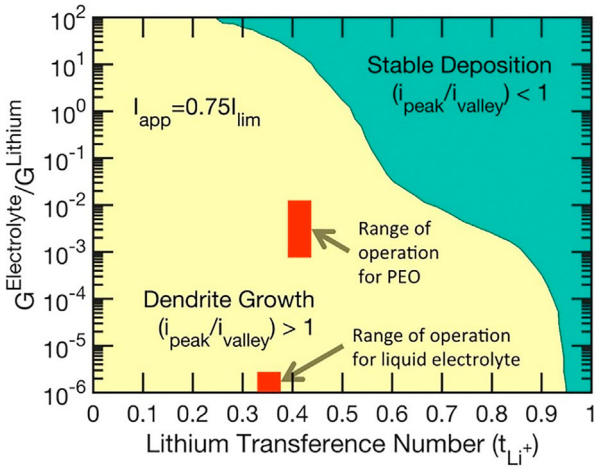

Figure 16. Phase-map showing the relationship between dendrite growth and Li^+ transference number. Copyright 2017, The Electrochemical Society, Inc.[96–98]

redox species. A high-performance separator needs high ionic conductivity together with high selectivity of charge carriers over redox species.

Changing the diffusivity of redox species in the membrane is feasible to limit the crossover of redox species. On the one hand, the diffusivity of redox species can be reduced by making the redox couples bulkier, corresponding to the developing direction of redox chemistries (Figure 17a). On the other hand, narrowing down the pore size and incorporating charged functional groups within membranes can block or repel redox species, which is the emerging concept of designing highly selective membranes (i.e., with ion transference numbers (t^+) >0.85 and permeability thresholds $<10^{-6}$ cm^2 s^{-1}).

Size-exclusion is a major theory for the explanation of membrane selectivity. The size-exclusion function can be achieved by decreasing membrane pore sizes or producing micropores (or mesopores depending on the applications).[101] For instance, a thin layer of polyamide with a pore size of below 0.6 nm was crosslinked on the surface of poly (ether sulfone)/sulfonated poly (ether ether ketone) membrane. This composite membrane exhibited a high selectivity of proton (H) over vanadium ion (V).[102] A similar approach was exploited in lithium-sulfur flow batteries in which the membrane consisted of a polycarbazole thin layer and a carbon nanotubes/polypropylene porous support.[103] The top layer with a pore size of 0.82 nm could effectively hinder the crossover of redox sulfides and thus maintain a reversible capacity. Polybenzimidazole (PBI) is another commonly used material in selective RFB membranes, as demonstrated by acid-doped PBI,[104] PBI/CMPSF membranes,[81,105] "fishnet-like" crosslinked PBI/PEI membranes,[106] and crosslinked PBI/SPEEK membranes.[107] These composite membranes with a decreased pore size can effectively minimize species crossover. "Acid–base pair" effect could be introduced to narrow down the size of water channels. Interactions of "Acid–base pairs" can be tuned by the content of acid and base materials. For example, tuning the ratios of quaternized PPO and sulfonated PEEK could control the "acid–base pair" effect and lead to a controllable and selective ionic channel.[108]

Donnan-exclusion is another mechanism for the selectivity of membranes. Donnan-exclusion is the function of a charged membrane to electrically repel species with the same charge while facilitating the transport of counterions (Figure 17b). For example, membranes with quaternized amine groups carry a positive charge and repel the transport of positive V^{3+}/V^{2+} ions, thereby increasing the selectivity of vanadium ions over protons. Sulfonated membranes (e.g., PVDF-g-PSSA,[109] SPEEK, PES) with negative charge could provide the repulsion toward negative redox chemistries, such as $Fe(CN)_6^{4-}$, $DHAQ^{2-}$, and FMN, and deliver good selectivity and cycling stability in RFBs (**Table 3**).

2.4. Failure Mechanisms in Separation

2.4.1. Root Causes of Low Transference Numbers

Low transference numbers, particularly regarding lithium ions, present a formidable obstacle in battery systems, resulting in complications such as nonuniform ion transport and dendrite formation. Two fundamental causes contribute to this predicament:

Inadequate anion immobilization and redox-species cross-contamination: Dominance of anion transport: In commercially available lithium-ion electrolytes, the transference number for lithium ions is generally low, typically ranging from 0.2 to 0.4. This phenomenon suggests that

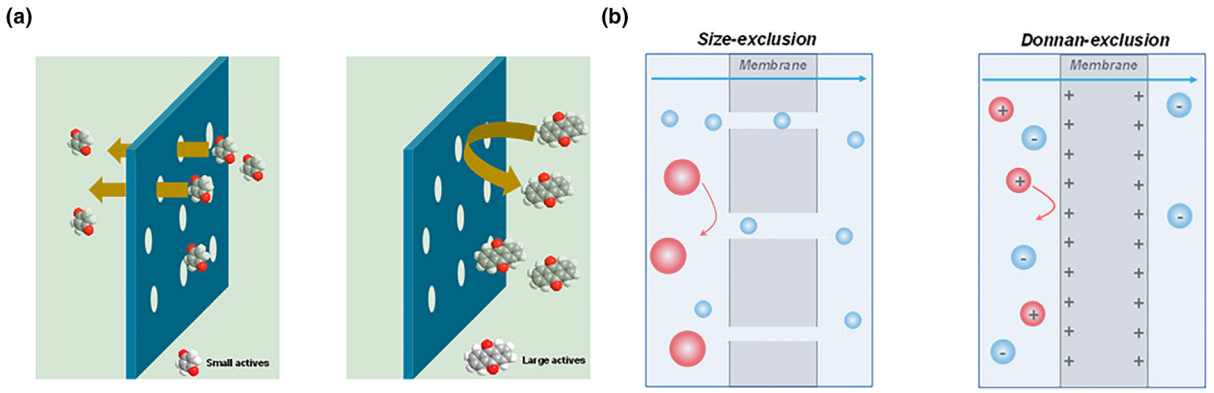

Figure 17. a) Diagram showing the crossover of small and large redox actives. (Benzenequinone and Anthraquinone are used as examples standing for small and large actives, respectively, in this figure) b) Schematics showing the working principles of size-exclusion and Donnan-exclusion.[100]

Table 3. Typical examples for the membrane with the size-exclusion function, Donnan-exclusion function, and the combination of both exclusion functions.

	Membrane	Structure	Principles	RFB system	Efficiency	Ref
Size-exclusion	Polyamide	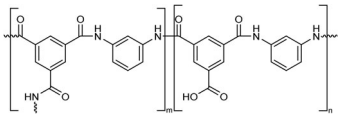	Micropores from interfacial polymerization	VRFBs C: VO^{2+}/VO_2^+ A: V^{2+}/V^{3+}	CE: 99.2% VE:92.8% EE: 92.1% 80 mA cm^{-2}	[102]
	Crosslinked polysulfone	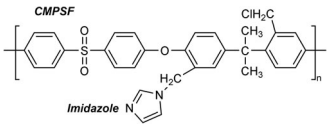	Narrow channels from chemically crosslinked network	VRFBs C: VO^{2+}/VO_2^+ A: V^{2+}/V^{3+}	CE:99.2% EE: 80.8% 120 mA cm^{-2}	[81]
	Acid–base composites	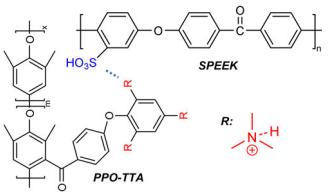	Narrow channels from hydrogen-bond network	VRFBs C: VO^{2+}/VO_2^+ A: V^{2+}/V^{3+}	CE:98.3% EE: 77.1% 200 mA cm^{-2}	[108]
	Crosslinked composite	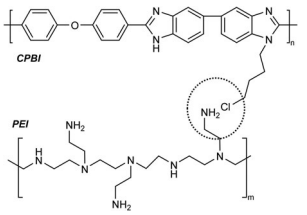	Narrow channels from chemically crosslinking network	VRFBs C: VO^{2+}/VO_2^+ A: V^{2+}/V^{3+}	CE:99.0% VE: 86.6% EE: 85.5% 120 mA cm^{-2}	[106]
Donnan-exclusion	Positive functional group (e.g., amine)	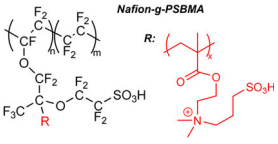	Graft positive charged constituent	VRFBs C: VO^{2+}/VO_2^+ A: V^{2+}/V^{3+}	CE:96.2% VE: 94.0% EE: 89.6% 40 mA cm^{-2}	[110]
	Negative functional group (e.g., -SO_3H)	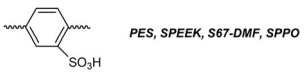	Graft negative charged part (sulfonated modification)	ORFBs C: $Fe(CN)_6^{3-}/Fe(CN)_6^{4-}$ A: $DHAQ^{2-}/DHAQ^{4-}$	CE:100% VE: 79.4% EE: 79.4% 100 mA cm^{-2}	[111,112]
Combination of Donnan and size exclusions	Acid-doped materials	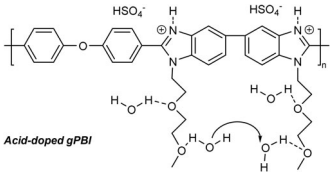	Nanophase separation +charge repulsion	VRFBs C: VO^{2+}/VO_2^+ A: V^{2+}/V^{3+}	CE:~100% EE: 93.6% 40 mA cm^{-2}	[78]
	Sulfonated PIMs	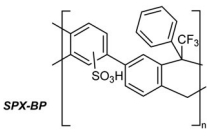	Micropores + charge repulsion	ORFBs C: $Fe(CN)_6^{3-}/Fe(CN)_6^{4-}$ A: $DHAQ^{2-}/DHAQ^{4-}$	CE: >99.0% EE:87.9% 60 mA cm^{-2}	[113]

anions, exhibiting a transference number between 0.6 and 0.8,[83] predominantly govern the ion transport mechanism. Such an imbalance may induce pronounced concentration gradients of ions and heightened internal resistance within battery systems.

Lack of selective properties: Conventional non-selective porous membranes facilitate the passage of both cations and anions. These membranes lack the capability to regulate ion transport or immobilize substantial anions, thereby exacerbating the low ion transference number.

Crossover of redox species: In redox flow batteries, the migration of redox species through membrane separators can culminate in diminished efficiency and loss of capacity. Likewise, in lithium-ion batteries, the transference of redox species, particularly diminutive ions, through the membrane separator may precipitate capacity deterioration. This challenge is intrinsically linked to the selectivity of the membrane, which denotes its capability to obstruct undesired species while permitting the passage of requisite charge carriers.

Electrolyte leakage from defective pore structures: Porous separator limitations: Traditional porous separators, particularly nonwoven variants, encounter difficulties in retaining the organic liquid electrolyte within their structure. This predicament can result in significant electrolyte leakage should the lithium-ion battery experience failure. The highly porous architecture of certain separators can absorb a substantial volume of organic liquid electrolyte, thereby augmenting the electrode-electrolyte contact area and potentially inciting side reactions at the interface between electrolytes and lithium metal anodes.

Inadequate Mechanical Strength and Thermal Stability: Conventional polyolefin separators, frequently employed in LIBs, often exhibit insufficient mechanical strength and suboptimal thermal stability. Such deficiencies may lead to thermal runaway, fires, and explosions in battery systems. The mechanical frailty may also result in separator failure due to penetration by formed lithium dendrites.

Swelling and Reduced Selectivity: Although certain modified membranes, such as ion-exchange membranes, may attain enhanced ionic conductivity, this improvement frequently compromises swelling and diminishes selectivity toward larger species. This swelling has the potential to enlarge ion transport channels, inadvertently forfeiting the desired selectivity. In essence, addressing the issue of low transference numbers necessitates innovations in separator design that prioritize effective anion fixation, preclude electrolyte leakage, and bolster the overall structural integrity and selectivity of the system membrane.

2.4.2. Dendrite Growth and Mechanical Stability

The phenomenon of dendrite growth, notably that of lithium, presents a significant challenge within the field of battery technology, engendering both safety hazards and a decline in performance efficacy. The mechanical stability inherent in battery separators is integral to alleviating this critical issue.

Inhomogeneous Li^+ deposition: SEI film formation dynamics: Dendrite formation: In lithium-metal batteries (LMBs), the employment of organic liquid electrolytes in conjunction with a lithium-metal anode frequently results in the emergence of dendrites on the surface of the metal. The presence of these dendrites may precipitate failure of the separator at the pack level. The uneven migration of lithium ions across the surface of lithium metal anodes can provoke erratic stripping and plating, culminating in the development of lithium dendrites. The utilization of functional microporous separators can facilitate the uniform transport of charge carriers, thereby diminishing the likelihood of localized overcharges occurring on the electrode surface.

Solid electrolyte interphase (SEI) film: The graphite porous electrode, which is prevalently utilized as an anode in commercially available LIBs, engenders a passivation layer referred to as the SEI. This SEI film possesses the capability to safeguard the electrolytes from extraneous reduction processes, thereby preserving a high coulombic efficiency. The structural characteristics of electrode surfaces, encompassing surface roughness and the formed passivating SEI layer, are intricately linked to the exchange current density, which, in turn, influences surface overpotential.

Membrane elastic modulus: critical threshold for dendrite suppression: Mechanical strength requirement: It is imperative that separators exhibit sufficient mechanical strength to endure the penetration of formed lithium dendrites. For example, conventional polyolefin separators frequently lack adequate mechanical strength, rendering them susceptible to failure due to penetration by lithium dendrites. The U.S. Advanced Battery Consortium (USABC) has established a target puncture strength exceeding 300 g for a thickness of 25.4 μm for commercial LIB separators.[114]

Solid electrolytes as physical barriers: Solid electrolytes serve not only as physical barriers to obstruct electrode contact but also facilitate lithium-ion conduction. Solid electrolytes exhibiting mechanical robustness are anticipated to thwart the penetration of lithium dendrites. Polymers of intrinsic microporosity (PIMs), characterized by their interconnected micropores, can modulate ion transport to achieve a uniform stripping and plating process of lithium ions, thereby effectively reducing the probability of dendrite formation.

Elastic modulus and dendrite suppression: While the document emphasizes the significance of mechanical strength, it does not explicitly delineate a "critical threshold" for the elastic modulus of the membrane concerning dendrite suppression. Nevertheless, it suggests that augmented mechanical strength is essential.

Separator swelling: dendrite initiation through topographical transformation and testing limitations: Separator swelling, driven by electrolyte absorption into the polymer's amorphous regions, is a critical factor governing lithium dendrite formation.[115] As the separator swells, surface wrinkles and local pore deformation develop due to mechanical softening; these topographical changes create preferential sites for dendrite initiation. Specifically, the wrinkled regions concentrate ionic flux and induce curvature-driven stress, synergistically promoting lithium nucleation and subsequent dendrite growth.

Notably, conventional methods for evaluating separator mechanical stability, such as puncture strength tests using free-standing films, fail to capture this behavior. These tests measure performance in isolation, whereas in practical batteries, the separator is compressed between electrodes under stack pressure. This operational environment alters both the mechanical response, for example, reduced stiffness from amorphous-phase plasticization[115] and electrochemical interactions, meaning isolated film testing overlooks key mechanisms like swelling-induced dendrite nucleation. In real batteries, for instance, swelling-induced wrinkles generate non-conformal contact gaps with electrodes, redirecting lithium plating into electrolyte-filled channels, an effect not observed in free-standing film tests.[116]

In conclusion, the regulation of dendrite growth constitutes a complex challenge that necessitates the management of both the dynamics of Li^+ deposition and SEI film formation, alongside the assurance of mechanical robustness of the separator through attributes such as an adequate elastic modulus to withstand dendrite penetration.

3. Engineering Applications of Separators in Energy Storage Systems

3.1. Separators in Redox Flow Batteries

RFB membranes have been extensively investigated. Although the rich diversity of materials allows many avenues for membrane innovation, it is very difficult to develop a membrane meeting all the requirements. The membrane properties are complicatedly correlated, in which the improvement of one feature likely decreases the efficacy for another. The main challenge is how to optimize membrane properties to match the redox flow battery chemistry.

Evaluating the performance of separators in RFBs does not simply rely on a sole metric (e.g., ionic conductivity, selectivity). The suitable membrane materials and optimization strategies must be taken into account for the specific battery systems. For example, VRFBs require the membrane with high proton conductivity, high V/H selectivity, and chemical stability to oxidative vanadium ions. Alkaline ORFBs need the alkaline-metal ion-conductive membrane with good selectivity to redox organics. To better evaluate an optimized membrane and its performance in RFBs, we summarized the relationships of improving strategies and membrane properties as presented in **Table 4**.

For the redox species, increasing the molecular size is beneficial to the limitation of crossover and the improvement of battery cycling capability. Balancing the properties (including thickness, ionic conductivity, pore structure, and polymer chemistries) of a separator is extremely complicated. For example, fabricating meso/macro pores and making thin film could effectively decrease the area-specific resistance of a battery and promote its output power. However, the redox-species crossover will become severe, leading to a reduced capacity retention and short lifetime. Crosslinking technique can help with the improvement of mechanical strength and restriction of the active-species crossover, but the ionic conductivity will be diminished due to the reduced electrolyte uptake. Introducing charged groups could increase the ionic conductivity, but this method may affect the mechanical properties of functionalized membranes and cause the fouling issue of membrane due to the interaction between charged membrane and redox species.

Ionic conductivity and selectivity are critical and correlated parameters as discussed above. Besides, stability, mechanical strength, cost-effectiveness, and sustainability are also very important for developing usable membranes. Here, the current progress of usable RFB membranes within the last 10 years is summarized below (**Figure 18**).

RFB membrane separators can be classified into four types: ion-exchange membranes (IEMs), non-ion-exchange membranes, porous membranes, and advanced membranes (combining the functions of pores and ionic functional groups). Commercially available ion-exchange membranes are commonly used in RFB stacks. Specifically, IEMs include cation-exchange membranes (CEMs), anion-exchange membranes (AEMs), amphoteric ion-exchange membranes (AIEMs), bipolar ion-exchange membranes (BIEMs), and mosaic ion.

3.1.1. *Anion-Exchange Membrane in Redox Flow Batteries*

AEMs possess anion-exchange groups, such as quaternized ammonium ($-NR_3^+$), imidazolium, benzimidazolium, pyridinium. These positively charged groups can not only offer the transport sites for charge carriers, such as OH-, Cl-, and SO_4^{2-}, but also repulse the positively charged redox species via the Donnan-exclusion mechanism. Introducing anion-exchange groups has become a new approach in hindering the crossover of vanadium redox species in VRFBs. The quaternary amine ($-NR_3^+$) groups are the main group in AEMs. For example, quaternized poly(p-phenylene oxide) (PPO) membrane was obtained by simply reacting the alkylhalide groups (-Br) from PPO with trimethylamine. This AEM enabled a stable cycling performance with a high retention of 99.988% per cycle for neutral TMAP-TEMPO/BTMAP-Vi ORFBs.

3.1.2. *Cation-Exchange Membrane in Redox Flow Batteries*

With cation-exchange functional groups (e.g., $-SO_3-$), CEMs could allow the transport of positive cations, such as H+, K+, Na+, Li+, and attract the counter species. Widely used commercial membranes, such as Nafion, suffer from a relatively high cost. To obtain cost-effective CEMs, the direct and effective method is to form a composite membrane by integrating cheap organic/inorganic fillers within CEMs. For example, a Nafion/lignin composite membrane was demonstrated with a high energy efficiency of 82.7% and decent cyclability over 1000 cycles in VRFBs. Inorganic fillers, such as ZrO_2, TiO_2, SiO_2, and GO, were also used to enhance mechanical strength, limit membrane swelling, and improve selectivity.[10,129] In addition, polyvinyl alcohol, polypyrrole, polyaniline, and amphoteric Nafion-g-PSBMA were evaluated as organic fillers in the Nafion composite membranes.[110,164–166] Although fillers possess a cost advantage, the stability, especially chemical stability in harsh acidic/alkaline conditions, is inadequate. It is hard

Table 4. Relationships of optimizing strategies, separator properties, and RFB performance.

Strategies	Membrane Properties			RFB performance		
	Ionic conductivity	Permeation of redox actives	Mechanical strength	Capacity retention	CE	Power density
Make larger actives	–	↓	–	↑	↑	–
Induce nanophase separation	↑	↓	–	↑	↑	↑
Introduce charged groups	↑	↓	–	↑	↑	↑
Narrow down pore-size	↓	↓	–	↑	↑	↓
Crosslink[a)]	⋮	⋮	↑	⋮	⋮	⋮
Make thin film/TFC	–	↑	↑	↓	↓	↑
Meso/macro porous structure	↑	↑	↓	↓	↓	↑

[a)]Crosslink may decrease the electrolyte uptake, and thus decrease the ionic conductivity. Crosslinked membranes normally have narrow channels to limit the permeate of redox actives.

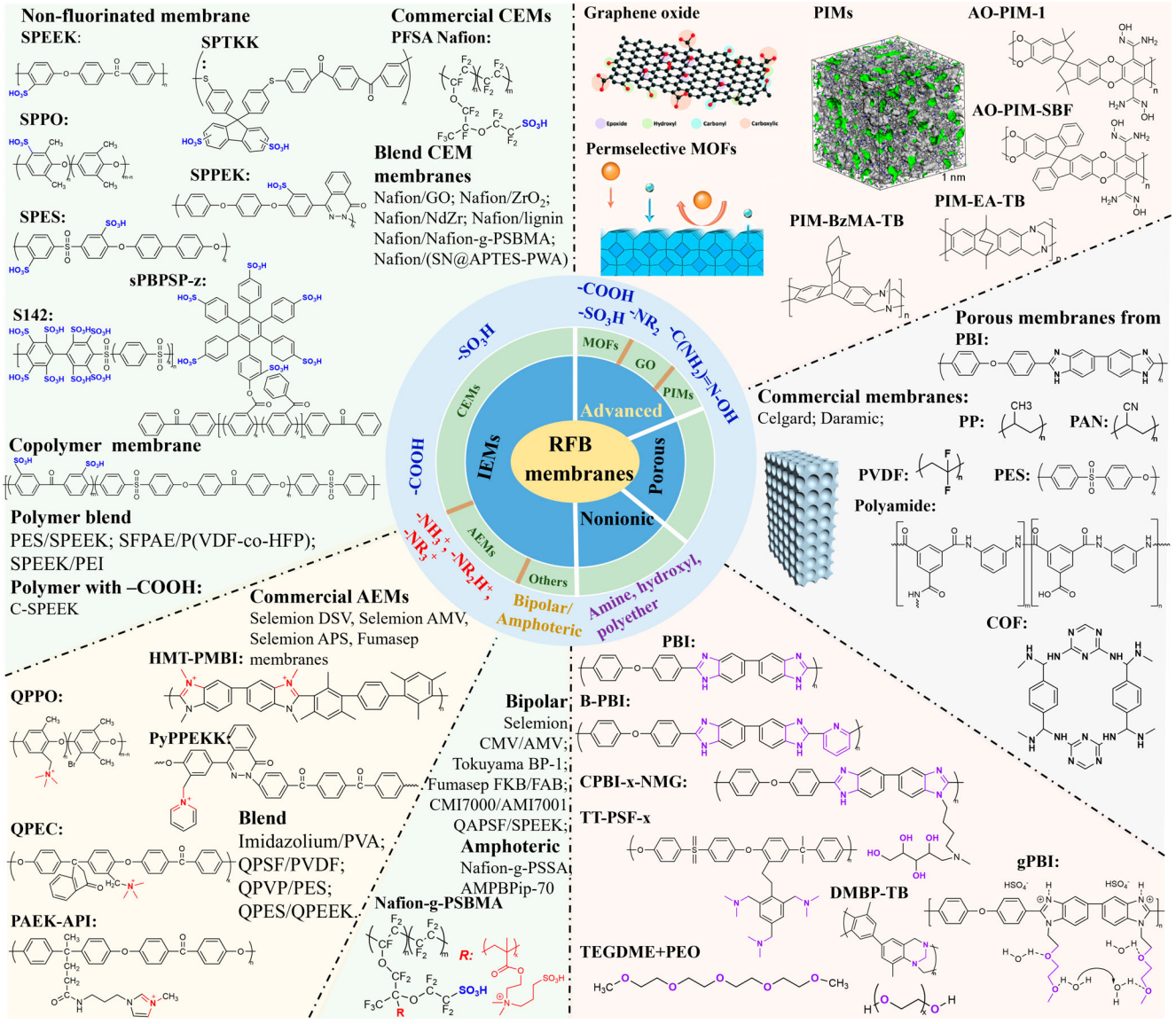

Figure 18. Summary of recent progress on RFB membranes, including CEMs, AEMs, Nonionic membranes, porous membranes, and next-generation membranes. CEMs: SPEEK,[111,117–119] SPTKK,[120] SPPO,[121] SPPEK,[122] S142,[123] sPBPSP-z,[76] copolymers,[124–126] Blends,[112,127,128] composites[129,130] and polymers with -COOH[131,132]; AEMs: QPPO,[121,133] QPEC,[134] PAEK-API,[135] PyPPEKK,[136] HMT-PMBI,[137] Blends[138–140] and others[141–144]; Bipolar or amphoteric membranes[145–147]: commercial bipolar membranes,[148] QAPSF-SPEEK,[149] Nafion-g-PSBMA;[110] Nonionic membranes: PBI,[150] B-PBI,[151] CPBI-x-NMG,[152] TT-PSF-x,[100] TEGDME-PEO,[153] DMBP-TB,[154], gPBI; Porous membranes: COF,[40,155,156] polyamide,[102,157] PBI.[81,150,157–159] Advanced membranes: GO (Reproduced with permission.[160–162] Copyright 2018, Elsevier Inc.), MOFs (Reproduced with permission.[163] Copyright 2020, Springer Nature Limited), PIMs (Reproduced with permission.[21] Copyright 2019, Springer Nature Limited).

to meet the longevity requirement for the RFBs using these composite CEMs.

3.1.3. *Other IEMs in Redox Flow Batteries*

Functional bipolar and amphoteric ion-exchange membranes are being increasingly studied, which combine the advantageous features from both CEMs and AEMs. Bipolar membranes comprise a cation-selective layer and an anionic layer, such as commercially available Selemion CMV/AMV, Tokuyama BP-1, Furmasep FKB/FAB,[145,148] and QAPSF/SPEEK.[149] The special configuration of bipolar membranes is favorable for the application of water splitting. Different from the bipolar membranes, amphoteric ion-exchange membranes possess both cation and anion-exchange functional groups at a molecular level. For example, PVDF film was integrated with styrene and dimethylaminoethyl methacrylate, which could undergo sulfonation and quaternization to generate positively and negatively charged groups.[146] The -SO3- groups facilitated the transport of charge carrying ions. Meanwhile, the quaternized ammonium groups could restrain the migration of vanadium ions by the Donnan-exclusion function, enabling improved selectivity for this membrane. Zwitterionic groups

(e.g., sulfobetaine methacrylate) were also introduced to the matrix of Nafion to improve its selectivity and ionic conductivity.[167]

3.2. Separators in Lithium-Ion Batteries

Separators in LIBs have received new requirements as the LIBs are being developed to power electric vehicles and energy storage stations. For example, the separators should be thermally and mechanically stable to prevent thermal runaway and internal short circuits. The separators should have the ability to regulate ion transport and reduce the possibility of Li-dendrite formation. High ionic conductivity is always important for membrane separators, which directly influences the output energy and efficiency of LIBs.

Separators should be chemically and electrochemically stable at varied states of charge (SOCs) during battery operation. The separators should also have enough puncture strength and tensile strength to prevent the penetration of formed dendrites or electrode particles. **Table 5** presents the United States Advanced Battery Consortium (USABC) targets for the properties of LIB batteries and summarizes the performance of the most developed Celgard separators. Despite the easy fabrication and relatively low cost, the thermal stability and mechanical strength of Celgard separators need significant improvement.

In the past decades, LIB separators had not been paid enough attention compared to the electrodes and electrolyte. However, the development of LIBs has faced bottlenecks in low energy density, poor cycling stability, and safety issues, which cannot be solved by solely improving the performance of electrode or electrolyte. Developing functional separators provide an alternative way to overcome these challenges.

Currently, the developed LIB separators are classified into polymeric porous membranes, nonwoven mats, gel polymer electrolytes, composite separators, and functional separators based on microporous materials. Typical examples of LIB separators are briefly presented in **Figure 19**. It should be noted that solid-state electrolyte and gel electrolyte are a special type of separator, which will be introduced specifically in the next section.

Table 5. U.S. Advanced Battery Consortium (USABC) requirements of a commercial LIB separator.[84]

Parameter	Goal	Celgard LLC
Sales price ($ m^{-2})	≤1.00	3.8–5
Thickness (μm)	≤25	12–40
Wettability	Complete wet-out in typical battery electrolyte	Complete wet-out
Chemically stability	Stable in battery for 10 years	Chemically stable
Pore size (μm)	<1	Micro/meso pores
Puncture strength	>300 g/25.4 μm	Young modulus: 0.3–0.8 GPa
Thermal stability	<5% shrinkage at 200 °C	Melt at 115–135 °C
Melt integrity	>200 °C	Melting point: 115–135 °C
Purity	<50 ppm H_2O	<50 ppm H_2O
Tensile strength	<2% offset at 1000 psi or >1000 kg cm^{-1} (98.06 MPa)	Machine direction (MD): ~150 Transverse direction (TD): ~10
Pin removal	Easy removal from all major brands of winding machines	Easy process

Polyolefin, such as PP and PE, is the most developed polymeric porous membrane for commercial separators.[11,168,169] This type of separator possesses good chemical stability. With the easy dry and wet processes, the porosity and pore size within polyolefin could be altered as required. The thickness of polyolefin separators is typically below 25 μm, which benefits the output power density of batteries. However, the anisotropic mechanical strength and thermal instability are challenging the safe operation of polyolefin separators. PP separators prepared by a dry process exhibit weak tensile strength in the transverse direction (TD),[86] indicating that PP cannot survive the penetration of the dendrites in the TD direction. PE separators have a low shutdown temperature due to their low melting temperature (~130 °C). One effective solution for the above issue is to prepare multilayer separators. For example, a PP/PE/PP multilayer separator demonstrates improved thermal and mechanical properties attributing to the isotropic mechanical strength of PE and high melting temperature of PP. The alternative approach is using thermally stable polymers, such as PAN,[27,177,178] PMMA,[33] PVDF,[170–172] PVDF-*co*-HFP,[173] cellulose,[181,182] etc.

In contrast to PP and PE separators, PVDF with C-F groups has good electrolyte wettability and high thermal stability with 3% shrinkage at 160 °C. Improving the porosity could significantly increase the electrolyte uptake so as to promote the ionic conductivity. The phase-inversion method was used to generate sponge-like or finger-like pores within PVDF membranes.[170–172] With a similar approach, hierarchical pores within the PVDF membrane can be created by extracting a mixed solvent, for example, N-methyl-2-pyrrolidone and acetonitrile. The enlarged pore size and porosity provide more space for the organic electrolyte. However, electrochemical stability is a problem when PVDF separators are used in LIBs for a long duration. The underlying mechanism involves multiple chemical degradation pathways in battery environments, including oxidative/radical attack, electrochemical decomposition, (de)hydrofluorination, and inorganic fluoride formation, each manifesting differently across their key applications as a cathode binder, coated separator, or solid-state electrolyte matrix.

At the cathode, reduced oxygen species (e.g., superoxide or singlet oxygen) generated during O_2 reduction attack PVDF's C-F backbone, causing oxidative cleavage and forming organic decomposition products (characterized by Raman bands at 1133 and 1525 cm^{-1}). This phenomenon not only misleads discharge chemistry identification but also consumes charge capacity.[213] Separately, electrochemical decomposition occurs when PVDF is exposed to electrode potentials exceeding the electrolyte's reduction onset, particularly on graphite anodes, where it correlates with increased interfacial resistance.[214] In Lewis-acidic or basic media, PVDF undergoes dehydrofluorination (HF elimination), forming unsaturated carbon backbones that carbonize into amorphous structures; this process releases fluoride ions that complex with cations (e.g., AlF_4^- observed in $AlCl_3$-based ionic liquids via ^{19}F NMR).[215] The accumulated fluoride from these reactions further precipitates as LiF or complex fluorometallates in electrodes and interphases, reducing active lithium availability and forming inactive surface films that impede battery performance.[216]

Beyond these general mechanisms, PVDF exhibits distinct degradation behaviors in its key applications. As a cathode binder, it physically entangles with active materials and forms weak hydrogen bonds between its -CH_2- segments and oxide surface -OH groups. However, long-term cycling induces two critical degradation modes: at the cathode's upper voltage window, oxidative attack from the electrolyte causes heterolytic cleavage of C-F bonds, generating carbonyl (-CO-) or carboxyl (-COOH) groups on the polymer backbone, which weaken

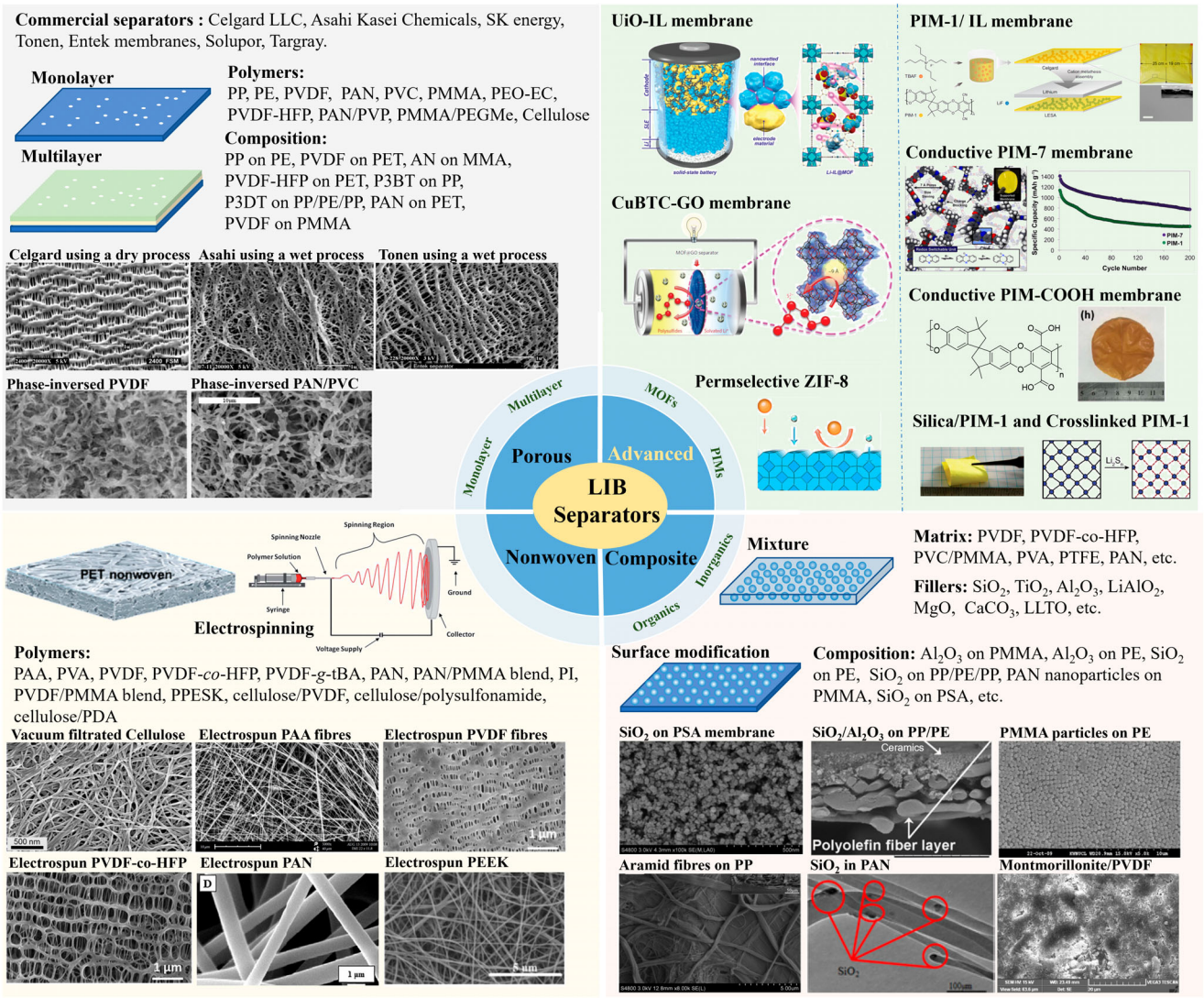

Figure 19. Categories of the LIB separators with their typical structure. Porous separators: PP/PE,[11,168,169] PVDF[170–172] (Reproduced with permission,[173] Copyright 2014, Springer-Verlag Berlin Heidelberg), PMMA,[174,175] PEO,[176] PAN,[27,177–180] cellulose,[181,182] and others[26] (Reproduced with permission.[26] Copyright 2014, Royal Society of Chemistry). Nonwovens,[28,31,183–188] Composites[33,173,189–192] (Reproduced with permission.[33] Copyright 2010, Elsevier B.V.; Reproduced with permission.[189] Copyright 2017, The Korean Fiber Society and Springer Science Business Media Dordrecht). Advanced separators: MOFs,[44,193–203] GO,[204] PIMs.[29,34,52,57,205–212] (Reproduced with permission.[190] Copyright 2013, IOP Publishing; Reproduced with permission.[191] Copyright 2010, Elsevier B.V.; Reproduced with permission.[192] Copyright 2013, Elsevier B.V.; Reproduced with permission.[198] Copyright 2020, WILEY-VCH Verlag GmbH & Co. KGaA, Weinheim; Reproduced with permission.[199] Copyright 2016, Nature Publishing Group; Reproduced with permission.[206] Copyright 2020, Springer Nature Limited; Reproduced with permission.[207] Copyright 2020, Royal Society of Chemistry; Reproduced with permission.[34] Copyright 2017, ACS. Org.)

interfacial adhesion and lead to electrode delamination.[213] Additionally, Li^+ intercalation into PVDF's amorphous regions during charge/discharge triggers phase transitions from the stable α-phase to polar β- or disordered γ-phases; uncontrolled transitions disrupt the binder's network, reducing mechanical integrity and compromising active material anchorage.[217]

As a coated separator material, PVDF may enhance thermal stability and electrolyte wettability. Yet, its coating layer faces degradation from two sources: first, hydrolysis of the electrolyte salt (taking $LiPF_6$, the most widely used electrolyte salt, as an example) in trace water generates HF (Equation 19). The formed HF, as a strong acid, reacts with PVDF's C–F bonds via dehydrofluorination $[(CH_2-CF_2)_n + nHF \rightarrow n(CH_2-CH_2) + nLiF]$, etching the surface and creating microcracks that increase electrolyte leakage risks.

$$LiPF_6 + H_2O \rightarrow LiF + 2HF + POF_3 \quad (19)$$

Second, prolonged exposure to temperatures above 120 °C, common in fast-charging, accelerates thermal chain scission, releasing fluorinated volatiles (e.g., CHF_3, CF_4) and reducing coating integrity.[218]

In composite solid electrolytes, PVDF acts as a polymer matrix to enhance ionic conductivity when blended with ceramic fillers (e.g., $Li_7La_3Zr_2O_{12}$, LLZO). Here, degradation arises from interfacial and bulk processes: PVDF's C-F groups react with Lewis acidic sites on

fillers (e.g., Al^{3+} in Al_2O_3 or Zr^{4+} in LLZO), forming stable fluorinated complexes that reduce amorphous content and limit Li^+ mobility;[219,220] meanwhile, preferential Li^+ transport along PVDF's amorphous phase induces chain alignment over time, creating anisotropic conductivity and localized stress concentrations that promote crack propagation.[221]

These application-specific degradation pathways, combined with the broader chemical mechanisms, underscore the need for targeted stabilization strategies to enhance PVDF's long-term performance in lithium-ion batteries.

PAN and PMMA separators also show good compatibility with organic electrolytes. Solution-processable PAN allows for the use of different methods for membrane preparation, such as phase inversion, casting method, and electrospinning. The weak interaction between Li ions and nitrile (-C ≡ N) groups within the structure of PAN will help with electrolyte retention and achieve high ionic conductivity. PMMA separators also have good stability and processability. However, polymeric separators intrinsically possess low mechanical strength due to their amorphous structure. Preparing blend or multilayer membranes is a useful method for improving the overall properties. For instance, a cyanoethylated cellulose derivative, that is, DH-4-CN, was added into the polymer matrix of PVDF-co-HFP to improve its mechanical strength, ionic conductivity, and electrochemical stability.[222]

Furthermore, the electrospinning technique is employed to fabricate porous polymeric membranes with enhanced electrolyte uptake. The approach undesirably sacrifices the mechanical strength of the membrane separators. To overcome this issue, fabricating composite membranes with the use of inorganic materials is feasible to enhance mechanical and thermal stability (Figure 19). However, the inorganic materials, such as Al_2O_3, generally exhibit poor processability.

3.3. Separators in Solid-State Batteries

Quasi-/solid-state LIBs consist of cathodic and anodic electrodes, and solid electrolyte (SSE) separators. (**Figure 20a**) SSEs function as a physical barrier to prevent contact between electrodes and work as an ionic conductor to complete the circuit loop during the passage of current. SSEs are well placed to solve the battery safety concerns due to their incombustible property. Solid-state batteries have been regarded as one of the promising energy storage technologies, which would potentially compete with traditional LIBs.[89,224]

In solid-state batteries, metal oxide electrodes are still the commonly used cathode materials. Instead of the porous graphite anode, a much thinner Li-metal anode can be securely deployed, allowing the batteries to achieve an improved volumetric energy density of.[13] Additionally, mechanically strong solid electrolytes are expected to prevent the penetration of lithium dendrites and stabilize the de-/lithiation process. Though promising, SSEs still face obstacles that limit their practical application. For example, the usable SSEs are extremely thick, as shown in Figure 20b. The volume of LIBs using this SSE is at least 10-fold larger than that of LIBs using 25-μm-thick Celgard.[223] Other critical issues, such as poor electrode-electrolyte compatibility, low ionic conductivity, complicated fabrication, and instability, are challenging the performance of SSEs in batteries.

The fundamentals of SSEs are introduced with a focus on the ionic conductivity.

The best fast ionic conductor has a "molten/soft" sub-lattice or "liquid like" structure for mobile ions. For example, soft and deformable sulfide-based SSEs possess a weak attraction of Li ions, of which the sulfide framework allows for the favorable migration of Li ions. The major advance was $Li_{9.54}Si_{1.74}P_{1.44}S_{11.7}Cl_{0.3}$ solid with an outstanding ionic conductivity of 25.3 mS cm^{-1}.[225] Nevertheless, the application of this SSE is difficult due to the poor electrochemical stability and relatively high resistance caused by grain boundaries.

Introducing soft materials and mimicking "liquid like" structure to produce composite electrolytes, which provide an alternative approach to developing fast ionic conductors. Liquid components can fill into the voids or gaps within electrolyte pellets or membranes to create continuous ion channels and improve the electrolyte-electrode compatibility, thereby reducing the overall resistance of batteries. This type of electrolyte can be denoted as quasi-solid-state electrolyte or composite solid electrolyte.[226] Both emerging sulfides and quasi-solid-state electrolytes have been considered as the new generation (3rd G) of SSEs.

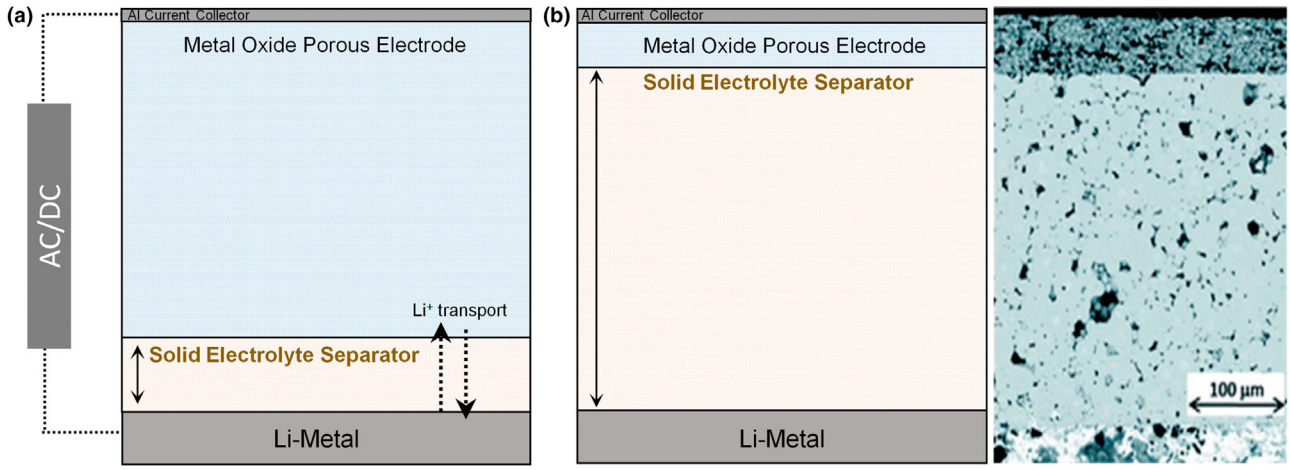

Figure 20. Schematics showing the cross-sections of ideal and practical solid-state LIBs. a) Schematic illustration of a quasi-/solid-state LIB with an ideal configuration. b) Diagram of a fabricated solid-state LIB and its cross-sectional SEM image. Reproduced with permission.[223] Copyright 2019, Royal Society of Chemistry.

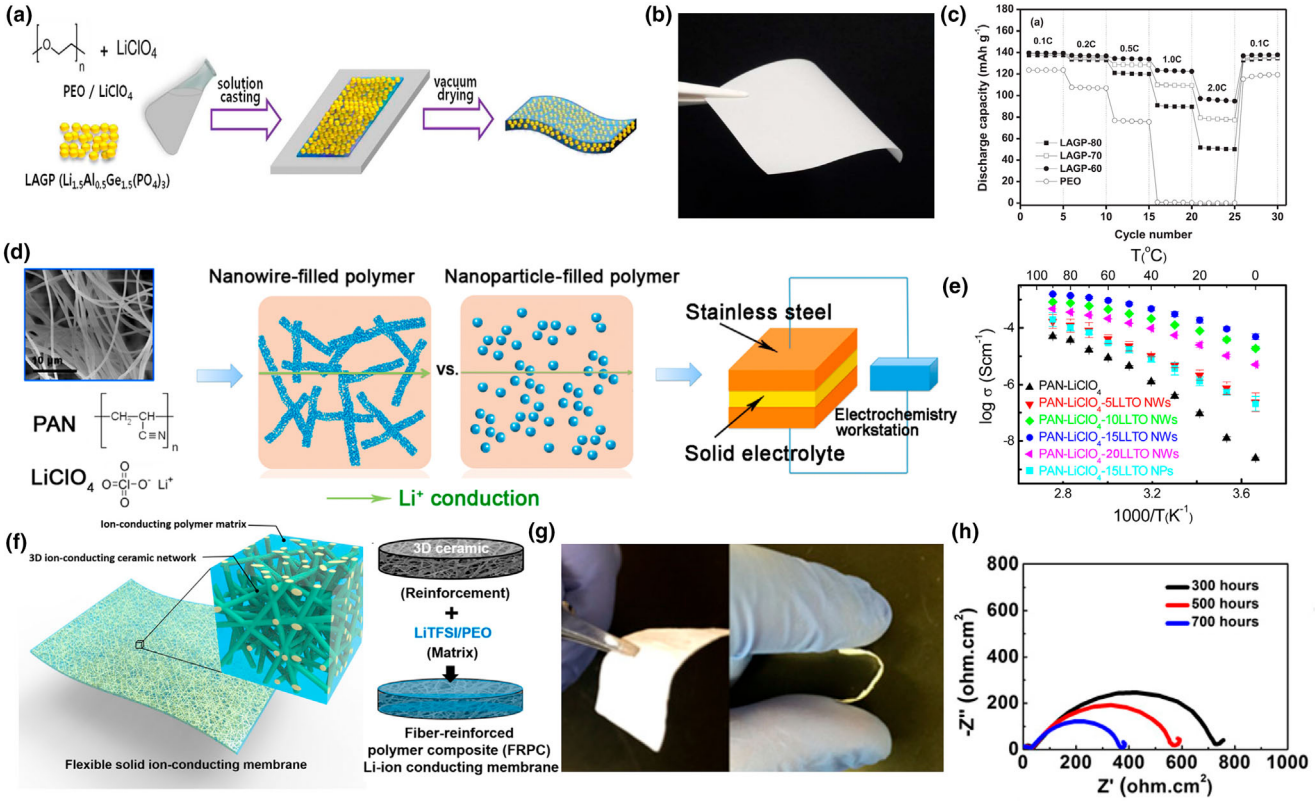

Figure 21. Examples of dry solid composite electrolytes and their applications. a) PEO/LAGP-based dry solid composite electrolyte. b) Photo of PEO/LAGP dry solid composite electrolyte. c) Rate performance of a LFP|Li solid-state battery. d) Nanowire-filled PAN dry solid composite electrolyte. e) Ionic conductivity at different temperatures. f) Preparation of LLZO fibers/PEO solid composite electrolyte. g) Photo of LLZO fibers/PEO solid composite electrolyte. h) Resistance of LLZO fibers/PEO solid composite electrolyte in polarization tests against time. a–c) reproduced with permission.[39] Copyright 2015, IOP Publishing. d–h) reproduced with permission.[243] Copyright 2016, The National Academy of Sciences.

SSEs are divided into inorganic solid electrolytes (ISEs), solid polymer electrolytes (SPEs), and solid composite electrolyte (SCEs),[242] examples shown in **Figure 21**. Typical examples of ISEs and SPEs, and their dis-/advantages, are summarized in **Table 6**. With regards to a practical application, properties including high ionic conductivity, high electronic resistance, good mechanical strength, wide electrochemical windows, and simple fabrication processes are also very crucial. Both ISEs and SPEs face inevitable challenges. The fabrication of ISEs are generally complicated, and grain boundaries derived from the pellet processing contribute to high apparent resistance. For SPEs, the ionic conductivity at ambient temperature is low, and the mechanical strength is insufficient. The employment of both electrolytes in LIBs doesn't match with the current manufacture process of LIBs. An increasingly research interest has been altered to SCEs, which take advantage of inorganic electrolytes and solid polymer electrolytes and compensate their drawbacks (the difficult process of inorganic electrolytes and the poor mechanical property of solid polymer electrolytes). For instance, Ma et al.[244] developed a PVDF-HFP-LLZTO composite electrolyte with in situ polymerized PVEC, which exhibits a high ionic conductivity of 1.21×10^{-1} mS cm^{-1} and enables dendrite-free lithium deposition. Which mitigates the low conductivity and poor interfacial stability issues of SPEs. Matsuda et al.[245] introduced a lithium salt-infused PAN nanofiber separator, leveraging the polar nitrile groups of PAN to enhance Li^+ diffusion (9.0×10^{-2} mS cm^{-1} at 60 °C) while its nanofiber structure suppresses dendrites, achieving 1000-hour stable cycling in symmetric cells and 99% Coulombic efficiency over 100 cycles, addressing both the mechanical weakness of SPEs and the complex fabrication of ISEs. Gong et al.[246] designed a h-BN@PEO/PVH ternary electrolyte with a thickness of only 26 µm, combining the high thermal conductivity of h-BN and the flexibility of PVH to achieve 3.3×10^{-1} mS cm^{-1} conductivity and a 0.74 Li^+ transference number. Its remarkable 4400-hour symmetric cell stability at 0.11 mV overpotential tackles the low ambient conductivity and short cycle life limitations of traditional SPEs. Khan et al.[247] fabricated an LLZTO@WO_3 hybrid filler electrolyte by integrating garnet-type LLZTO with semiconducting WO_3, creating synergistic ion pathways that yield 1.9×10^{-1} mS cm^{-1} conductivity and 0.67 Li^+ transference number at 40 °C. The hybrid filler reduces interfacial resistance, enabling $LiFePO_4$ cells with 95.2% capacity retention after 400 cycles, a significant advancement over the high interfacial resistance and poor rate performance of ISEs. Hu et al.[248] reinforced PEO with a polyurethane polymer of intrinsic microporosity (PPU), enhancing ionic conductivity to 1.82 mS cm^{-1} at 50 °C, with a 0.68 Li^+ transference number and 5.3 V stability window, overcoming the low conductivity and mechanical fragility of SPEs. Li et al.[249] developed an Al-doped garnet nanofiber CSE by embedding LLZAO nanofibers (15 wt%) into PEO, which reduces crystallinity and expands amorphous regions to achieve 6.19×10^{-1} mS cm^{-1} conductivity. The cathode-supported design

Table 6. Summary of ISEs and SPEs.

Type		Materials	Conductivity (mS cm^{-1})	Advantages	Disadvantages	Ref.
ISEs	Oxides	Garnet: $Li_7La_3Zr_2O_{12}$	10^{-3}–10^{-1}	High mechanical strength and thermal stability	Non-flexible	[227]
		LISICON: $Li_{1.5}Al_{0.5}Ge_{1.5}(PO_4)_3$		High conductivity of bulk electrolyte	Side reaction with Li-metal	[228,229]
		NASICON: $LiTi_2(PO_4)_3$		Air stability	Grain boundary resistance	[230]
		Perovskite $Li_{3.3}La_{0.56}TiO_3$			Expensive large-scale production	[231]
	Sulfides	Li_2S-P_2S_5	10^{-1}-10	High ionic conductivity	Sensitive to moisture	[232]
		Thio-LISICON: $Li_{10}GePS_{12}$		Good mechanical strength	Side reaction with Li-metal	[38]
		$LiBH_4$-LiX (X = Cl, Br, or I)			Grain boundary resistance	[225]
					Complicated process	
	Halides	$LiBH_4$	10^{-5}–10^{-2}	Good mechanical strength	Sensitive to moisture	[233,234]
		$LiBH_4$-LiX (X = Cl, Br, or I)		Good compatibility with Li-metal	Low oxidation window	[233]
					Grain boundary resistance	
					Low ionic conductivity	
SPEs	Ethers	PEO	10^{-1}-10 (>60 °C)	Good mechanical flexibility	Limited thermal stability	[88]
		PEO-fillers		Good compatibility with Li-metal	Low oxidation window	[234–241]
				Easy manufacture	Insufficient mechanical strength	

enables $LiFePO_4$//Li cells with 94.1% capacity retention over 115 cycles and 99% Coulombic efficiency, effectively addressing the complex fabrication (e.g., grain boundary issues) of ISEs and the poor mechanical property of SPEs.

In practical devices, SSEs must possess the following characteristics: i) minimized interfacial and grain boundary resistance; ii) negligible electronic conductivity and wide electrochemical windows (at least >4.2 V vs Li/Li$^+$); iii) a high apparent ionic conductivity of above 0.1 mS cm^{-1}; iv) chemical stability toward Li-metal anode; and v) easy synthesis, facile processing, and manufacture.

Low ionic conductivity is the main obstacle limiting the practical implementation of SSEs.[224] The restrictions to ion conduction can be explained based on three aspects: bulk limitation, interface/surface limitation, and grain boundary limitation. Firstly, the ionic conductivity of the bulk of inorganics and solid polymers is generally low at room temperature. In crystalline ISEs, there is limited space to accommodate mobile ions. In SPEs, the motion of polymer chains is too weak to facilitate ion transport below T_g. Secondly, the surface of SSEs and the SSE-electrode interface is unstable. The surface of ISEs, for example, LGPS,[38] is very sensitive to moisture, with a tendency to generate harmful H_2S gas. ISEs that contain Ti^{4+} can be reduced by the lithium metal anode. SPEs that consist of ether units tend to be oxidized by high-voltage cathodes. The poor surface/interface stability restricts the stable transport of ions from electrolytes to electrodes. Last but not least, grain boundaries existing in pelletized ISEs and dry SCEs increase the length of ion pathways between cathodes and anodes and thus increase the apparent resistance. The grain boundaries cannot be easily avoided during the electrolyte fabrication process.

Quasi-solid electrolyte is a promising solution to solve the above issues. The solidified liquid electrolyte (not limited in RTILs) creates sufficient channels for ion transport. With the addition of active fillers or matrices, the bulk ionic conductivity can be further improved. On the other hand, the electrode-electrolyte interface and grain boundaries will be wetted by electro-/chemically stable liquid, lowering the risk of interfacial side reaction. For a traditional quasi-solid electrolyte, the matrices are soft polymer, such as PEO, PVDF, and PAN. These polymers are too mechanically soft to survive the penetration by dendrites. Inorganic materials are useful to develop mechanically robust quasi-solid electrolyte either.

4. Scientific Challenges

4.1. Separators for RFB Applications

Research progress of the separators applied in RFBs, including typical ion-exchange membranes, non-ion-exchange membranes, and porous membranes as well as some emerging membranes prepared by PIM materials has been reviewed. There remain general challenges for the development of high-performance membranes for batteries:

- Selectivity: Perfluorinated sulfonic acid membranes are the state-of-the-art RFB separators which inspired a series of follow-up work to develop membranes with nanophase separation. However, this membrane suffers from low selectivity to redox species, for example, vanadium-based species. Although Donnan-exclusion is introduced by grafting the same charged functional groups, obvious crossover of redox actives still occurs due to the large-sized ionic channels.
- Conductivity: Nonionic membranes and porous membranes (e.g., PBI separators) exhibit an improved selectivity toward redox species, but feature relatively low ionic conductivity. Increasing the ionic conductivity will unexpectedly sacrifice the selectivity. Overcoming or balancing the trade-off is necessary to develop practically usable RFB membranes.
- Cost: Commercial perfluorinated membranes, such as Nafion, are expensive.
- Stability: As the operating conditions of most RFBs are acidic or alkaline, membrane needs to be stable in the harsh alkaline or acidic solutions. The developed substitutes for Nafion membranes are mainly hydrocarbon-based materials that are unstable in the above solutions for a long time.

Here is summarized the typical examples of cation-exchange membranes, anion-exchange membranes, nonionic and porous membranes, and recently reported advanced membranes (**Table 7**). New materials including PIMs and GO were explored as RFB separators aiming to overcome the above challenges and improve the performance. However, these new membranes are still limited by the following issues.

Table 7. Typical examples for the CEMs, AEMs, nonionic membranes, and advanced membranes with their functional groups, conductivity or resistance, permeability of redox species, and the performance in RFBs. Based on the functional groups, only one or two typical reports are summarized as examples in this table.

	Functional groups	Membrane	Conductivity (mS cm^{-1})[a)]	Permeability ($cm^2 s^{-1}$)	RFB types	Performance	Ref
CEMs	Sulfonic	SPEEK	H^+: 9.1	$VOSO_4$: 3.6×10^{-9}	VRFBs	CE: 97.5% VE:82.5% EE: 80.3% ($120\ mA\ cm^{-2}$)	[111]
		SPPO	ASR in KOH: $1.3\ \Omega\ cm^2$	$Fe(CN)_6$: 2.50×10^{-10} DHAQ: 4.80×10^{-9}	ORFBs $Fe(CN)_6$/DHAQ	CE: 99.9% VE:83.1% EE: 83.0% ($60\ mA\ cm^{-2}$)	[121]
		SPAEK	H^+: 53	$VOSO_4$: 1.8×10^{-8}	VRFBs	CE: 89.5% VE:92.2% EE: 82.6% ($20\ mA\ cm^{-2}$)	[250]
	Carboxyl	C-SPEEK	ASR in H_2SO_4: $0.16\ \Omega\ cm^2$	N/A	VRFBs	CE: 97.3% VE:84.5% EE: 82.2% ($80\ mA\ cm^{-2}$)	[131]
AEMs	Quaternized ammonium	QPPO	ASR in KCl: $2.55\ \Omega\ cm^2$	TMAP-TEMPO: 3.38×10^{-9} BTMP-Vi: 9.6×10^{-9}	ORFBs TMAP-TEMPO/ BTMAP-Vi	CE: 100% VE:81.0% EE: 81.0% ($60\ mA\ cm^{-2}$)	[121]
		PQVB-b-PVBF	NaCl: 9.5	N/A	ORFBs TEMPO/BTMAP-Vi	CE: 97.0% VE:80% EE: 79% ($10\ mA\ cm^{-2}$)	[141]
		QPEK-C	H^+: 15.2	Ce: below detection limit	V/Ce RFBs	CE: 100% VE:67.8% EE: 67.8% ($10\ mA\ cm^{-2}$)	[134]
	Imidazolium	PAEK-API	H^+: 5.3	$VOSO_4$: 2.1×10^{-9}	VRFBs	CE: 100% VE:67.8% EE: 67.8% ($10\ mA\ cm^{-2}$)	[135]
	Benzimidazolium	PBI-hex-BIm	ASR in H_2SO_4: $0.132\ \Omega\ cm^2$	$VOSO_4$: 8×10^{-13}	VRFBs	CE: 99.4% VE:59.9% EE: 59.4% ($65\ mA\ cm^{-2}$)	[135]
	Pyridinium	BrPPO/Py-56	H^+: 28.4	$VOSO_4$: 3.96×10^{-10}	VRFBs	CE: 98.6% VE:78.2% EE: 77.1% ($250\ mA\ cm^{-2}$)	[144]
Nonionic	Amine	PBI	ASR: $\sim 0.6\ \Omega\ cm^2$	N/A	VRFBs	CE: 100% VE:73.5% EE: 73.5% ($200\ mA\ cm^{-2}$)	[151]
	Polyether	GPBI-3	ASR in H_2SO_4: $0.15\ \Omega\ cm^2$	$VOSO_4$: 1.30×10^{-9}	VRFBs	CE: 99.8% VE:76.1% EE: 75.9% ($200\ mA\ cm^{-2}$)	[78]
	Hydroxyl	CPBI-70-NMG	ASR in H_2SO_4: $0.32\ \Omega\ cm^2$	$VOSO_4$: 8.58×10^{-10}	VRFBs	CE: 99.2% VE:78.4% EE: 77.9% ($250\ mA\ cm^{-2}$)	[152]

Table 7. Continued

	Functional groups	Membrane	Conductivity (mS cm^{-1})[a)]	Permeability ($cm^2 s^{-1}$)	RFB types	Performance	Ref
Advanced Membranes	Carboxyl	GO	H^+: 17	∼100% rejection of all actives	ORFBs	CE: ∼98%	[160]
	Hydroxyl		KOH: ∼5		$Fe(CN)_6$/FMN	(40 mA cm^{-2})	
	N/A	PIM-1	ASR in H_2SO_4: 1.44 Ω cm^2	N/A (infinite)	VRFBs	CE: 97.1% VE:92.5% EE: 89.9% (20 mA cm^{-2})	[20]
	Sulfonic	SPX-BP	KOH: 20.1	$Fe(CN)_6$: 4.7×10^{-10} DHAQ: 3.9×10^{-9}	ORFBs $Fe(CN)_6$/DHAQ	CE: 100% VE:79.4% EE: 79.4% (250 mA cm^{-2})	[113]
		S-F-abSPI/1% PFMPP	H^+: 116	$VOSO_4$: 7.20×10^{-9}	VRFBs	CE: 98.61% VE:83.12% EE: 81.95% (200 mA cm^{-2})	[251]
		SCOF/SPEEK-75	H^+: 65	$VOSO_4$: 1.98×10^{-9}	VRFBs	CE: 98.6% VE:N/A (100 mA cm^{-2})	[252]
		S/GO-TpTG	H^+: 82.7	$VOSO_4$: 1.38×10^{-8}	VRFBs	CE: 95% VE:85% EE: 79.4% (250 mA cm^{-2})	[253]
		SP/TpTGC1	H^+: 142	$VOSO_4$: 2.15×10^{-8}	VRFBs	CE: 98.3% VE:78.8% EE: 77.4% (180 mA cm^{-2})	[254]
	Imidazole Ring	P/STpPa-3	H^+: 69.2	$VOSO_4$: 2.74×10^{-10}	VRFBs	CE: 99.39% VE: increased by >12%; EE: 83.3% (80 mA cm^{-2})	[255]
		DP-PBI	H^+: 30.33	$VOSO_4$: 1–2 times that of ordinary PBI	VRFBs	CE: 98.3% VE:78.8% EE: 77.4% (180 mA cm^{-2})	[256]
	Amidoxime	AquaPIMs	KOH: 7.9	N/A (D_{sol}/D_{eff})	Hybrid RFBs $Fe(CN)_6$/Zn	CE: ∼99% VE:60% EE: 59.4% (250 mA cm^{-2})	[35]

[a)]Some reports provided the area-specific resistance (ASR) instead of ionic conductivity.

- Stability: Mechanical property and chemical stability of membranes are key challenges. For example, the GO membrane cannot withstand the mechanical pressure in a flow mode of RFBs. The structure of PIM-1 is not chemically stable in both acidic and alkaline solutions. The PIM backbones with amidoxime functional groups could not survive in alkaline solutions for a long time.
- Match of membranes and redox species: These newly developed membranes have a high potential of being applied in a diverse system with different redox couples. Selecting suitable operating conditions and matchable redox species could maximize the working ability of these membranes.

4.2. Separators for LIBs and SSBs

The separators being developed mainly involve the conventional porous separators based on polyolefins, nonwoven separators, composite separators (e.g., Al_2O_3 modified membranes), and emerging separators fabricated by new microporous materials, MOFs and PIMs. The challenges for the typical separators include (**Table 8**):

- Thermal stability and mechanical strength: Commercially available separators are thermally unstable and own a large thermal shrinkage at above 120 °C. The mechanical strength of this separator is not strong enough to prevent the puncture of formed Li dendrites. Thus, LIBs with the use of these separators have a severe safety issue.
- Side reactions: On the one hand, some polymer separators are not electro-/chemical stable. For example, the C-F groups of PVDF can react with reductive lithium metals and produce a Li-F passivating layer, leading to the reduced coulombic efficiency. On the other hand, the highly porous structure can absorb a large amount of organic liquid electrolyte and enlarge the electrode-electrolyte contact area. Side reactions will occur at the interface between electrolytes and Li metal anodes.
- Electrolyte leakage: The porous separator cannot maintain the organic liquid electrolyte in its bulk and may cause a serious electrolyte when Li-ion battery failure occurs. This is a common issue for nonwoven separators.
- Low lithium-ion transference number: The conventional separators generally feature a low Li-ion transference number of around 0.2–0.3, which means the transport of cations is not homogenous. The nonuniform migration of Li ions probably induce the random stripping/plating of Li ions on the surface of Li metal anodes, leading to the formation of Li dendrites.

Separators based on microporous materials, such as COFs, MOFs, and PIMs, were developed to overcome the above issues. Typical examples of MOF and PIM-based separators are summarized in Table 8. Microporous materials can indeed improve the membrane stability, enhancing the cation transference number, avoiding the side reactions and electrolyte leakage by confining the liquid electrolytes in the bulk. However, challenges still remain in the development of new separators:

- Processability: MOFs have been extensively studied as separators in LIBs. Processing the MOF particles into flexible membranes or grain-boundary free pellets are extremely difficult.
- Ionic conductivity: Solution-processable PIMs are a leading candidate for LIB separators. However, PIMs without ionic functional groups have low ionic conductivity and lead to the decreased power density of devices.

For a solid-state electrolyte separator (e.g., PEO and inorganic electrolytes), the low apparent ionic conductivity at room temperature is the key issue. Besides the limited ionic conductivity of the bulk of electrolytes, resistance originating from grain boundaries contributes to the low battery power. This challenge could not be easily avoided during the membrane fabrication process. To develop usable solid-state electrolyte, smart strategies need to be adopted, for example, the design of semi-solid electrolyte, in which the liquid can be impregnated into the boundaries to create continuous ion channels.

4.3. Recent Progress in Separator Design Strategies for Lithium Dendrite Suppression

4.3.1. *Electric/Ionic Field Regulation*

This approach leverages electric or ionic field gradients to guide uniform Li ion flux and suppress dendritic nucleation. For instance, the GFC@PVDF membrane[267] employs gradient Fe_2O_3 particles that attenuate from the bottom to the top of the membrane, creating a lithiophilic gradient. This gradient induces a bottom-up "pumping" of Li^+ ions via localized electric fields, directing Li^+ flux toward the substrate rather than the separator surface. During cycling, Fe_2O_3 gradually converts to a Fe/Li_2O hybrid conductor, which decouples charge-transfer processes, enabling fast Li ion transport pathways and promoting the formation of spherical, amorphous Li deposits rather than sharp dendrites. Similarly, the ion-management membrane (IMM)[268] uses vertically aligned, polydopamine (PDA)-modified nanochannels to act as "ion distributors," equalizing Li ion concentration beneath each. Its electronegative surface forms an electric double layer (EDL) with a ζ-potential of −22.8 mV, enhancing Li ion adsorption and suppressing anion migration.

4.3.2. *Alloying Reaction-Based Suppression*

This strategy utilizes reactive alloy formation to "digest" dendritic hotspots and modulate Li^+ adsorption. A representative example is the PZEM superlithiophilic membrane,[269] where localized Li ion overdeposition triggers $ZnCl_2$–Li alloying reactions. These reactions dissolve dendritic Li into a LiZn alloy, effectively eliminating dendritic growth. The membrane's porous architecture and Zn–F bonds (binding energy: −4.64 eV, significantly stronger than the −0.35 eV binding energy of PVDF) ensure uniform Li ion adsorption across the membrane.

4.3.3. *Ion Transport Regulation*

This strategy is aimed at enhancing Li^+ conductivity, structuring transport pathways, and stabilizing Li^+ flux. The Zn-MOF composite electrolyte,[270] for example, combines zeolitic imidazolate framework-8 (ZIF-8) nanoparticles with $TFSI^-$ anions. ZIF-8's Lewis acidic sites coordinate with $TFSI^-$, releasing free Li^+ ions and enhancing ionic conductivity to 2.39×10^{-1}

Table 8. Typical examples of LIB separators and their properties, preparation method, and performance.

Type	Material	Processing method	Organic electrolyte	Electrolyte uptake (wt%)	Ionic conductivity (mS cm^{-1})	t_{Li}	Performance	Ref.
Porous polymer separator	PP, PE	Wet and dry processes	$LiPF_6$ in EC/DMC	150–400	0.4–2.1	0.2–0.3	✓: High porosity, thin thickness, good chemical stability ✗: **Thermal instable, Weak mechanical strength in TD**	[257,258]
	PVDF	Casting method	$LiPF_6$ in EC/DMC/DEC	180–230	1.3	0.48	Good mechanical strength, high porosity, good chemical stability **C-F/Li by-reaction**	[22,259]
	PAN	Phase inversion	$LiPF_6$ in EC/DMC	8.2 times to polymer weight	2.8	0.2–0.3	Better ion transport, high porosity, good chemical stability **Electrolyte leakage**	[179,260]
Nonwovens	PVDF	Electrospinning	$LiPF_6$ in EC/DMC/DEC	320–350	1.0	N/A	High electrolyte uptake, good cycling performance **Poor mechanical strength**	[261]
	PVDF-*co*-HFP	Electrospinning	$LiPF_6$ in EC/DMC	160–210	0.4	N/A	Good cycling performance **Poor mechanical strength**	[262]
	PAN	Electrospinning	$LiPF_6$ in EC/DMC/DEC	1100	0.017	N/A	Mechanical stability, high electrolyte uptake **Low ionic conductivity (20 °C)**	[263]
Composites	Al_2O_3/PEO/PVDF-HFP on PP	Solution casting method	$LiPF_6$ in EC/DMC/EMC	170–273	3.8	0.52–0.62	Good rate and cycle stability **Low shutdown temperature and C-F/Li by-reaction**	[264]
	Al_2O_3/PLSS on PE	Solution coating method	$LiPF_6$ in EC/DMC	206–248	0.72–0.83	N/A	Excellent wettability, improved mechanical strength **Low ionic conductivity**	[265]
	Al_2O_3/PVDF-*co*-HFP	Solution casting method	$LiClO_4$ in EC/DEC	N/A	0.8–2.1	0.66	High Li+ transference number, stable cycling performance **C-F/Li by-reaction**	[266]
MOFs	HKUST-1/ GO	Vacuum filtration method	LiTFSI in DOL/DME	N/A	0.07	N/A	High selectivity to Li-polysulfides, stable cycling performance **Low ionic conductivity, electrochemical instability of HKUST-1**	[199]
	HKUST-1/PTFE	Solution casting method and compression	$LiClO_4$ in PC	N/A	>1.0	0.65	High selectivity to TFSI−, improved mechanical strength, stable cycling **Low ionic conductivity, electrochemical instability of HKUST-1**	[202]
	UiO-LiTFSI	Pelletizing method	MOFs and LiTFSI 7:3	PC added	0.21	0.84	High Li+ transference number, improved mechanical strength **Instable cycling capacity, complicated membrane process**	[201]
	UiO-66 on PP	Dip coating method	LiTFSI in DOL/DME	N/A	0.04–0.2	N/A	High selectivity to Li-polysulfides, improved cycling performance **Reduced conductivity**	[200]
PIMs	PIM-1	Casting method	LiTFSI in DOL/DME	N/A	0.0059	N/A	High selectivity to Li-polysulfides, improved cycling performance **Low ionic conductivity**	[205]
	PIM-7	Casting method	LiTFSI in DOL/DME	N/A	0.007	N/A	Improved selectivity to Li-polysulfides **Low ionic conductivity**	[34]
	Silica/ PIM-1	Solution casting method	$LiPF_6$ in EC/DMC/EMC	240	0.82	N/A	Enhanced ionic conductivity **Mesoporous structure and low selectivity**	[29]

Text in ✓: green indicates the advantages of the corresponding materials, while text in ✗: red highlights their disadvantages or limitations.

$mS\,cm^{-1}$. Meanwhile, the F-PMIA (fluorinated polyamide) backbone provides mechanical reinforcement that resists dendrite penetration. Another example is the starfish-inspired fluorinated alkyl imidazolium electrolyte (FAEI),[271] which merges rigid polyacrylonitrile (PAN)/metal–organic framework (MOF) skeletons with [EMIM][TFSI] ionic liquid matrices. This design creates a 3D conductive network with a high Li^+ transference number ($t_+ = 0.69$) and a multi-component solid electrolyte interphase (SEI) composed of organic $ROCO_2Li$ and inorganic Li_2CO_3/LiF. Additionally, the PBI-Cu coordination membrane[272] leverages Cu^{2+}-mediated Li^+ solvation in PBI-Cu complexes to enhance transport kinetics (ionic conductivity: 10.13×10^{-1} $mS\,cm^{-1}$) and induce interconnected pores. These pores guide flat Li ion fronts, enabling 1000 h of stable cycling with consistent voltage profiles.

4.3.4. Physical Barrier Approaches

This strategy aims to block dendrite penetration through mechanical or structural barriers while maintaining Li^+ transport. The imidazole-functionalized polyamide (PABZ-20-ISM),[273] for instance, uses hydrogen-bond networks (imidazole N–H···N interactions) to form a crosslinked structure with a tensile strength of 11.8 MPa, effectively resisting dendrite penetration. By suppressing polymer crystallinity, it also enables amorphous Li^+ transport pathways, achieving a high ionic conductivity of 2.46 $mS\,cm^{-1}$.

4.3.5. Ferroelectric Effects

This emerging strategy exploits piezoelectric fields to repel Li ions from dendrite tips and induce self-healing. The P(VDF-TrFE) separator[274] generates localized piezoelectric fields (E_pz) when compressed by growing dendrites, which repel Li ions from dendrite protrusions. This process reverses the surface energy landscape, flattening the electrode surface (surface roughness S_a reduced from 2.42 to 0.45 μm). Repeated cycling further smooths pre-formed dendrites through a self-healing mechanism. Experimental evidence shows that Zn foils coated with membranes exhibit featureless surfaces after 10 hours of electrodeposition, whereas uncoated foils develop whisker-like dendrites on bare glass fiber (GF) separators.

4.4. Modeling Strategies for Separators in Lithium-Ion, Redox Flow, and Solid-State Batteries

Separators play a pivotal role in governing the electrochemical performance, safety, and longevity of energy storage systems. Modeling approaches for separators in LIBs, RFBs, and SSBs must address distinct physicochemical mechanisms while confronting common challenges in multiscale integration and experimental validation (**Table 9**).

In RFBs, the non-selective permeability of separators leads to active-species crossover and capacity decay, driving the development of models that link transport phenomena to electrochemical kinetics. Classical porous electrode theory, combined with the Nernst–Planck equation, describes ionic transport across separators, while the Marcus–Hush–Chidsey (MHC) kinetics simulate interfacial reaction dynamics.[275] Two-dimensional transient models further integrate electrolyte flow fields and pressure distributions to quantify the relationship between capacity utilization and Damköhler numbers, offering a framework for optimizing separator selectivity.[275] Complementary in situ spectroscopic techniques, such separation efficiency with cost remains a critical challenge due to the inherent trade-off between selectivity and membrane permeability.

For LIBs, separator modeling focuses on reconciling ionic conductivity, mechanical stability, and thermal safety. Finite element analysis (FEA) simulates stress distributions to predict mechanical failure thresholds under puncture or compression scenarios.[116] Porous medium models coupled with computational fluid dynamics (CFD) link effective ionic conductivity ($\sigma_{eff} = \varepsilon/\tau \cdot \sigma$) to microstructural parameters like porosity (ε) and tortuosity (τ), enabling pore-structure optimization.[8] Molecular dynamics (MD) simulations further reveal polymer chain degradation mechanisms in polyethylene or polypropylene separators at elevated temperatures, informing thermal runaway mitigation strategies.[276] However, achieving synergy between high porosity (favoring ion transport) and mechanical robustness (preventing short circuits) remains a persistent challenge.

SSB separators demand modeling strategies to address interfacial impedance and dendrite suppression. Multiscale simulations integrate 3D microstructure reconstructions with macroscopic electrochemical models to predict ion transport pathways and mechanical strength in solid electrolytes (SEs).[277] Phase-field modeling elucidates lithium dendrite growth dynamics and their interaction with SEs, guiding thickness optimization (<5 μm) and material stability enhancements (e.g., garnet-type LLZO).[278] Additionally, machine learning-assisted design identifies polymer binders and carbon additives that improve cathode composite conductivity and mechanical flexibility.[278] However, interfacial side reactions between SEs and electrodes, along with degradation under operational thermal stress, pose unresolved hurdles.

Cross-battery modeling integration strategies increasingly leverage multiphysics coupling and data-driven approaches. Tools like COMSOL Multiphysics unify electrochemical, thermal, and fluid dynamic modules to simulate separator behaviors across systems, with RFB flow-reaction models adaptable to SSB solid-state transport.[116,279] Material property databases (e.g., porosity, ionic conductivity, thermal expansion coefficients) enable rapid parameter optimization across chemistries.[277,280] Neural networks trained on experimental datasets[275,278,281] predict separator performance metrics (e.g., crossover rates, thermal stability) to reduce empirical trial-and-error. Standardized protocols for electrochemical impedance spectroscopy (EIS) and pressure testing further ensure model validity and cross-comparability.[116,276]

These advancements highlight the necessity of closed-loop modeling frameworks that bridge atomic-scale mechanisms, such as ion transport and dendrite growth, with macro-scale performance optimization, while addressing interdisciplinary barriers in battery system design.

4.5. Scalable Manufacturing and Lifecycle Sustainability

The advancement of sustainable battery separators, critical for next-generation energy storage systems, hinges on resolving dual challenges: adopting environmentally benign synthesis methodologies and establishing circular end-of-life material recovery systems. Traditional fabrication routes for ion-conducting materials, such as polymer electrolytes, metal–organic frameworks (MOFs), and covalent organic frameworks (COFs), rely heavily on toxic solvents like N-methyl-2-

Table 9. Modeling focus and computational methods for battery separators in lithium-ion, redox flow, solid-state, and cross-battery systems.

Battery type	Modeling focus	Methods
RFBs	Quantify active-species crossover and capacity decay	Nernst-Planck equation (ion transport) + Marcus-Hush-Chidsey kinetics (interfacial reactions)
	Optimize flow field and capacity utilization	2D transient model (coupled flow-pressure distribution; Damköhler number[a)] analysis)
LIBs	Predict mechanical failure under stress	Finite element analysis (FEA) for stress distribution in separators
	Optimize porous structure for ion transport	Porous media CFD with effective ionic conductivity[b)] ($\sigma eff = \varepsilon/\tau \cdot \sigma$)
	Simulate thermal degradation of polymers	Molecular dynamics (MD) with ReaxFF force field (polymer chain scission at high temperatures)
SSBs	Suppress Li-dendrite growth in solid electrolytes	Phase-field model[c)] (Li-dendrite-stress interaction in SE; <111> crystallographic growth)
	Predict 3D ion pathways and mechanical strength	Multiscale FEM (3D FIB-SEM reconstruction of SE microstructure)
	Design stable cathode-electrolyte interfaces	Machine learning (ML) for binder-additive screening (bond energy prediction)
Cross-battery	Unified multiphysics simulation	COMSOL Multiphysics (electrochemical-thermal-fluid coupling; SEI growth modeling)
	Rapid performance prediction	Neural networks (NN) trained on experimental datasets (crossover rates, ionic conductivity)

FEM, finite element method.
[a)]Damköhler number = reaction rate/mass transfer rate.
[b)]$\sigma_{eff} = \varepsilon$ (porosity)/τ (tortuosity)·σ (bulk conductivity).
[c)]Phase-field model includes lattice strain energy and electrochemical potential coupling.

pyrrolidone (NMP) and petroleum-derived monomers, generating hazardous waste and significant carbon emissions.[282,283] For instance, solution-based synthesis of sulfonated polymers involves carcinogenic solvents and produces persistent organic byproducts, while the thermal instability of MOFs complicates metal–ligand bond recycling.[283] In response, emerging solvent-free techniques like melt polycondensation, electrospinning, and microwave-assisted synthesis offer promising alternatives. Melt-condensed polylactic acid (PLA) electrolytes derived from bio-sourced lactide demonstrate an 80% reduction in hazardous waste compared to solution-based methods, though scalability is limited by challenges in controlling melt viscosity without compromising ionic conductivity.[284] Similarly, cellulose acetate sourced from agricultural biomass shows potential as a renewable polymer electrolyte host, but its rigid structure and low polarity necessitate chemical modifications (e.g., esterification) to enhance ion solubility, with underlying mechanisms poorly understood.[285,286]

As illustrated in **Table 10**, the environmental footprint of these materials extends beyond synthesis to encompass manufacturing processes. Dry routes (e.g., melt-extrusion) eliminate solvent hazards but demand extreme thermal energy (15–20 kWh kg^{-1}) for polymer processing, contributing to high carbon footprints.[285] Wet processes like phase-inversion casting, while enabling precise pore control (23–66% porosity in P(VDF-TrFE-CFE) membranes), rely on toxic solvents like NMP and generate wastewater (10–20 L kg^{-1} separator), necessitating energy-intensive recovery systems.[282,283] Phase-transition methods (e.g., thermally induced phase separation) balance pore tunability and reduced solvents but suffer from inconsistent morphologies and thermal inefficiencies.[282] Emerging techniques such as electrospun lignin separators, as well as papermaking-based cellulose composites circumvent toxic solvents and enable biomass feedstocks, yet industrial scalability remains elusive due to undefined metrics for water/energy consumption and lifecycle costs.[286,287,289] For example, while lignin-based electrospun membranes exhibit thermal stability advantages,[287] their high-voltage production energy inputs and cellulose dispersion water footprints remain undocumented.[286,289]

Equally pressing is the need for end-of-life strategies aligned with circular economy principles. Current systems lack pathways to recover value from degraded materials, leading to landfill accumulation. Chemical recycling methods like PFSA membrane hydrolysis recover fluorinated monomers but require energy-intensive conditions incompatible with industrial scalability.[283] MOF/COF recovery faces additional hurdles: acid leaching or thermal calcination extracts metals like Zr^{4+} but degrades organic ligands, reducing reusability.[283] Innovations in selective degradation pathways, such as enzymatic cleavage for bio-based MOFs, are essential to overcome these limitations.[283] Bridging these gaps demands a systems-level approach integrating process engineering, material science, and lifecycle analysis. Standardized metrics for water/energy consumption and solvent recovery efficiencies are urgently needed to enable quantitative sustainability comparisons.[285,293] Ultimately, translating qualitative "green" claims into actionable roadmaps will require interdisciplinary collaboration to harmonize technical feasibility with ecological responsibility.

5. Conclusions and Outlooks

This review highlights the pivotal role of membrane separators in advancing electrochemical energy storage systems, including redox flow batteries (RFBs), lithium-ion batteries (LIBs), and solid-state batteries. By governing ion transport kinetics, suppressing parasitic reactions, and ensuring mechanical stability, separators directly influence energy efficiency, cycling durability, and operational safety. Despite diverse chemistries and operating principles, these systems share common design paradigms: achieving fast and selective ion conduction, mitigating concentration polarization, and balancing mechanical robustness with chemical compatibility. Addressing these challenges demands a paradigm shift in materials engineering, particularly through the development of microporous architectures that integrate multifunctional properties.

Emerging microporous materials defined by subnanometer pore channels, tailorable surface chemistries, and hierarchical architectures

Table 10. Comparative table of separator manufacturing methods: environmental footprint and techno-economic metrics.

Metric	Dry process	Wet process (Phase-inversion)	Phase-transition methods (TIPS/SIPS)	Emerging methods (Electrospinning)	Ref
Resource consumption	High thermal energy (15–20 kWh kg^{-1}) due to polymer melting/fibrillation Zero solvent use	High organic solvent use Energy-intensive solvent recovery (3.8–5.2 kWh kg^{-1})	Moderate thermal energy (10–15 kWh kg^{-1}) for phase separation Solvent-dependent (e.g., water for salt leaching)	Aqueous systems (e.g., lignin/PVA) avoid organic solvents Dry electrospinning avoids solvents but requires high-voltage energy inputs	[285–288]
Environmental impact	Low liquid waste but high CO_2 emissions from energy-intensive drying No solvent pollution	Severe aquatic toxicity from solvents Hazardous waste generation (e.g., $LiPF_6$ hydrolysis byproducts)	Reduced solvent risks versus wet processes Thermal pollution from phase-separation heat sources	Reduced VOCs and solvent risks Biomass feedstocks (e.g., cellulose) lower fossil carbon footprint	[282,283,287,289,290]
Technical advantages	Simplified process flow (no solvent recovery) High throughput for electrode-compatible materials	Precise pore control Established scalability for commercial separators	Tunable pore structures via temperature/precipitant control Improved mechanical strength in some systems	Nanofiber mats enable high ionic conductivity Papermaking yields thermal-shutdown separators	[282,286,288,291]
Economic costs	High capital costs for specialized extrusion/drying equipment Limited cost reduction potential	Dominant market share due to low material costs High operational costs for solvent recycling and waste treatment	Moderate costs for thermal systems Salt-leaching methods cheaper but less scalable	Low material costs for biomass-based separators Scalability barriers (e.g., very low electrospinning throughput)	[283,285,292]
Sustainability potential	Reduced solvent risks but energy-intensive Shortcomings in circular economy integration	High environmental liabilities Regulatory pressures to replace NMP with greener solvents	Improved safety profiles (e.g., ceramic-filled separators) Challenges in recycling phase-separated polymers	High theoretical sustainability (water-based, biodegradable polymers) Lack of LCA data for commercial-scale production	[286,287,289,293,294]

TIPS/SIPS, temperature-induced phase separation/solvent-induced phase separation.

offer unprecedented opportunities to decouple ionic conductivity from selectivity. Their ability to combine size-exclusion sieving with tunable electrostatic interactions positions them as a transformative platform for next-generation separators. However, critical gaps persist: conductivity-selectivity trade-offs often arise due to competing requirements, while scalability barriers hinder the fabrication of defect-free membranes from brittle frameworks like MOFs or COFs. Additionally, dynamic stability remains a concern, particularly under harsh electrochemical conditions or prolonged cycling.

To bridge these gaps, future research must adopt a multiscale design philosophy. First and foremost, hierarchical pore engineering—integrating interconnected subnanometer channels with mesoporous scaffolds—could harmonize rapid ion transport and molecular-level selectivity. Simultaneously, surface functionalization with charged or polar groups may enable dual-mode separation, leveraging both size-exclusion and Donnan-exclusion mechanisms without compromising electrolyte compatibility. Furthermore, controlled lattice or interfacial defects within microporous frameworks could serve as low-energy pathways for ion migration, enhancing conductivity while maintaining structural integrity.

Advancements in manufacturing will also be critical. Solvent-free or additive fabrication methods could enable large-scale production of uniform, defect-free microporous films, while hybridizing microporous fillers with flexible polymer matrices might resolve mechanical fragility without sacrificing conductivity. Equally vital is the integration of in situ characterization and computational modeling to unravel ion transport dynamics and degradation mechanisms under realistic conditions. For instance, operando X-ray tomography and solid-state NMR could reveal real-time ion distribution, while machine learning tools may accelerate the discovery of materials with optimized pore geometries and surface chemistries.

Finally, application-specific optimization must guide material development. Tailoring separators for niche scenarios—such as aqueous RFBs requiring acid/base stability, Li-metal anodes demanding dendrite suppression, or flexible electronics needing mechanical stretchability—will ensure practical relevance. The successful implementation of microporous separators hinges on interdisciplinary collaboration spanning materials science, electrochemistry, and process engineering. By addressing scalability, stability, and functional integration, these materials could redefine the performance boundaries of energy storage systems, enabling high-density, long-lifetime, and inherently safe batteries for grid-scale renewables and electrified transportation.

In summary, the paper emphasizes that a deeper understanding of the structure–property–function relationships of membrane separators is crucial for guiding the development of advanced materials. Future efforts must focus on innovative design strategies to overcome existing limitations and unlock the full potential of these materials for next-generation battery technologies.

Conflict of Interest

The authors declare no conflict of interest.

Data Availability Statement

Data will be made available on request.

Keywords

lithium-ion batteries, membrane separators, modeling, redox flow batteries, solid-state batteries

Received: August 10, 2025
Revised: August 31, 2025
Published online: September 25, 2025

[1] S. Bouckaert, A. F. Pales, C. McGlade, U. Remme, B. Wanner, L. Varro, D. D'Ambrosio, T. Spencer, *Net Zero by 2050: A Roadmap for the Global Energy Sector*, International Energy Agency, Paris, France **2021**.
[2] X. Tian, S. Zhou, H. Hao, H. Ruan, R. R. Gaddam, R. C. Dutta, T. Zhu, H. Wang, B. Wu, N. P. Brandon, R. Tan, *Chain* **2024**, *1*, 150.
[3] Z. Feng, I. Eiubovi, Y. Shao, Z. Fan, R. Tan, *Chain* **2024**, *1*, 54.
[4] Z. Feng, Y. Luo, D. Li, J. Pan, R. Tan, Y. Chen, *Chain* **2025**, *2*(1), 1.
[5] P. Alotto, M. Guarnieri, F. Moro, *Renew. Sust. Energ. Rev.* **2014**, *29*, 325.
[6] B. Dunn, H. Kamath, J. M. Tarascon, *Science* **2011**, *334*, 928.
[7] M. Armand, P. Axmann, D. Bresser, M. Copley, K. Edström, C. Ekberg, D. Guyomard, B. Lestriez, P. Novák, M. Petranikova, *J. Power Sources* **2020**, *479*, 228708.
[8] E. Sánchez-Díez, E. Ventosa, M. Guarnieri, A. Trovò, C. Flox, R. Marcilla, F. Soavi, P. Mazur, E. Aranzabe, R. Ferret, *J. Power Sources* **2021**, *481*, 228804.
[9] D. Duerkop, H. Widdecke, C. Schilde, U. Kunz, A. Schmiemann, *Membranes* **2021**, *11*, 214.
[10] M. Park, J. Ryu, W. Wang, J. Cho, *Nat. Rev. Mater.* **2016**, *2*(1), 1.
[11] G. Venugopal, J. Moore, J. Howard, S. Pendalwar, *J. Power Sources* **1999**, *77*, 34.
[12] Y. Pan, S. Chou, H. K. Liu, S. X. Dou, *Natl. Sci. Rev.* **2017**, *4*, 917.
[13] P. Albertus, S. Babinec, S. Litzelman, A. Newman, *Nat. Energy* **2018**, *3*, 16.
[14] H. Chen, G. Cong, Y.-C. Lu, *J. Energy Chem.* **2018**, *27*, 1304.
[15] C. Zhang, L. Zhang, Y. Ding, S. Peng, X. Guo, Y. Zhao, G. He, G. Yu, *Energy Storage Mater* **2018**, *15*, 324.
[16] M. Skyllas-Kazacos, *ECS Trans.* **2019**, *89*, 29.
[17] C. Minke, U. Kunz, T. Turek, *J. Power Sources* **2017**, *361*, 105.
[18] C. Minke, T. Turek, *J. Power Sources* **2015**, *286*, 247.
[19] H. Prifti, A. Parasuraman, S. Winardi, T. M. Lim, M. Skyllas-Kazacos, *Membranes (Basel)* **2012**, *2*, 275.
[20] I. S. Chae, T. Luo, G. H. Moon, W. Ogieglo, Y. S. Kang, M. Wessling, *Adv. Energy Mater.* **2016**, *6*, 1600517.
[21] R. Tan, A. Wang, R. Malpass-Evans, R. Williams, E. W. Zhao, T. Liu, C. Ye, X. Zhou, B. P. Darwich, Z. Fan, *Nat. Mater.* **2020**, *19*, 195.
[22] H.-q. Liang, L.-s. Wan, Z.-k. Xu, *Chin. J. Polym. Sci.* **2016**, *34*, 1423.
[23] M. Yang, J. Hou, *Membranes (Basel)* **2012**, *2*, 367.
[24] J. Janek, W. G. Zeier, *Nat. Energy* **2016**, *1*(9), 1.
[25] Z. Tian, X. He, W. Pu, C. Wan, C. Jiang, *Electrochim. Acta* **2006**, *52*, 688.
[26] H. Lee, M. Yanilmaz, O. Toprakci, K. Fu, X. Zhang, *Energy Environ. Sci.* **2014**, *7*, 3857.
[27] Y. Huai, J. Gao, Z. Deng, J. Suo, *Ionics* **2010**, *16*, 603.
[28] N. Sabetzadeh, A. A. Gharehaghaji, M. Javanbakht, *Solid State Ionics* **2018**, *325*, 251.
[29] Y. Tian, C. Lin, Z. Wang, J. Jin, *RSC Adv.* **2019**, *9*, 21539.
[30] M. R. Asghar, M. T. Anwar, T. Rasheed, A. Naveed, X. Yan, J. Zhang, *IOP Conf. Ser. Mater. Sci. Eng.* **2019**, *654*, 12017.
[31] S. Yang, W. Ma, A. Wang, J. Gu, Y. Yin, *RSC Adv.* **2018**, *8*, 23390.
[32] S. Ferrari, E. Quartarone, P. Mustarelli, A. Magistris, M. Fagnoni, S. Protti, C. Gerbaldi, A. Spinella, *J. Power Sources* **2010**, *195*, 559.
[33] J.-H. Park, W. Park, J. H. Kim, D. Ryoo, H. S. Kim, Y. U. Jeong, D.-W. Kim, S.-Y. Lee, *J. Power Sources* **2011**, *196*, 7035.
[34] A. L. Ward, S. E. Doris, L. Li, M. A. Hughes Jr., X. Qu, K. A. Persson, B. A. Helms, *ACS Cent. Sci.* **2017**, *3*, 399.
[35] M. J. Baran, M. N. Braten, S. Sahu, A. Baskin, S. M. Meckler, L. Li, L. Maserati, M. E. Carrington, Y.-M. Chiang, D. Prendergast, *Joule* **2019**, *3*, 2968.
[36] S. E. Doris, A. L. Ward, A. Baskin, P. D. Frischmann, N. Gavvalapalli, E. Chenard, C. S. Sevov, D. Prendergast, J. S. Moore, B. A. Helms, *Angew. Chem. Int. Ed. Engl.* **2017**, *56*, 1595.
[37] M. Liu, L. Chen, S. Lewis, S. Y. Chong, M. A. Little, T. Hasell, I. M. Aldous, C. M. Brown, M. W. Smith, C. A. Morrison, *Nat. Commun.* **2016**, *7*, 12750.
[38] N. Kamaya, K. Homma, Y. Yamakawa, M. Hirayama, R. Kanno, M. Yonemura, T. Kamiyama, Y. Kato, S. Hama, K. Kawamoto, A. Mitsui, *Nat. Mater.* **2011**, *10*, 682.
[39] Y.-C. Jung, S.-M. Lee, J.-H. Choi, S. S. Jang, D.-W. Kim, *J. Electrochem. Soc.* **2015**, *162*, A704.
[40] M. Di, L. Hu, L. Gao, X. Yan, W. Zheng, Y. Dai, X. Jiang, X. Wu, G. He, *Chem. Eng. J.* **2020**, *399*, 125833.
[41] J. H. Park, K. Suh, M. R. Rohman, W. Hwang, M. Yoon, K. Kim, *Chem. Commun.* **2015**, *51*, 9313.
[42] Y. Du, H. Yang, J. M. Whiteley, S. Wan, Y. Jin, S. H. Lee, W. Zhang, *Angew. Chem. Int. Ed.* **2016**, *55*, 1737.
[43] Y. Hu, N. Dunlap, S. Wan, S. Lu, S. Huang, I. Sellinger, M. Ortiz, Y. Jin, S.-h. Lee, W. Zhang, *J. Am. Chem. Soc.* **2019**, *141*, 7518.
[44] M. Li, Y. Wan, J.-K. Huang, A. H. Assen, C.-E. Hsiung, H. Jiang, Y. Han, M. Eddaoudi, Z. Lai, J. Ming, *ACS Energy Lett.* **2017**, *2*, 2362.
[45] C. Sun, J.-h. Zhang, X.-f. Yuan, J.-n. Duan, S.-w. Deng, J.-m. Fan, J.-K. Chang, M.-s. Zheng, Q.-f. Dong, *ACS Appl. Mater. Interfaces* **2019**, *11*, 46671.
[46] C. Lu, X. Chen, *J. Power Sources* **2020**, *448*, 227587.
[47] H. Yang, B. Liu, J. Bright, S. Kasani, J. Yang, X. Zhang, N. Wu, *ACS Appl Energy Mater* **2020**, *3*, 4007.
[48] K. Wang, L. Yang, Z. Wang, Y. Zhao, Z. Wang, L. Han, Y. Song, F. Pan, *Chem. Commun.* **2018**, *54*, 13060.
[49] H. Zhu, X. Yang, E. D. Cranston, S. Zhu, *Adv. Mater.* **2016**, *28*, 7652.
[50] P. M. Budd, B. S. Ghanem, S. Makhseed, N. B. McKeown, K. J. Msayib, C. E. Tattershall, *Chem. Commun.* **2004**, *2*, 230.
[51] M. Carta, R. Malpass-Evans, M. Croad, Y. Rogan, J. C. Jansen, P. Bernardo, F. Bazzarelli, N. B. McKeown, *Science* **2013**, *339*, 303.
[52] L. Wang, Y. Zhao, B. Fan, M. Carta, R. Malpass-Evans, N. B. McKeown, F. Marken, *Electrochem. Commun.* **2020**, *118*, 106798.
[53] D. K. Karthikeyan, G. Sikha, R. E. White, *J. Power Sources* **2008**, *185*, 1398.
[54] M. Daigle, S. C. Kulkarni, *Annu. Conf. Progn. Health Manag. Soc.* **2013**, *5*(1), 1.
[55] M. Ghassemi, M. Kamvar, R. Steinberger-Wilckens, *Fundamentals of Heat and Fluid Flow in High Temperature Fuel Cells*, Academic Press, San Diego **2020**.
[56] L. Qi, Z. Wu, B. Zhao, B. Liu, W. Wang, H. Pei, Y. Dong, S. Zhang, Z. Yang, L. Qu, W. Zhang, *Chemistry* **2020**, *26*, 4193.
[57] Q. Yang, W. Li, C. Dong, Y. Ma, Y. Yin, Q. Wu, Z. Xu, W. Ma, C. Fan, K. Sun, *J. Energy Chem.* **2020**, *42*, 83.
[58] J. Wu, L. Yuan, W. Zhang, Z. Li, X. Xie, Y. Huang, *Energy Environ. Sci.* **2021**, *14*, 12.
[59] M. J. Baran, M. E. Carrington, S. Sahu, A. Baskin, J. Song, M. A. Baird, K. S. Han, K. T. Mueller, S. J. Teat, S. M. Meckler, C. Fu, D. Prendergast, B. A. Helms, *Nature* **2021**, *592*, 225.
[60] Z. Xue, D. He, X. Xie, *J Mater Chem A* **2015**, *3*, 19218.
[61] T. Miyake, M. Rolandi, *J. Phys. Condens. Matter* **2016**, *28*, 23001.
[62] Z. Zou, Y. Li, Z. Lu, D. Wang, Y. Cui, B. Guo, Y. Li, X. Liang, J. Feng, H. Li, C. W. Nan, M. Armand, L. Chen, K. Xu, S. Shi, *Chem. Rev.* **2020**, *120*, 4169.

[63] C. León, J. Santamaria, M. Paris, J. Sanz, J. Ibarra, L. Torres, *Phys. Rev. B* **1997**, *56*, 5302.
[64] P. Utpalla, S. K. Sharma, S. K. Deshpande, J. Bahadur, D. Sen, M. Sahu, P. K. Pujari, *Phys. Chem. Chem. Phys.* **2021**, *23*, 8585.
[65] D. Diddens, A. Heuer, *ECS Meet Abstr* **2019**, *4*, 196.
[66] Z. L. Peng, B. Wang, S. Q. Li, S. J. Wang, *J. Appl. Phys.* **1995**, *77*, 334.
[67] Z. Wojnarowska, H. Feng, Y. Fu, S. Cheng, B. Carroll, R. Kumar, V. N. Novikov, A. M. Kisliuk, T. Saito, N.-G. Kang, J. W. Mays, A. P. Sokolov, V. Bocharova, *Macromolecules* **2017**, *50*, 6710.
[68] S. D. Jones, J. Bamford, G. H. Fredrickson, R. A. Segalman, *ACS Polymers Au* **2022**, *2*, 430.
[69] X. C. Chen, R. L. Sacci, N. C. Osti, M. Tyagi, Y. Wang, M. J. Palmer, N. J. Dudney, *Mol. Syst. Des. Eng.* **2019**, *4*, 379.
[70] X. Chen, P. M. Vereecken, *Adv. Mater. Interfaces* **2019**, *6*, 1800899.
[71] S. B. Aziz, T. J. Woo, M. Kadir, H. M. Ahmed, *J. Sci. Adv. Mater. Devices* **2018**, *3*(1), 1.
[72] C. Granqvist, O. Hunderi, *Phys. Rev. B* **1978**, *18*, 1554.
[73] P. Knauth, *J. Electroceram.* **2000**, *5*, 111.
[74] C. Liang, *J. Electrochem. Soc.* **1973**, *120*, 1289.
[75] K. Schmidt-Rohr, Q. Chen, *Nat. Mater.* **2008**, *7*, 75.
[76] H. Y. Shin, M. S. Cha, S. H. Hong, T.-H. Kim, D.-S. Yang, S.-G. Oh, J. Y. Lee, Y. T. Hong, *J Mater Chem A* **2017**, *5*, 12285.
[77] K. Kreuer, *J. Membr. Sci.* **2001**, *185*, 29.
[78] S. Peng, X. Wu, X. Yan, L. Gao, Y. Zhu, D. Zhang, J. Li, Q. Wang, G. He, *J Mater Chem A* **2018**, *6*, 3895.
[79] T. Kimura, R. Akiyama, K. Miyatake, J. Inukai, *J. Power Sources* **2018**, *375*, 397.
[80] J. Si, Y. Lv, S. Lu, Y. Xiang, *J. Power Sources* **2019**, *428*, 88.
[81] Y. Zhao, M. Li, Z. Yuan, X. Li, H. Zhang, I. F. Vankelecom, *Adv. Funct. Mater.* **2016**, *26*, 210.
[82] M. Stucki, M. Loepfe, W. J. Stark, *Adv. Eng. Mater.* **2018**, *20*, 1700611.
[83] R. Bouchet, S. Maria, R. Meziane, A. Aboulaich, L. Lienafa, J.-P. Bonnet, T. N. Phan, D. Bertin, D. Gigmes, D. Devaux, *Nat. Mater.* **2013**, *12*, 452.
[84] X. Huang, *J. Solid State Electrochem.* **2011**, *15*, 649.
[85] M. F. Lagadec, R. Zahn, V. Wood, *Nat. Energy* **2019**, *4*, 16.
[86] S. Kalnaus, Y. Wang, J. A. Turner, *J. Power Sources* **2017**, *348*, 255.
[87] B. Zhang, R. Tan, L. Yang, J. Zheng, K. Zhang, S. Mo, Z. Lin, F. Pan, *Energy Storage Mater* **2018**, *10*, 139.
[88] Z. Gadjourova, Y. G. Andreev, D. P. Tunstall, P. G. Bruce, *Nature* **2001**, *412*, 520.
[89] M. V. Reddy, C. M. Julien, A. Mauger, K. Zaghib, *Nanomaterials* **2020**, *10*, 1606.
[90] S. Ohta, Y. Kihira, T. Asaoka, *Front. Energy Res.* **2016**, *4*, 30.
[91] J. Van Den Broek, S. Afyon, J. L. Rupp, *Adv. Energy Mater.* **2016**, *6*, 1600736.
[92] D. I. Kushner, A. R. Crothers, A. Kusoglu, A. Z. Weber, *Current Opinion in Electrochemistry* **2020**, *21*, 132.
[93] R. Epsztein, R. M. DuChanois, C. L. Ritt, A. Noy, M. Elimelech, *Nat. Nanotechnol.* **2020**, *15*, 426.
[94] M. Sogami, S. Era, M. Murakami, Y. Seo, H. Watari, N. Uyesaka, *Biochim. Biophys. Acta* **2001**, *1511*, 42.
[95] J. S. Babu, S. P. Sathian, *Phys. Rev. E* **2012**, *85*, 51205.
[96] P. Barai, K. Higa, V. Srinivasan, *Impact of Electrolyte Transference Number on Lithium Dendrite Growth Process, Electrochemical Society Meeting Abstracts 232*, The Electrochemical Society, Inc., Pennington **2017**, p. 66.
[97] M. D. Tikekar, L. A. Archer, D. L. Koch, *Sci. Adv.* **2016**, *2*, e1600320.
[98] C. Brissot, M. Rosso, J.-N. Chazalviel, S. Lascaud, *J. Power Sources* **1999**, *81*, 925.
[99] W. Wang, Q. Luo, B. Li, X. Wei, L. Li, Z. Yang, *Adv. Funct. Mater.* **2013**, *23*, 970.
[100] Q. Tan, S. Lu, J. Si, H. Wang, C. Wu, X. Li, Y. Xiang, *Macromol. Rapid Commun.* **2017**, *38*, 1600710.
[101] K. H. Hendriks, S. G. Robinson, M. N. Braten, C. S. Sevov, B. A. Helms, M. S. Sigman, S. D. Minteer, M. S. Sanford, *ACS Cent Sci* **2018**, *4*, 189.
[102] Q. Dai, Z. Liu, L. Huang, C. Wang, Y. Zhao, Q. Fu, A. Zheng, H. Zhang, X. Li, *Nat. Commun.* **2020**, *11*, 13.
[103] D. Guo, X. Li, F. Ming, Z. Zhou, H. Liu, M. N. Hedhili, V. Tung, H. N. Alshareef, Y. Li, Z. Lai, *Nano Energy* **2020**, *73*, 104769.
[104] M. Mamlouk, K. Scott, *Int. J. Hydrog. Energy* **2010**, *35*, 784.
[105] G. Venugopalan, K. Chang, J. Nijoka, S. Livingston, G. M. Geise, C. G. Arges, *ACS Appl Energy Mater* **2019**, *3*, 573.
[106] L. Hu, L. Gao, C. Zhang, X. Yan, X. Jiang, W. Zheng, X. Ruan, X. Wu, G. Yu, G. He, *J Mater Chem A* **2019**, *7*, 21112.
[107] L. Qiao, H. Zhang, M. Li, Z. Yuan, Y. Zhao, X. Li, *J Mater Chem A* **2017**, *5*, 25555.
[108] H. Zhang, X. Yan, L. Gao, L. Hu, X. Ruan, W. Zheng, G. He, *ACS Appl. Mater. Interfaces* **2019**, *11*, 5003.
[109] X. Luo, Z. Lu, J. Xi, Z. Wu, W. Zhu, L. Chen, X. Qiu, *J. Phys. Chem. B* **2005**, *109*, 20310.
[110] J. Dai, H. Zhang, Z. Sui, H. Hu, P. Gao, Y. Zhu, Y. Dong, X. Teng, *Ionics* **2020**, *26*, 801.
[111] J. Xi, Z. Li, L. Yu, B. Yin, L. Wang, L. Liu, X. Qiu, L. Chen, *J. Power Sources* **2015**, *285*, 195.
[112] S. Liu, L. Wang, Y. Ding, B. Liu, X. Han, Y. Song, *Electrochim. Acta* **2014**, *130*, 90.
[113] P. Zuo, Y. Li, A. Wang, R. Tan, Y. Liu, X. Liang, F. Sheng, G. Tang, L. Ge, L. Wu, Q. Song, N. B. McKeown, Z. Yang, T. Xu, *Angew. Chem. Int. Ed. Engl.* **2020**, *59*, 9564.
[114] USABC, *Lithium Battery Separator Goals*, The United States Advanced Battery Consortium LLC The United States Advanced Battery Consortium LLC (USABC), Southfield **2021**.
[115] A. V. Maksimov, M. Molina, O. G. Maksimova, G. Y. Gor, *ACS Appl. Polymer Mater.* **2023**, *5*, 2026.
[116] A. Li, A. C. Yuen, W. Wang, I. M. De Cachinho Cordeiro, C. Wang, T. B. Chen, J. Zhang, Q. N. Chan, G. H. Yeoh, *Molecules* **2021**, *26*, 478.
[117] D. De Porcellinis, B. Mecheri, A. D'Epifanio, S. Licoccia, S. Granados-Focil, M. Aziz, *J. Electrochem. Soc.* **2018**, *165*, A1137.
[118] F. Niccolai, E. Guazzelli, Z. El Koura, I. Pucher, E. Martinelli, *Adv. Sustain. Syst.* **2024**, *9*, 2400661.
[119] F. Niccolai, E. Guazzelli, Z. El Koura, I. Pucher, E. Martinelli, *J Energy Storage* **2025**, *130*, 117366.
[120] D. Chen, S. Wang, M. Xiao, Y. Meng, *Energy Environ. Sci.* **2010**, *3*, 622.
[121] Y. Li, Y. Liu, Z. Xu, Z. Yang, *Ind. Eng. Chem. Res.* **2019**, *58*, 10707.
[122] N. Wang, J. Yu, Z. Zhou, D. Fang, S. Liu, Y. Liu, *J. Membr. Sci.* **2013**, *437*, 114.
[123] S. Takamuku, A. Wohlfarth, A. Manhart, P. Räder, P. Jannasch, *Polym. Chem.* **2015**, *6*, 1267.
[124] L. Chen, D. T. Hallinan Jr., Y. A. Elabd, M. A. Hillmyer, *Macromolecules* **2009**, *42*, 6075.
[125] T. Miyahara, T. Hayano, S. Matsuno, M. Watanabe, K. Miyatake, *ACS Appl. Mater. Interfaces* **2012**, *4*, 2881.
[126] C. Wang, D. W. Shin, S. Y. Lee, N. R. Kang, Y. M. Lee, M. D. Guiver, *J. Membr. Sci.* **2012**, *405*, 68.
[127] Z. Yuan, X. Liu, W. Xu, Y. Duan, H. Zhang, X. Li, *Nat. Commun.* **2018**, *9*, 3731.
[128] D. Chen, S. Kim, V. Sprenkle, M. A. Hickner, *J. Power Sources* **2013**, *231*, 301.
[129] S.-H. Cha, *J. Nanomater.* **2015**, *2015*(1), 1.
[130] J. Xi, Z. Wu, X. Teng, Y. Zhao, L. Chen, X. Qiu, *J. Mater. Chem.* **2008**, *18*, 1232.
[131] D. Chen, X. Li, *J. Power Sources* **2014**, *247*, 629.
[132] Y. Ma, N. A. Qaisrani, L. Ma, P. Li, L. Li, S. Gong, F. Zhang, G. He, *J. Membr. Sci.* **2018**, *560*, 67.
[133] Y. Li, J. Sniekers, J. C. Malaquias, C. Van Goethem, K. Binnemans, J. Fransaer, I. F. Vankelecom, *J. Power Sources* **2018**, *378*, 338.
[134] S. Yun, J. Parrondo, V. Ramani, *ChemPlusChem* **2015**, *80*, 412.

[135] Y. Ahn, D. Kim, *J. Ind. Eng. Chem.* **2019**, *71*, 361.
[136] S. Zhang, B. Zhang, D. Xing, X. Jian, *J Mater Chem A* **2013**, *1*, 12246.
[137] B. Shanahan, T. Böhm, B. Britton, S. Holdcroft, R. Zengerle, S. Vierrath, S. Thiele, M. Breitwieser, *Electrochem. Commun.* **2019**, *102*, 37.
[138] J. Ren, Y. Dong, J. Dai, H. Hu, Y. Zhu, X. Teng, *J. Membr. Sci.* **2017**, *544*, 186.
[139] Q. Zhang, Q.-F. Dong, M.-S. Zheng, Z.-W. Tian, *J. Membr. Sci.* **2012**, *421*, 232.
[140] Z. Li, X. He, Z. Jiang, Y. Yin, B. Zhang, G. He, Z. Tong, H. Wu, K. Jiao, *Electrochim. Acta* **2017**, *240*, 486.
[141] J. Hou, Y. Liu, Y. Liu, L. Wu, Z. Yang, T. Xu, *Chem. Eng. Sci.* **2019**, *201*, 167.
[142] Z. Li, Z. Jiang, H. Tian, S. Wang, B. Zhang, Y. Cao, G. He, Z. Li, H. Wu, *J. Power Sources* **2015**, *288*, 384.
[143] K. Emmanuel, C. Cheng, B. Erigene, A. N. Mondal, M. M. Hossain, M. I. Khan, N. U. Afsar, G. Liang, L. Wu, T. Xu, *J. Membr. Sci.* **2016**, *497*, 209.
[144] L. Zeng, T. Zhao, L. Wei, Y. Zeng, Z. Zhang, *J. Power Sources* **2016**, *331*, 452.
[145] R. Parnamae, L. Gurreri, J. Post, W. J. van Egmond, A. Culcasi, M. Saakes, J. Cen, E. Goosen, A. Tamburini, D. A. Vermaas, M. Tedesco, *Membranes* **2020**, *10*, 409.
[146] J. Qiu, J. Zhang, J. Chen, J. Peng, L. Xu, M. Zhai, J. Li, G. Wei, *J. Membr. Sci.* **2009**, *334*, 9.
[147] L. Liu, C. Wang, Z. He, R. Das, B. Dong, X. Xie, Z. Guo, *J. Mater. Sci. Technol.* **2021**, *69*, 212.
[148] G.-M. Weng, C.-Y. V. Li, K.-Y. Chan, *J. Electrochem. Soc.* **2013**, *160*, A1384.
[149] J. Dai, Y. Dong, P. Gao, J. Ren, C. Yu, H. Hu, Y. Zhu, X. Teng, *Polymer* **2018**, *140*, 233.
[150] S. Peng, X. Yan, X. Wu, D. Zhang, Y. Luo, L. Su, G. He, *RSC Adv.* **2017**, *7*, 1852.
[151] D. Chen, H. Qi, T. Sun, C. Yan, Y. He, C. Kang, Z. Yuan, X. Li, *J. Membr. Sci.* **2019**, *586*, 202.
[152] L. Hu, L. Gao, X. Yan, W. Zheng, Y. Dai, C. Hao, X. Wu, G. He, *J Mater Chem A* **2019**, *7*, 15137.
[153] R. E. Ruther, G. Yang, F. M. Delnick, Z. Tang, M. L. Lehmann, T. Saito, Y. Meng, T. A. Zawodzinski Jr., J. Nanda, *ACS Energy Lett.* **2018**, *3*, 1640.
[154] J. Zhou, Y. Liu, P. Zuo, Y. Li, Y. Dong, L. Wu, Z. Yang, T. Xu, *J. Membr. Sci.* **2021**, *620*, 118832.
[155] Y. Zhang, H. Wang, W. Wang, Z. Zhou, J. Huang, F. Yang, Y. Bai, P. Sun, J. Ma, L. E. Peng, C. Y. Tang, L. Shao, *Matter* **2024**, *7*, 1406.
[156] Y. Wang, L. Ren, H. Wang, J. Wang, Q.-b. Chen, T. Han, *Chem. Eng. J.* **2024**, *485*, 149742.
[157] A. Pasadakis-Kavounis, F. Arslan, M. Radmer Almind, D. Aili, J. Hjelm, *Batteries Supercaps* **2023**, *6*, e202300176.
[158] X. Che, H. Zhao, X. Ren, D. Zhang, H. Wei, J. Liu, X. Zhang, J. Yang, *J. Membr. Sci.* **2020**, *611*, 118359.
[159] D. Chen, S. Yu, X. Liu, X. Li, *J. Power Sources* **2015**, *282*, 323.
[160] L. Zhang, Y. Ding, C. Zhang, Y. Zhou, X. Zhou, Z. Liu, G. Yu, *Chem* **2018**, *4*, 1035.
[161] T. Lin, X. Wen, X. Ren, V. Quintano, D. V. Andreeva, K. S. Novoselov, R. Joshi, *Small Struct.* **2024**, *6*, 2400320.
[162] M. Wang, J. J. Urban, B. Mi, *J. Membr. Sci.* **2024**, *697*, 122548.
[163] S. Bai, B. Kim, C. Kim, O. Tamwattana, H. Park, J. Kim, D. Lee, K. Kang, *Nat. Nanotechnol.* **2021**, *16*, 77.
[164] B. Schwenzer, S. Kim, M. Vijayakumar, Z. Yang, J. Liu, *J. Membr. Sci.* **2011**, *372*, 11.
[165] J. Zeng, C. Jiang, Y. Wang, J. Chen, S. Zhu, B. Zhao, R. Wang, *Electrochem. Commun.* **2008**, *10*, 372.
[166] J. Ye, D. Yuan, M. Ding, Y. Long, T. Long, L. Sun, C. Jia, *J. Power Sources* **2021**, *482*, 229023.
[167] J. Dai, Y. Dong, C. Yu, Y. Liu, X. Teng, *J. Membr. Sci.* **2018**, *554*, 324.
[168] C. T. Love, *J. Power Sources* **2011**, *196*, 2905.
[169] M.-S. Wu, P.-C. J. Chiang, J.-C. Lin, Y.-S. Jan, *Electrochim. Acta* **2004**, *49*, 1803.
[170] J. A. Morehouse, L. S. Worrel, D. L. Taylor, D. R. Lloyd, B. D. Freeman, D. F. Lawler, *J. Porous. Mater.* **2006**, *13*, 61.
[171] J. Saunier, F. Alloin, J.-Y. Sanchez, G. Caillon, *J. Power Sources* **2003**, *119*, 454.
[172] Z. Jiang, B. Carroll, K. Abraham, *Electrochim. Acta* **1997**, *42*, 2667.
[173] M. Raja, T. P. Kumar, G. Sanjeev, L. Zolin, C. Gerbaldi, A. M. Stephan, *Ionics* **2014**, *20*, 943.
[174] M.-H. Lee, H. J. Kim, E. Kim, S. B. Rhee, M. J. Moon, *Solid State Ionics* **1996**, *85*, 91.
[175] G. Appetecchi, F. Croce, B. Scrosati, *Electrochim. Acta* **1995**, *40*, 991.
[176] A. Yarin, E. Zussman, *Polymer* **2004**, *45*, 2977.
[177] Z. Tian, W. Pu, X. He, C. Wan, C. Jiang, *Electrochim. Acta* **2007**, *52*, 3199.
[178] X. Fu, C. Shang, M. Yang, E. M. Akinoglu, X. Wang, G. Zhou, *J. Power Sources* **2020**, *475*, 228687.
[179] H.-S. Min, J.-M. Ko, D.-W. Kim, *J. Power Sources* **2003**, *119*, 469.
[180] M. Latifatu, J. M. Ko, Y.-G. Lee, K. M. Kim, J. Jo, Y. Jang, J. J. Yoo, J. H. Kim, *Korean Chem. Eng. Res.* **2013**, *51*, 550.
[181] J. H. Jo, C. H. Jo, Z. Qiu, H. Yashiro, L. Shi, Z. Wang, S. Yuan, S. T. Myung, *Front. Chem.* **2020**, *8*, 153.
[182] R. Pan, R. Sun, Z. Wang, J. Lindh, K. Edström, M. Strømme, L. Nyholm, *Nano Energy* **2019**, *55*, 316.
[183] Y. Li, Q. Li, Z. Tan, *J. Power Sources* **2019**, *443*, 227262.
[184] H. Y. Nguyen Thi, B. T. D. Nguyen, J. F. Kim, *Membranes* **2020**, *11*, 19.
[185] O. Jirsak, P. Sysel, F. Sanetrnik, J. Hruza, J. Chaloupek, *J. Nanomater.* **2010**, *2010*(1), 1.
[186] M. Alcoutlabi, H. Lee, J. V. Watson, X. Zhang, *J. Mater. Sci.* **2013**, *48*, 2690.
[187] H. Li, B. Zhang, B. Lin, Y. Yang, Y. Zhao, L. Wang, *J. Electrochem. Soc.* **2018**, *165*, A939.
[188] H. Lee, M. Alcoutlabi, J. V. Watson, X. Zhang, *J. Appl. Polym. Sci.* **2013**, *129*, 1939.
[189] Y. Li, X. Ma, N. Deng, W. Kang, H. Zhao, Z. Li, B. Cheng, *Fibers Polym.* **2017**, *18*, 212.
[190] J. Zhang, L. Yue, Q. Kong, Z. Liu, X. Zhou, C. Zhang, S. Pang, X. Wang, J. Yao, G. Cui, *J. Electrochem. Soc.* **2013**, *160*, A769.
[191] T.-H. Cho, M. Tanaka, H. Ohnishi, Y. Kondo, M. Yoshikazu, T. Nakamura, T. Sakai, *J. Power Sources* **2010**, *195*, 4272.
[192] J. Zhang, Q. Kong, Z. Liu, S. Pang, L. Yue, J. Yao, X. Wang, G. Cui, *Solid State Ionics* **2013**, *245*, 49.
[193] B. M. Wiers, M. L. Foo, N. P. Balsara, J. R. Long, *J. Am. Chem. Soc.* **2011**, *133*, 14522.
[194] K. Fujie, R. Ikeda, K. Otsubo, T. Yamada, H. Kitagawa, *Chem. Mater.* **2015**, *27*, 7355.
[195] Z. Wang, Z. Wang, L. Yang, H. Wang, Y. Song, L. Han, K. Yang, J. Hu, H. Chen, F. Pan, *Nano Energy* **2018**, *49*, 580.
[196] Y. Du, X. Gao, S. Li, L. Wang, B. Wang, *Chin. Chem. Lett.* **2020**, *31*, 609.
[197] S. S. Park, Y. Tulchinsky, M. Dinca, *J. Am. Chem. Soc.* **2017**, *139*, 13260.
[198] Z. Wang, R. Tan, H. Wang, L. Yang, J. Hu, H. Chen, F. Pan, *Adv. Mater.* **2018**, *30*, 1704436.
[199] S. Bai, X. Liu, K. Zhu, S. Wu, H. Zhou, *Nat. Energy* **2016**, *1*(7), 1.
[200] Y. Fan, Z. Niu, F. Zhang, R. Zhang, Y. Zhao, G. Lu, *ACS Omega* **2019**, *4*, 10328.
[201] F. Zhu, H. Bao, X. Wu, Y. Tao, C. Qin, Z. Su, Z. Kang, *ACS Appl. Mater. Interfaces* **2019**, *11*, 43206.
[202] L. Shen, H. B. Wu, F. Liu, J. L. Brosmer, G. Shen, X. Wang, J. I. Zink, Q. Xiao, M. Cai, G. Wang, Y. Lu, B. Dunn, *Adv. Mater.* **2018**, *30*, e1707476.
[203] S. Fischer, J. Roeser, T. C. Lin, R. H. DeBlock, J. Lau, B. S. Dunn, F. Hoffmann, M. Fröba, A. Thomas, S. H. Tolbert, *Angew. Chem. Int. Ed.* **2018**, *57*, 16683.
[204] X. Lv, T. Lei, B. Wang, W. Chen, Y. Jiao, Y. Hu, Y. Yan, J. Huang, J. Chu, C. Yan, *Adv. Energy Mater.* **2019**, *9*, 1901800.
[205] C. Li, A. L. Ward, S. E. Doris, T. A. Pascal, D. Prendergast, B. A. Helms, *Nano Lett.* **2015**, *15*, 5724.
[206] C. Fu, V. Venturi, J. Kim, Z. Ahmad, A. W. Ells, V. Viswanathan, B. A. Helms, *Nat. Mater.* **2020**, *19*, 758.

[207] Y. Zhao, X. Ma, P. Li, Y. Lv, J. Huang, H. Zhang, Y. Shen, Q. Deng, X. Liu, Y. Ding, *J Mater Chem A* **2020**, *8*, 3491.
[208] L. Ma, J. Meng, Y. Pan, Y. J. Cheng, Q. Ji, X. Zuo, X. Wang, J. Zhu, Y. Xia, *Langmuir* **2020**, *36*, 2003.
[209] S. E. Doris, A. L. Ward, P. D. Frischmann, L. Li, B. A. Helms, *J Mater Chem A* **2016**, *4*, 16946.
[210] L. Qi, L. Shang, K. Wu, L. Qu, H. Pei, W. Li, L. Zhang, Z. Wu, H. Zhou, N. B. McKeown, W. Zhang, Z. Yang, *Chemistry* **2019**, *25*, 12052.
[211] L. Ma, C. Fu, L. Li, K. S. Mayilvahanan, T. Watkins, B. R. Perdue, K. R. Zavadil, B. A. Helms, *Nano Lett.* **2019**, *19*, 1387.
[212] G. HyeonáMoon, H. JongáKim, I. SeokáChae, S. ChanáPark, B. SuáKim, Y. SooáKang, *Chem. Commun.* **2019**, *55*, 6313.
[213] J. K. Papp, J. D. Forster, C. M. Burke, H. W. Kim, A. C. Luntz, R. M. Shelby, J. J. Urban, B. D. McCloskey, *J. Phys. Chem. Lett.* **2017**, *8*, 1169.
[214] M. J. Kim, C. H. Lee, M. H. Jo, S. K. Jeong, *Mater. Sci. Forum* **2017**, *893*, 127.
[215] X. Yao, T. Šamořil, J. Dluhoš, J. F. Watts, Z. Du, B. Song, S. R. P. Silva, T. Sui, Y. Zhao, *Energy Environ. Mater.* **2022**, *5*, 662.
[216] M. Wang, K. Liu, J. Yu, Q. Zhang, Y. Zhang, M. Valix, D. C. W. Tsang, *Glob. Chall.* **2023**, *7*, 2200237.
[217] Z. Yu, S. Wu, C. Ji, F. Tang, L. Zhang, F. Huang, *ACS Appl. Nano Mater.* **2023**, *6*, 10340.
[218] H. J. Im, Y. J. Park, *Sci. Rep.* **2022**, *12*, 527.
[219] V. C. Nguyen, T. Dam, H.-B. Na, C.-J. Park, *ACS Appl Energy Mater* **2025**, *8*, 3120.
[220] W. He, H. Ding, X. Chen, W. Yang, *J. Membr. Sci.* **2023**, *665*, 121095.
[221] Z. Zhang, M. Ye, J. Chen, X. Fu, X. Zhou, L. Zheng, L. He, Z. Wu, A. Kumar, L. Li, F. Wan, X. Guo, *Chem. Sci.* **2025**, *16*, 5028.
[222] L. Liu, Z. Li, Q. Xia, Q. Xiao, G. Lei, X. Zhou, *Ionics* **2012**, *18*, 275.
[223] C.-L. Tsai, Q. Ma, C. Dellen, S. Lobe, F. Vondahlen, A. Windmüller, D. Grüner, H. Zheng, S. Uhlenbruck, M. Finsterbusch, *Sustain. Energy Fuels* **2019**, *3*, 280.
[224] Z. Wang, J. Liu, M. Wang, X. Shen, T. Qian, C. Yan, *Nanoscale Adv* **2020**, *2*, 1828.
[225] Y. Kato, S. Hori, T. Saito, K. Suzuki, M. Hirayama, A. Mitsui, M. Yonemura, H. Iba, R. Kanno, *Nat. Energy* **2016**, *1*(4), 1.
[226] A. Manthiram, X. Yu, S. Wang, *Nat. Rev. Mater.* **2017**, *2*(4), 1.
[227] V. Thangadurai, S. Narayanan, D. Pinzaru, *Chem. Soc. Rev.* **2014**, *43*, 4714.
[228] H. Chung, B. Kang, *Chem. Mater.* **2017**, *29*, 8611.
[229] A. V. Kirianova, I. I. Yakovlev, D. S. Zimbovskii, S. Xiong, D. P. Sadykov, L. G. Grigoryan, X. Xu, D. Zhou, D. I. Yakubovsky, P. V. Evdokimov, I. A. Veselova, A. V. Arsenin, V. S. Volkov, F. S. Napolskiy, A. V. Merkulov, A. A. Rudnyh, V. A. Krivchenko, O. O. Kapitanova, *J Energy Storage* **2025**, *132*, 117687.
[230] L. Xiong, Z. Ren, Y. Xu, S. Mao, P. Lei, M. Sun, *Solid State Ionics* **2017**, *309*, 22.
[231] Z. Hu, J. Sheng, J. Chen, G. Sheng, Y. Li, X.-Z. Fu, L. Wang, R. Sun, C.-P. Wong, *New J. Chem.* **2018**, *42*, 9074.
[232] A. Santhosha, L. Medenbach, J. R. Buchheim, P. Adelhelm, *Batteries Supercaps* **2019**, *2*, 524.
[233] M. Matsuo, Y. Nakamori, S.-i. Orimo, H. Maekawa, H. Takamura, *Appl. Phys. Lett.* **2007**, *91*, 224103.
[234] V. Epp, M. Wilkening, *Phys. Rev. B* **2010**, *82*, 20301.
[235] M. R. Johan, O. H. Shy, S. Ibrahim, S. M. M. Yassin, T. Y. Hui, *Solid State Ionics* **2011**, *196*, 41.
[236] N. S. T. Do, D. M. Schaetzl, B. Dey, A. C. Seabaugh, S. K. Fullerton-Shirey, *J. Phys. Chem. C* **2012**, *116*, 21216.
[237] K. Zhu, Y. Liu, J. Liu, *RSC Adv.* **2014**, *4*, 42278.
[238] B. W. Zewde, S. Admassie, J. Zimmermann, C. S. Isfort, B. Scrosati, J. Hassoun, *ChemSusChem* **2013**, *6*, 1400.
[239] R. Tan, R. Gao, Y. Zhao, M. Zhang, J. Xu, J. Yang, F. Pan, *ACS Appl. Mater. Interfaces* **2016**, *8*, 31273.
[240] R. Tan, J. Yang, J. Zheng, K. Wang, L. Lin, S. Ji, J. Liu, F. Pan, *Nano Energy* **2015**, *16*, 112.
[241] L. Yang, Z. Wang, Y. Feng, R. Tan, Y. Zuo, R. Gao, Y. Zhao, L. Han, Z. Wang, F. Pan, *Adv. Energy Mater.* **2017**, *7*, 1701437.
[242] R. Chen, W. Qu, X. Guo, L. Li, F. Wu, *Mater. Horizons* **2016**, *3*, 487.
[243] K. K. Fu, Y. Gong, J. Dai, A. Gong, X. Han, Y. Yao, C. Wang, Y. Wang, Y. Chen, C. Yan, Y. Li, E. D. Wachsman, L. Hu, *Proc. Natl Acad. Sci. USA* **2016**, *113*, 7094.
[244] X. Ma, D. Mao, W. Xin, S. Yang, H. Zhang, Y. Zhang, X. Liu, D. Dong, Z. Ye, J. Li, *Polymers* **2024**, *16*, 565.
[245] Y. Matsuda, S. Nakazawa, M. Tanaka, H. Kawakami, *Macromol. Chem. Phys.* **2025**, *226*, 2400196.
[246] X. Gong, Y. Pan, L. Zhong, J. Wang, F. Liu, G. Qi, J. Li, C. Liu, D. Yu, *Chem. Commun.* **2024**, *60*, 13530.
[247] K. Khan, M. B. Hanif, H. Xin, A. Hussain, H. G. Ali, B. Fu, Z. Fang, M. Motola, Z. Xu, M. Wu, *Small* **2024**, *20*, 2305772.
[248] X. Hu, B. Zhang, *J. Membr. Sci.* **2024**, *701*, 122710.
[249] M. Li, W. Yang, L. Sun, Y. Li, X. Chen, *J Energy Storage* **2025**, *118*, 116247.
[250] S. Yang, Y. Ahn, D. Kim, *J Mater Chem A* **2017**, *5*, 2261.
[251] G. Wang, Y. Jing, Y. Yu, S. Wei, X. Li, S. Zhang, C. Zuo, J. Chen, Y. Zhou, J. Zhang, J. Chen, R. Wang, *ACS Appl. Mater. Interfaces* **2024**, *16*, 64020.
[252] Afzal, Y. Ren, S. Wang, H. Ma, S. Yuan, Q. Zhao, M. B. Wadud, X. Liang, Q. Pan, G. He, Z. Jiang, *J. Membr. Sci.* **2025**, *722*, 123863.
[253] Y. Zhang, H. Liu, M. Liu, X. Li, Y. Zhang, H. Sun, H. Shi, Y. Feng, *J. Membr. Sci.* **2025**, *714*, 123410.
[254] H. Liu, M. Liu, Y. Zhang, H. Sun, C. Ding, P. Qian, Y. Zhang, *J. Membr. Sci.* **2025**, *713*, 123314.
[255] J. Wang, W. Xu, F. Xu, L. Dai, Y. Wu, Y. Wang, S. Li, Z. Xu, *J. Membr. Sci.* **2024**, *695*, 122470.
[256] Y. Su, S. Liu, B. Shao, W. Zhu, Z. He, J. Wang, *Chem. Eng. J.* **2024**, *485*, 149838.
[257] Y. Zhu, F. Wang, L. Liu, S. Xiao, Y. Yang, Y. Wu, *Sci. Rep.* **2013**, *3*, 3187.
[258] D. Djian, F. Alloin, S. Martinet, H. Lignier, J.-Y. Sanchez, *J. Power Sources* **2007**, *172*, 416.
[259] J. Liu, C. Wang, X. Wu, F. Zhu, M. Liu, Y. Xi, *J. Solid State Electrochem.* **2019**, *23*, 277.
[260] B. Liu, Y. Huang, H. Cao, L. Zhao, Y. Huang, A. Song, Y. Lin, X. Li, M. Wang, *J. Membr. Sci.* **2018**, *545*, 140.
[261] J. R. Kim, S. W. Choi, S. M. Jo, W. S. Lee, B. C. Kim, *Electrochim. Acta* **2004**, *50*, 69.
[262] X. Li, G. Cheruvally, J.-K. Kim, J.-W. Choi, J.-H. Ahn, K.-W. Kim, H.-J. Ahn, *J. Power Sources* **2007**, *167*, 491.
[263] P. Carol, P. Ramakrishnan, B. John, G. Cheruvally, *J. Power Sources* **2011**, *196*, 10156.
[264] Y. Liao, X. Li, C. Fu, R. Xu, L. Zhou, C. Tan, S. Hu, W. Li, *J. Power Sources* **2011**, *196*, 2115.
[265] J.-A. Choi, S. H. Kim, D.-W. Kim, *J. Power Sources* **2010**, *195*, 6192.
[266] V. Kumar, P. Kumar, A. Nandy, P. P. Kundu, *RSC Adv.* **2016**, *6*, 23571.
[267] X. Wang, B. Zhao, X. Li, X. Qi, Y. Dai, T. Li, G. He, F. Chu, X. Jiang, *Energy Storage Mater* **2025**, *77*, 104200.
[268] Q. Zhang, B. Hou, X. Wu, X. Li, Z. Guo, J. Liu, D. Cao, X. Huang, J. Duan, D. Mo, J. Liu, H. Yao, *Adv. Energy Mater.* **2024**, *14*, 2401377.
[269] Y. Hu, Z. Li, Z. Wang, X. Wang, W. Chen, J. Wang, W. Zhong, R. Ma, *Adv. Sci.* **2023**, *10*, 2206995.
[270] S. Luo, N. Deng, H. Wang, Q. Zeng, Y. Li, W. Kang, B. Cheng, *Chem. Eng. J.* **2023**, *474*, 145683.
[271] L. Liu, L. Zhu, Y. Wang, X. Guan, Z. Zhang, H. Li, F. Wang, H. Zhang, Z. Zhang, Z. Yang, T. Ma, *Angew. Chem. Int. Ed.* **2025**, *64*, e202420001.
[272] N. u. R. Lashari, A. Mehmood, A. Hussain, W. Raza, I. Ahmed, M. A. Mushtaq, L. Wei, X. Cai, D. Liu, *J. Power Sources* **2024**, *624*, 235590.
[273] A. Liu, Z. Lv, H. Wang, X. Zhou, Q. Chen, S. Kang, Q. Zhang, N. Li, *J. Membr. Sci.* **2025**, *735*, 124511.
[274] Y. Dong, W. Liu, C. Carlos, Z. Zhang, J. Li, F. Pan, J. Sui, X. Wang, *Nano Lett.* **2024**, *24*, 4785.

[275] V. P. Nemani, K. C. Smith, *J. Electrochem. Soc.* **2018**, *165*, A3144.
[276] H. Xu, C. Bae, *J. Power Sources* **2019**, *430*, 67.
[277] K. Yang, L. Zhang, W. Wang, C. Long, S. Yang, T. Zhu, X. Liu, *Carbon Neutralization* **2024**, *3*, 348.
[278] J. H. Teo, F. Strauss, Đ. Tripković, S. Schweidler, Y. Ma, M. Bianchini, J. Janek, T. Brezesinski, *Cell Rep. Phys. Sci.* **2021**, *2*, 100465.
[279] E. Fraser, K. R. Dinesh, R. Wills, *Energy Rep.* **2021**, *7*, 49.
[280] M. D'Adamo, N. Daub, L. Trilla, J. A. Saez-Zamora, J. M. Paz-Garcia, *Batteries* **2025**, *11*, 8.
[281] E. J. Latchem, T. Kress, P. A. A. Klusener, R. V. Kumar, A. C. Forse, *J. Phys. Chem. Lett.* **2024**, *15*, 1515.
[282] S. H. Senthilkumar, B. Ramasubramanian, R. P. Rao, V. Chellappan, S. Ramakrishna, *Polymers* **2023**, *15*, 1622.
[283] X. H. G. Kia, Method of making thermally-stable composite separators for lithium batteries. **2020**.
[284] T. Maharana, B. Mohanty, Y. S. Negi, *Prog. Polym. Sci.* **2009**, *34*, 99.
[285] M. D. Bouguern, A. K. Madikere Raghunatha Reddy, X. Li, S. Deng, H. Laryea, K. Zaghib, *Batteries* **2024**, *10*, 39.
[286] N. Pavlin, S. Hribernik, G. Kapun, S. D. Talian, C. Njel, R. Dedryvère, R. Dominko, *J. Electrochem. Soc.* **2019**, *166*, A5237.
[287] H. Jia, J. Liu, B. Liu, R. Kuphal, V. Mottini, P. Monday, M. Ball, J. Li, M. Nejad, C. Fang, *Adv. Mater.* **2025**, *37*, 2419694.
[288] R. S. Pinto, J. P. Serra, J. C. Barbosa, M. M. Silva, M. Salado, A. Fidalgo Marijuan, E. Amayuelas, Y. Grosu, R. Gonçalves, S. Lanceros-Mendez, C. M. Costa, *J. Colloid Interface Sci.* **2025**, *680*, 714.
[289] Y. Wang, X. Zhang, X. Lang, Z. Li, C. Zhang, X. Feng, C. Shi, *Chem. Eng. J.* **2025**, *508*, 160824.
[290] Y. Li, J. Long, Y. Liang, J. Hu, *ACS Appl. Polym. Mater.* **2023**, *5*, 5305.
[291] S. Luiso, M. J. Petrecca, A. H. Williams, J. Christopher, O. D. Velev, B. Pourdeyhimi, P. S. Fedkiw, *ACS Appl. Polym. Mater.* **2022**, *4*, 3676.
[292] W. Lu, Z. Yuan, Y. Zhao, H. Zhang, H. Zhang, X. Li, *Chem. Soc. Rev.* **2017**, *46*, 2199.
[293] D. V. C. K. L. Passerini, Separator for an electrochemical device and method for the production thereof. **2015**.
[294] Q. Zhang, K. Liu, F. Ding, X. Liu, *Nano Res* **2017**, *10*, 4139.